Phytoplankton growth mainly depends on nutrient and light availability. Highly dynamic oceanic environments are dominated by physical processes that generally alter phytoplankton dynamics by controlling the access to these resources. Mesoscale motions have been considered the most important factor modulating the distribution of biogeochemical properties at the upper levels of the ocean. Nevertheless, recent studies have highlighted the role played by smaller processes that operate below the local Rossby radius of deformation, referred to here as submesoscale. Due to the inherent complexity of sampling at such high-resolution levels, our knowledge about submesoscale-influenced phytoplankton distribution and variability is mostly constrained to theoretical and modeling studies. In addition, little is known about the fate of meso-submesoscale impacts on phytoplankton communities under climate change stressors. Ocean warming leads to enhanced stratification in the oligotrophic ocean but also to the intensification of cross-shore wind gradients and thus of the eddy kinetic energy across eastern boundary regions of the subtropical gyres. Phytoplankton thriving in a warmer, acidified ocean could then be fertilized by enhanced meso-submesoscale activity. Consequently, meso-submesoscale contribution to global net primary production could be increased. In order to contribute to understand how physical and biogeochemical factors, resolved at a resolution close to submesoscale could affect the spatiotemporal distribution and variability of pico- and nanoplankton, the main components of planktonic communities in the Canary Islands waters, we conducted two interdisciplinary surveys across a highly variable mesoscale field and a submesoscale front south of Gran Canaria island (Canary Island).

ULPGC
Instituto Universitario de Oceanografía y Cambio Global
IOCAG
GOB OCEANOGRAFÍA BIOLÓGICA
Gobierno de Canarias
Consejería de Economía, Conocimiento y Empleo
Agencia Canaria de Investigación, Innovación y Sociedad de la Información
Canarias avanza con Europa

Short-term Drivers of Phytoplankton Distribution and Primary Production in the Canary Current Region

ULPGC

ULPGC
Universidad de Las Palmas de Gran Canaria

Doctoral Thesis

Short-term Drivers of Phytoplankton Distribution and Primary Production in the Canary Current Region

Nauzet Hernández Hernández

Doctorado en Oceanografía y Cambio Global

Telde
Octubre, 2021

D/Dª Santiago Manuel Hernández León coordinador del programa de doctorado en Oceanografía y Cambio global de la Universidad de Las Palmas de Gran Canaria

INFORMA,

De que la Comisión Académica del Programa de Doctorado, en su sesión de fecha tomó el acuerdo de dar el consentimiento para su tramitación, a la tesis doctoral titulada *" Short-term Driver of Phytoplankton Community Structure and Primary Production in the Canary Current Region"* presentada por el/la doctorando/a D/Dª **Nauzet Hernández Hernández** y dirigida por el/la Doctor/a **Javier Arístegui Ruiz.**

Y para que así conste, y a efectos de lo previsto en el Artº 11 del Reglamento de Estudios de Doctorado (BOULPGC 04/03/2019) de la Universidad de Las Palmas de Gran Canaria, firmo la presente.

Las Palmas de Gran Canaria, a de de

ULPGC Universidad de Las Palmas de Gran Canaria | Instituto Universitario de Oceanografía y Cambio Global

IOCAG

Short-term Drivers of Phytoplankton Community Structure and Primary Production in the Canary Current Region

Moduladores de la Estructura de la Comunidad de Fitoplancton y la Producción Primaria en la Región de la Corriente de Canarias a Pequeña Escala

Tesis doctoral presentada por **Nauzet Hernández Hernández** dentro del Programa de Doctorado en Oceanografía y Cambio Global, y dirigida por el **Prof. Dr. Javier Arístegui Ruiz**

El Doctorando

El Director

Las Palmas de Gran Canaria, 25 de octubre de 2021

ULPGC Universidad de Las Palmas de Gran Canaria | Instituto Universitario de Oceanografía y Cambio Global

IOCAG

Short-term Drivers of Phytoplankton Community Structure and Primary Production in the Canary Current Region

Moduladores de la Estructura de la Comunidad de Fitoplancton y la Producción Primaria en la Región de la Corriente de Canarias a Pequeña Escala

Tesis doctoral presentada por **Nauzet Hernández Hernández** dentro del Programa de Doctorado en Oceanografía y Cambio Global, y dirigida por el **Prof. Dr. Javier Arístegui Ruiz**

Short-term drivers of phytoplankton community structure and primary production in the Canary Current region

Author: Nauzet Hernández Hernández

Advisor: Javier Arístegui Ruiz

Grupo de Oceanografía Biológica (GOB),

Instituto de Oceanografía y Cambio Global (IOCAG),

Facultad de Ciencias del Mar, Universidad de Las Palmas de Gran Canaria (ULPGC), 35214, Taliarte, Telde, Gran Canaria, Islas Canarias

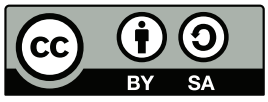

Test printed in Las Palmas de Gran Canaria

First edition, November 2021

A Tete, por acompañarme
en todas las veredas

El mar es a mi vida
lo que al hambriento el pan;
para saciar mi espíritu
tengo que ver el mar.

el mar me da la norma
y el ansia de vivir:
su majestad es ciencia
suprema para mí.

Saulo Torón, El Caracol Encantado.
1926, Telde (Gran Canaria).

Gracias también se llaman las tres hermanas,
Que una da, otra recibe, otra agradece.

Bartolomé Cairasco de Figueroa (Gran Canaria, 1538-1610)

Acknowledgments

Lleva razón ese refrán tan usado en los campos canarios; 'Buey sólo no ara". Este buey por si sólo tampoco hubiera podido llevar a cabo esta tesis sin todas aquellas personas, de las cuales, de una u otra forma, he tenido la suerte de recibir ayuda durante este periplo. Y es que periplo es la palabra que mejor define, en mi opinión, esta tesis doctoral. Ha sido un viaje largo, por numerosos lugares y con muchos escollos, pero también repleto de personas increíbles de las cuales he intentado aprender todo lo que he podido. Con mayor o menor éxito. Me siento afortunado de pedir perdón a todas aquellas personas que, aún habiendo sido parte de esta 'aventura', sus nombres no aparecen en lo que es una síntesis de todos aquellos agradecimientos que se merecen.

Si hay una persona sin la cual esta tesis no hubiera podido ser, ese es mi director. Javier, muchas gracias por darme la oportunidad de ser parte de la ciencia, de guiarme y de enseñarme. Pero, sobre todo, te agradezco cada uno de los retos que me has ido lanzando durante estos años. Al intentar superarlos, superarlos, fallar y fallar estrepitosamente (si me refiero a las trampas de sedimento), he aprendido valiosas lecciones que me han ayudado a evolucionar. Con tu permiso me llevo tu pasión por la

ciencia, el sentido crítico que con ella tienes y tus ganas incansables de seguir aprendiendo. Te estoy igual de agradecido por todos esos buenos momentos “fuera de la ciencia”. Imposible no acordarme de tus conciertos en medio de La Mar con Mine como corista de lujo, de tu conducción al estilo cretense, o de nuestros viajes en las guaguas no oficiales, ni recomendables de Lima.

Todo periplo tiene, un puerto de partida y unos personajes principales, en este caso, personajes en todas sus acepciones. Pero que tres personajes. El día que entré a formar parte de este grupo Javier me presentó al que sería mi “superbecario”. Yera, muchísimas gracias por acogerme desde el primer día. Gracias por tantas y tantas risas. Por los cafés de maquina en la facultad y por esas cervezas improvisadas en las que nunca se sabía cuando, ni dónde acabaría uno. También hicimos cosas saludables. Correr contigo y con los majalulos se hacía cuesta arriba. Gracias por esas largas conversaciones de bar sobre ciencia y por tu eterno buen humor. Me quedo, con tu permiso, con tu forma de entender la ciencia y, ojalá pudiera decir, que con la parsimonia que te caracteriza. Los siguientes dos personajes las voy a presentar juntas, pero no revueltas, que bastante revoltosas son ya ellas por separado. Mine, Cory, tengo tanto que agradecerles que no se por dónde empezar. Gracias por enseñarme como se debe trabajar en un laboratorio, aunque en este caso el alumno no supera a las maestras. ¡Buff, es que está jodido! Trabajar con ustedes hace que a uno le den ganas de levantarse a trabajar cada día. Gracias por esos cafés de marujas y por tantas, y tantas cervezas. Tantas como buenas y pisadas conversaciones, pero nunca tantas como risas. Si reírse da años de vida, gracias a ustedes tres sigo teniendo la misma edad que cuando empecé la tesis. A los tres gracias

por su amistad. No puedo continuar sin agradecer a Manu, el hijo de Maricarmen. Aunque por esta época aun quedaban años para conocerte, cuando apareciste, completaste las cuatro patas de la mesa de las viejas del visillo. Parte de esos años de vida extra son gracias a ti.

Creo que todo oceanógrafo recuerda perfectamente su primera campaña. De mi primera campaña recuerdo con especial cariño dos cosas. La oportunidad de ver de cerca el volcán submarino Tagoro de El Hierro, y a dos majoreros. Iván, un aventurero que ya había completado con éxito el periplo que yo estaba comenzando, y Vero. A los dos, gracias por recibirme con los brazos abiertos allá dónde nos encontramos.

Me gustaría expresar mi especial agradecimientos a aquellas personas que me han recibido y me han hecho sentir como en casa. Gracias Pepe por hacerme sentir parte de tu grupo durante mi estancia en Vigo. Oírte hablar de biogeoquímica es una de las experiencias más enriquecedoras que he tenido. Gracias también a su grupo, especialmente a Mar y Vane, con las que además he tenido la suerte de compartir varias campañas en las que nunca han faltado las risas. Aún saboreo el pincho de tortilla de la hora del café. No puedo dejar de agradecer a Toño y Carla, no sólo me hicieron sentir como en casa, sino que además me hicieron sentir un gallego más. Graciñas a todos.

I would like to thank to Ulf Riebesell for welcoming me to his team during my research stay in Kiel, and in every mesocosms experiment in which I have had the good fortune to participate. I would also like to thank to Ulf's group for making me feel like one more. In special to my

office mate Allanah, and Joaquín, Jan, Lennart, Mischa, Paul and Andrea. Vielen Dank!

Se me viene una lista enorme de nombres a la cabeza con los cuales he vivido buenos momentos durante esta tesis. Espero ser capaz de recordarlos todos. A los que no, les pido disculpas de antemano. Gracias a los majalulos Ale, Zeben, Juan Carlos, Yeray e Iván por dejarme sin aire corriendo, y de la risa. Gracias a Dani, Xabi, Xoel y Gustavo de la UTM por su valiosa ayuda y tantos buenos ratos en La Mar. A Mayi, Gara, María y Miguel por una precampaña apasionante en Boipeba. Gracias Fran por convertir RAPROCAN y VULCANO en una aventura. To Søren, for our short but amazing days in Gran Canaria. Gracias Tere por tu constante amabilidad y buen humor durante tu visita a Gran Canaria y la campaña HOTMIX. Gracias Bieito por los buenos momentos de la campaña FLUXES y Viena. Dirty Sanchez sigue estando en el top 10 de mis canciones favoritas. Gracias a Jose, María, Airam y Abel por lo buenos momentos vividos en la campaña SUMMER y los que le han seguido. Se que se me olvidan muchos nombres, a todos ellos, muchas gracias.

Por último, pero no por ello menos importante, quiero agradecer a mi familia. Por que lo que soy, no es más que una mezcla de todos ellos.

Mah, Papá, gracias por todo el esfuerzo que han hecho para que yo pudiera llegar hasta aquí. Gracias por darme la libertad de elegir mis pasos y apoyarme en cada uno de ellos. Gracias por estar siempre ahí. Y por no desheredarme por lo poco que llamo.

Tete, me haría falta otra tesis para agradecerte por todo lo que quiero. Que yo haya llegado hasta aquí se debe a ti. Gracias por apoyarme incondicionalmente, por acompañarme y por dejarme acompañarte. Gracias por ser mi orza y la mayor. Pero sobre todo gracias por hacerme mejor persona.

Idaira, Ayoze, gracias por ser los mejores hermanos mayores que uno puede tener. A ustedes dos se debe gran parte de mi personalidad. Me la cambiaron a base de cogotazos, pero aún así, es gracias a ustedes. Iván, gracias por ser y tratarme siempre como a un hermano. Gracias a los tres por mis sobrinos Asier, Naroa y Nairam.

A mis abuelos Nena y Emeterio, y Antonia y Rafael. Sin ustedes no existirían las dos familias Hernández, a las cuales tengo la inmensa suerte de pertenecer. Gracias también a los Hernández, si vuelvo a nacer espero que sea otra vez en estas dos familias.

Gracias Rita y Felipe por tratarme como un hijo. Y a Cira, Luis, Luisillo e Inés por hacerme sentir parte de su familia. Gracias a todos por hacer que la magua de estar lejos de la familia sea más llevadera.

Rubio, quién les iba a decir a aquellos dos chinijos en el campamento de La Santa, que más de 20 años después iban a seguir “bobiacando”. Gracias por ser mi oráculo, por todos los ‘surfins’ y las parrandas. Gracias también por la portada de la tesis, no se me ocurre un diseñador mejor para hacerla. Javivi, no sé que carajo andabas haciendo que te dio por hablarme “antier”. Salvaje, que eres un salvaje. No hay mejor plan que cocinar, escuchar música y arreglar el mundo contigo. Óscar, dónde estás tú, no hay problemas. A menos que te pongas “morrúo” con la

política. Gracias por tu eterno buen humor y por perdonarme tan rápido cuando nos gritamos. Barre pasar un rato contigo es salir con dolor de mandíbula y si te descuidas con los pantalones "meaos". Gracias por convertir todo en una fiesta. Damián, si a ti y a mi nos dicen el día que nos conocimos todo lo que íbamos a vivir juntos, tu hubieras dicho, ¡yo con el hippy ese no voy a ningún lado! Y yo hubiera estado de acuerdo. Lo que me hubiera perdido. Gracias por ser el alma de todas las fiestas y reuniones, y por haber hecho nuestra época universitaria mucho más emocionante. Rohan, otro descubrimiento tardío, pero chiquito descubrimiento. El momento del discurso de Damián en perojo puede ser de las veces que más me he reído en mi vida. Gracias por estar siempre dispuesto a apuntarte a un bombardeo. No hay problema que no se olvide con una cena, un viajito o unos indianos con ustedes. Si de algo me siento afortunado en esta vida es de pertenecer a Salitre S.A.

A todos ustedes, y en especial a los que no están…

Gracias,
Nau.
22 de octubre de 2021

Forewords

This Thesis, entitled *Short-term Drivers of Phytoplankton Community Structure and Primary Production in the Canary Current Region* was conducted under the supervision of Prof. Dr. Javier Arístegui Ruiz at the Grupo de Oceanografía Biológica (GOB) belonging to the Instituto de Oceanografía y Cambio Global (IOCAG) of the Universidad de Las Palmas de Gran Canaria (ULPGC), within the Doctoral program in Oceanografía y Cambio Global. The thesis compiles three distinct original studies: Two studies are based on in situ data collected during oceanographic surveys carried out in the frame of projects RODA (Oceanic eddies and atmospheric deposition in the Canary Current; CMT2004-06842-C03/MAR) and PUMP (Study of the Vertical Oceanic Pump in Mesoscale Eddies; CTM2012-33355) headed by Prof. Dr. Javier Arístegui Ruiz and Prof. Dr. Pablo Sangrá Inciarte, respectively. The third study is based on a mesocosms experiment carried out in Gran Canaria in the frame of project BIOACID (Biological Impacts of Ocean Acidification; FKZ 03F06550) headed by Prof. Dr. Ulf Riebesell. The candidate was supported by a pre-doctoral grant of the Agencia Canaria de Investigación, Innovación, y Sociedad de la Información (ACIISI, TESIS2015010036). Three research stays were conducted during the thesis: at the Instituto de Investigacións Mariñas of Vigo (IIM-CSIC; Spain) under the supervision of Prof. Dr. Xosé Antón Álvarez Salgado; at the Instituto del Mar del Perú (IMARPE, Peru), and at Helmholtz-Zentrum für Ozeanforschung Kiel (GEOMAR, Germany), both under

the supervision of Prof. Dr. Ulf Riebesell. The research stays were granted by the ULPGC (IIM-CSIC) and the ACIISI (IMARPE and GEOMAR). Furthermore, this study has benefited from the active participation in oceanographic cruises and mesocosms experiments that resulted from the research projects SFB 754 (Prof. Dr. Ulf Riebesell), FLUXES (Prof. Dr. Javier Arístegui; CTM2015-63392-C31-R), Ocean ArtUp (Prof. Dr. Ulf Riebesell), SUMMER (Prof. Dr. Xabier Irigoien) and OceanNET's (Prof. Dr. Ulf Riebesell).

This thesis is organized as required by the PhD Thesis Regulations from the Universidad de Las Palmas de Gran Canaria (BOULPGC, Chap: III, Art. 11 and 12, October 7th, 2016): A general introduction provides the essential background information and outline the objectives and hypothesis to be examined; the three original research designed to test our hypothesis are presented afterwards following conventional research article structure; We finally synthesized our results in a general discussion, giving rise to the main conclusions and future lines of research. A summary in Spanish language is attached at the end of the dissertation.

Abstract

This thesis presents novel results on phytoplankton spatiotemporal distribution and variability at submesoscale range, and on the potential effects of climate change over primary productivity in the oligotrophic waters of the Canary region.

Phytoplankton growth mainly depends on nutrient and light availability. Highly dynamic oceanic environments are dominated by physical processes that generally alter phytoplankton dynamics by controlling the access to these resources. Mesoscale motions have been considered the most important factor modulating the distribution of biogeochemical properties at the upper levels of the ocean. Nevertheless, recent studies have highlighted the role played by smaller processes that operate below the local Rossby radius of deformation (~40 in the Canary region), referred to here as submesoscale. Due to the inherent complexity of sampling at such high-resolution levels, our knowledge about submesoscale-influenced phytoplankton distribution and variability is mostly constrained to theoretical and modeling studies. In addition, little is known about the fate of meso-submesoscale impacts on phytoplankton communities under climate change stressors. Ocean warming leads to enhanced stratification in the oligotrophic ocean but also to the intensification of cross-shore wind gradients and thus of the eddy kinetic energy across eastern boundary regions of the subtropical gyres. Phytoplankton thriving in a warmer, acidified ocean could then be fertilized by enhanced meso-submesoscale activity. Consequently,

meso-submesoscale contribution to global net primary production could be increased. In order to contribute to understand how physical and biogeochemical factors, resolved at a resolution close to submesoscale could affect the spatiotemporal distribution and variability of pico- and nanoplankton, the main components of planktonic communities in the Canary Islands waters, we conducted two interdisciplinary surveys across a highly variable mesoscale field and a submesoscale front south of Gran Canaria island (Canary Island). We found that autotrophic and heterotrophic pico- and nanoplanktonic organisms presented a heterogeneous distribution in response to nutrient inputs caused by meso- and submesoscale processes. On the other hand, temporal variability, which is rarely studied, was found to be a significant source of error in phytoplankton variability. Finally, we have tested the response of three size classes (0.2-2, 2-20 and >20 μm) of subtropical phytoplankton communities in terms of primary production, chlorophyll and cell biomass, to increasing CO_2 concentrations and nutrient fertilization during an *in situ* mesocosm experiment in oligotrophic waters off Gran Canaria. Our results suggest that in a future acidified subtropical ocean, mesoscale and submesoscale features would drive nutrient pumping to the surface ocean favouring the development of diatoms and increasing new production in the global ocean.

List of Contents

List of Figure

List of tables

Chapter One

General Introduction

Principiar quiero,
principiar quiero.
A ver si principiando,
lograrte puedo.

Canary Island folklore

1.1. Background

1.1.1. The Phytoplankton

The sunlit layers of the world's oceans are dominated by a plethora of drifting, single-celled organisms, collectively called as phytoplankton. They primarily obtain energy by harvesting the sun light to convert inorganic matter into organic biomass (i.e., the photosynthesis), fueling most of the ocean food webs. It has been estimated that roughly half of the global organic carbon net production (approximately 50 Gt $C \cdot yr^{-1}$) is performed by these small organism (Falkowski, 1994; Field et al., 1998; Behrenfeld et al., 2005; McClain, 2009; Buitenhuis et al., 2013a), which conversely represent less than 1% of the total autotrophic biomass on Earth (~1 Gt C; Field et al., 1998; Le Quéré et al., 2005; Bar-On et al., 2018).

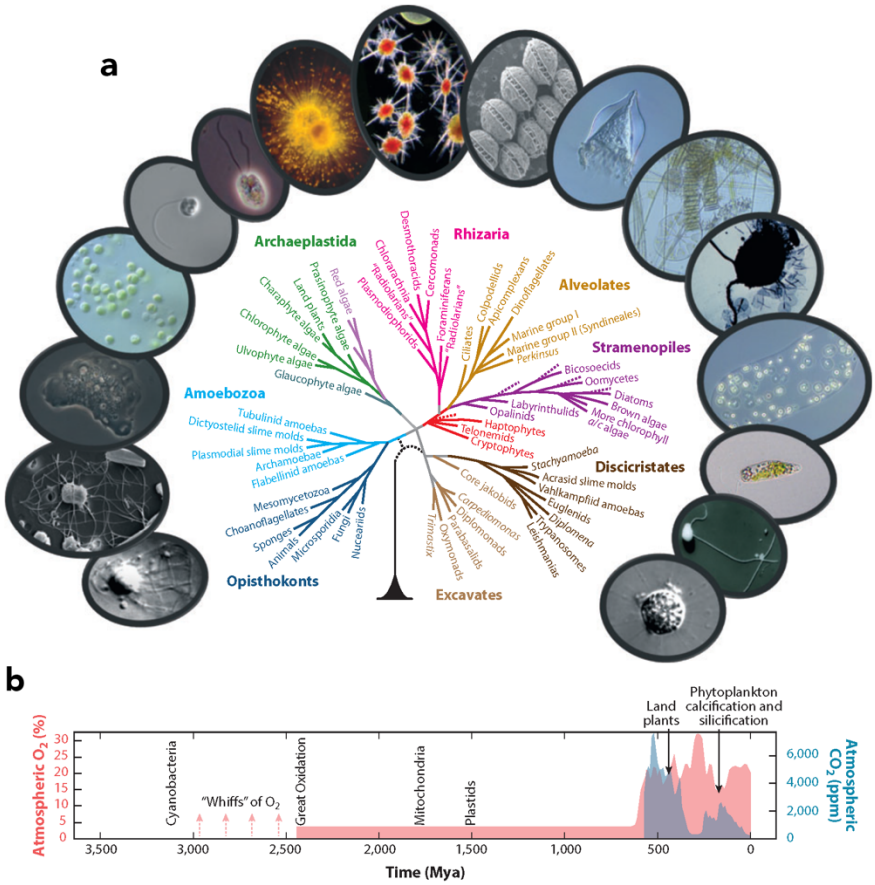

Figure 1.1. **(a)** Phylogenetic breadth among eukaryotic plankton. The pictures depict (clockwise from lower left): two micrographs of choanoflagellates, a free-living lobose amoeba, minute chlorophyte algae, the prasinophyte *Pyramimonas*, the heterotrophic cercozoan flagellate *Cryothecomonas*, the planktonic foraminiferan *Orbulina*, a mixed natural assemblage of *Acantharia*, the photosynthetic dinoflagellate *Alexandrium*, a tintinnid ciliate, a mixed diatom assemblage, the heterotrophic chrysomonad *Paraphysomonas*, the colonial haptophyte *Phaeocystis*, the euglenid flagellate *Eutreptiella*, a heterotrophic bodonid flagellate, and a heliozoan. Taken from Caron et al. (2012). **(b)** Temporal relationships between trends in atmospheric O_2 and CO_2 concentrations and major evolutionary events during the evolution of life on Earth. Taken from Karlusich et al. (2020).

First phytoplankton organisms (similar to actual marine cyanobacteria) appeared circa ~2.6 billion years ago, evolving through diverse global biogeochemical scenarios (Hedges et al., 2001; Falkowski et al., 2004;

Yoon et al., 2004; Simon et al., 2009; Cardona, 2019) into the tens of thousands of described phytoplankton species extant in the modern ocean (Fig. 1.1; Zeidner et al., 2003; Katz et al., 2004; De Vargas et al., 2015). This miscellanea of evolutionary histories implies plenty of distinguishing morphological (Chrétiennot-Dinet et al., 1993; Smetacek, 2001) and physiological traits (Beardall et al., 2009; Litchman et al., 2015; Worden et al., 2015; Stoecker et al., 2017). Such differences controls phytoplankton distribution and variability and their role in the biogeochemical cycles (Litchman et al., 2015; Worden et al., 2015; Acevedo-Trejos et al., 2018; Pierella Karlusich et al., 2020).

Body size is arguably the most important trait of phytoplankton cells as it affects its biology at every ecological level, from individual to the entire community (Brown et al., 2004; Litchman and Klausmeier, 2008; Litchman et al., 2010; Marañón, 2015). Due to the key role played by cell size in plankton ecology, it has been historically used as a gathering factor for phytoplankton communities but also for other plankton components as viruses, zooplankton or even small fishes (Fig. 1.2; Sieburth and Smetacek, 1978). Phytoplankton's cell size spectrum spans through four different orders of magnitude, from ~0.2 μm to >200 μm, being gathered in three size-dependent groups named as picoplankton, nanoplankton and microplankton (Beardall et al., 2009; Finkel et al., 2010).

The picophytoplankton comprises organisms ranging between 0.2 – 2.0 μm of cell diameter. Its small size confers them high nutrient diffusion per unit of cell volume (Raven, 1998; Marañón, 2015) and elevated light absorption per unit of chlorophyll *a* (Finkel, 2001; Finkel et al., 2004).

Owing to these fundamental biophysical traits, picophytoplankton dominates the vast nutrient-poor tropical and subtropical oligotrophic regions, contributing >50% to the total phytoplankton biomass (Agawin et al., 2000; Buitenhuis et al., 2013a) and being responsible of 25 – 50 % of the total ocean primary production (Marañón et al., 2001; Uitz et al., 2010). The picophytoplankton is mainly represented by prokaryotic cyanobacteria genera *Prochlorococcus* and *Synechococcus*, and many eukaryotic algae, grouped as picoeukaryotes (Vaulot et al., 2008).

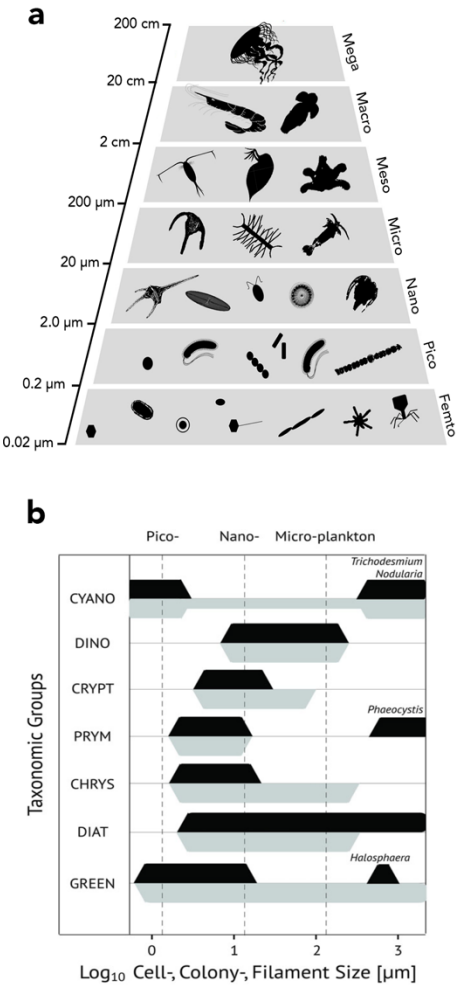

Figure 1.2. **(a)** Schematic representation of plankton size classes. Taken from Colombet et al. (2020). **(b)** Size ranges of higher phytoplankton taxa in marine (black) and freshwater (gray) phytoplankton. CYAN: cyanobacteria; DINO: dinoflagellates; CHRYS: chrysophytes; DIAT: diatoms; GREEN: green algae. Taken from Sommer et al. (2017)

Less is known about the immediately next size-group, the nanophytoplankton (2 – 20 µm ø), beside recent studies suggest that they are the major contributors to primary production at global scale (~44 %, i.e. ~20 Gt C·yr^{-1}; Uitz et al., 2010). It is mostly formed by flagellated organisms belonging to the taxa

Cryptophytes, *Prymnesiophytes* and *Chrysophytes* (Sommer et al., 2017). Traditionally, nanophytoplankton were thought to be strictly either photoautotroph or heterotroph (Caron et al., 2012; Flynn et al., 2013; Caron, 2016) but an increasing number of studies points out that they may behave as both "at the same time" (Mixotrophy; e.g., Worden et al., 2015; Stoecker et al., 2017; Edwards, 2019). Laboratory studies have reported that pigmented nanoflagellates may be responsible of up to 95 % of total bacterivory in oligotrophic waters, thus playing a pivotal role in ocean ecosystems as primary producer and primary consumers (Zubkov and Tarran, 2008; Hartmann et al., 2012; Mitra et al., 2014).

Due to its relatively large size (20 - >200 µm), the microplankton is the most studied size fraction of the phytoplankton community. Indeed, species of the two principal groups composing the microplankton, diatoms and dinoflagellates, were first described by Danish naturalist Otto Friedrich Müller in 1773-1774 (Müller, 1773, 1774). Diatoms and dinoflagellates share three distinguishing characteristics. (1) They are shielded by relatively solid covers; Diatoms build ornate silica cell walls (Frustules; Hamm et al., 2003; Armbrust, 2009), while cellulose plates (Theca or lorica) covers one part of the dinoflagellates species (Janouskovec et al., 2017). (2) Under favourable conditions, both may present exponential growth dominating the phytoplankton community in a short period of time (Blooms; Wyatt, 2014). (3) Both present bloom-forming species capable of to produce toxic or harmful substances against marine organisms and the humankind, the so-called Harmful Algal Blooms (HAB's; Moestrup et al., 2009).

Despite their similarities, diatoms and dinoflagellates perform two different roles in ocean biogeochemistry and ecology. Diatoms are ubiquitous in all marine environments wherever there are sufficient light and nutrients. They quickly build up large amounts of biomass because of their high capacity of new nutrient uptake (r-strategist) dominating community production and biomass in temperate and cold areas, and in the recently upwelled waters of Eastern Boundary Upwelling Systems (EBUS's; Uitz et al., 2010; Malviya et al., 2016; Tréguer et al., 2018) though decreasing rapidly. Dinoflagellates, conversely, are K-strategist. They grow slower compare to diatoms, but they may maintain blooms longer because of their ability of vertical migration which allows them to use nutrients from deeper water layers (Ross and Sharples, 2007; Spilling and Markager, 2008; Spilling et al., 2014).

1.1.2. Phytoplankton community structure

The growth of some phytoplankton groups may be favoured against others due to their distinct metabolic requirements (Beardall et al., 2009; Worden et al., 2015). Consequently, phytoplankton biomass is used to be unequally distributed among the size fractions. This partitioning of biomass among major functional groups, known as phytoplankton community structure, is a key trait of pelagic ecosystem (Falkowski and Oliver, 2007; Finkel et al., 2010; Marañón, 2015). It plays a crucial role in most of the processes involved in the biological carbon pump (BCP), including carbon fixation, export into the deep ocean and sequestration (Arrigo, 2005; Fuhrman, 2009; Guidi et al., 2009, 2016; Marañón, 2015), and hence, in the oceanic regulation of the global climate (Boyd, 2015; Basu and Mackey, 2018; Buesseler et al., 2020). In general terms,

phytoplankton community structure is constrained by a complex interplay of physical factors such as temperature or light availability (Fuhrman et al., 2008; Righetti et al., 2019); biotic interactions as competition and grazing (Vallina et al., 2014; Ward et al., 2014); dispersion (Fuhrman, 2009; Ward et al., 2021) and inorganic nutrients availability (Acevedo-Trejos et al., 2013; Marañón et al., 2014; Mousing et al., 2018).

In regions where the scarcity of nutrients limits primary production as in the subtropical gyres, picoplankton dominates the community structure thanks to their advantages over larger cells in nutrient uptake (Raven, 1998; Marañón, 2015; Dutkiewicz et al., 2020). The low daily biomass produced in these regions is rapidly consumed by protist microbial grazers resulting in a somewhat constant phytoplankton biomass stock along the year (Buitenhuis et al., 2013a). High phytoplankton exudation and microzooplankton excretion of dissolved organic matter fuels bacterial production which are also controlled by protist microbial grazing (Hagström et al., 1988; Anderson and Turley, 2003). The complex food web of pelagic ecosystems dominated by picoplankton is then characterized by high rates of organic matter recycling and reduced efficiency of carbon transfers toward upper trophic levels (Azam et al., 1993; Legendre and Le Fevre, 1995). In addition, due to the small size of the major components of plankton assemblage losses through sedimentation remains low (Mouw et al., 2016, Arístegui et al., in prep.).

A contrasting scenario occurs in nutrient rich waters as equatorial and coastal upwelling zones where continuous inputs of new nutrients into the euphotic layers support not only smalls cells, but also a huge amount

of large phytoplankton biomass (Alvain et al., 2008; Buitenhuis et al., 2013b). Large organisms as diatoms and dinoflagellates dominate the phytoplankton community structure in these regions thanks to their advantages in new nutrient utilization and their mechanical protection from grazers (Leblanc et al., 2012; Tréguer et al., 2018). The massive microplankton biomass production of upwelling region support 20 % of global marine fish catch while covering less than 1% of the surface ocean (Carr, 2001; Chavez and Messié, 2009; Messié and Chavez, 2015). Due to their large size and the essential role of the opal cell wall in ballasting sinking particles (Klaas and Archer, 2002) these regions also present high carbon export efficiency into the deep ocean, which is rapidly remineralized due to their relative labile nature (Guidi et al., 2016; Mouw et al., 2016). Accordingly, eutrophic regions dominated by microplankton are characterized by high transfer efficiency of carbon toward high trophic levels and into the deep ocean.

1.1.3. Physical control over phytoplankton community

The presence of minimum levels of nutrient and light are fundamental for phytoplankton growth. Unlike terrestrial ecosystems, the phytoplankton landscape is dominated by ocean dynamics. Horizontal and vertical motions occurring in the water column at different spatiotemporal scales change nutrients and light availability by dragging phytoplankton cells away from these energy sources or bringing them closer; or by changing the physical-biogeochemical conditions of the surrounding environment.

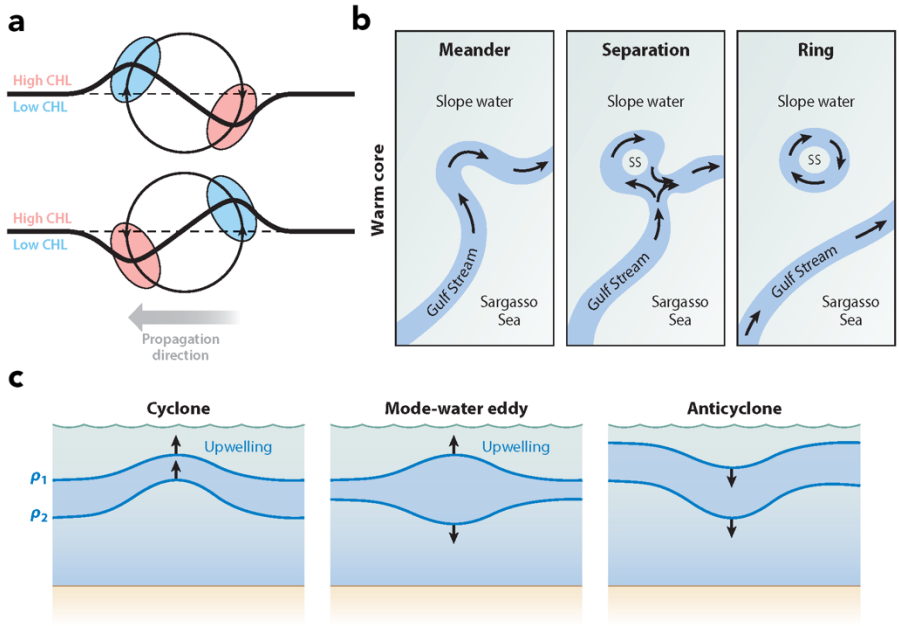

Figure 1.3. (a) Schematic diagram of eddy-driven stirring of chlorophyll (CHL) for eddies rotating clockwise (top) and counterclockwise (bottom) and propagating westward in regions where the CHL gradient is northward. An otherwise smooth contour of CHL (dashed lines) is distorted by the rotational velocity field within the eddy, as shown by the solid lines. Advection of CHL within the large-scale background CHL gradient results in the positive and negative CHL anomalies shown by the red and blue regions, respectively. (b) Processes of Gulf Stream ring formation. SS, Sargasso Sea water in warm-core rings; SW, slope water in cold-core rings. (c) Isopycnal displacements associated with three types of eddies. Two density surfaces are depicted in each case: one in the seasonal thermocline (ρ1) and one in the main thermocline (ρ2). Taken from McGuillicudy et al. (2016).

Until the mid-20th century, it was thought that gyre-scale currents and meter-scale turbulence characterized the ocean physics with little in between. The first descriptions of oceanic eddies in the 60's, however, revealed strong physical-biological-biogeochemical interactions at mesoscale (Swallow,1961;Crease, 1962, Fuglister, 1972). Mesoscale eddies are ubiquitous, long-lived (months) vortices of 100-200 km in diameter which may reach up to 2000 m depth in the water column, flowing superimposed on large-scale currents (Chelton et al., 2007,

2011; Chaigneau et al., 2009; Carpenter and Timmermans, 2012). They can be divided into two types depending on their sense of rotation. In the Northern Hemisphere, cyclonic eddies (CE) have negative vertical relative vorticity (rotate counterclockwise), while anticyclonic eddies (AE) present positive vorticity (rotate clockwise). Intrathermocline eddies (ITE) are a particular type of subsurface intensified AE which present dome-shaped isopycnals in the upper layers but still rotate anticyclonically (Barceló-Llull et al., 2017b).

The rotational flow of mesoscale eddies tends to perturb the local biological-biogeochemical conditions (McGillicuddy, 2016). Nevertheless, the core and the periphery of these structures act in very different ways. At the periphery, passive tracers as phytoplankton cells are stirred by the eddy field redistributing tracer's anomalies (Fig. 1.3.a)("Eddy Stirring"; Abraham, 1998; Martin, 2003). The eddy core, on other hand, tends to retain and transports water parcels, and hence their biotic content for weeks/months (Fig. 1.3.b) ("Eddy Trapping"; d'Ovidio et al., 2013; Gaube et al., 2014). Furthermore, during eddy formation and intensification shoaling of the isopycnals in CE and ITE cores lifts deep nutrient-rich waters into the euphotic layer, while in AE downward motions sink nutrient-poor waters from the surface (Fig. 1.3.c) ("Eddy Pumping"; Falkowski et al., 1991; Arístegui et al., 1997; Mcgillicuddy Jr et al., 1998).

The intense research carried out during the past half-century about mesoscale eddies have highlighted the key role played by these physical features on ocean biogeochemistry. Vertical fluxes of nutrients driven by mesoscale eddies dynamics have been hypothesized to be responsible to

balance nutrient budget in the subtropical gyre supporting ~40 % of phytoplankton new production (Jenkins, 1988; Falkowski, 1994; Mcgillicuddy Jr et al., 1998). In contrast to oligotrophic regions, eddy-driven processes in eutrophic waters as upwelling regions may reduce local productivity by transporting offshore or subducting phytoplankton biomass (Gruber et al., 2011; Lathuiliere et al., 2011). Eddy-driven processes may also modulate the phytoplankton community structure. Enhanced diatom and dinoflagellate biomass has been observed in ITE (McGillicuddy et al., 2003; Benitez-Nelson and McGillicuddy, 2008; Arístegui et al., in prep.) while cyanobacteria-like *Synechococcus* and *Prochlorococcus* have been observed dominating the core of AE (Sweeney et al., 2003; Baltar et al., 2009; Mouriño-Carballido, 2009). Davis and McGillicuddy (2006) reported high biomass of cyanobacteria-like *Trichodesmiun spp.* in an AE. Even though, the factors driving those changes in the community structure are less known so far.

Other mesoscale processes such as filaments and fronts have been reported to impact local biological-biogeochemical features. Filaments are ubiquitous zonal structures in EBUS, which are typically generated by the interactions of large-scale currents with coastal irregularities, i.e., capes and headlands (Haynes et al., 1993; Arístegui et al., 2009). They mediate exchange of water parcels from the near-shore upwelling region towards the open ocean and hence its biological-biogeochemical content (Álvarez-Salgado et al., 2007; Santana-Falcón et al., 2020). Mesoscale fronts, on the other hand, are continually formed by the stretching and deformation of the large or mesoscale evolving flow field. They play an important role in the vertical supply of nutrients into the euphotic layers and the subduction of organic matter (Mahadevan and Archer, 2000;

Stukel et al., 2017). Nevertheless, the processes involved in these biogeochemical fluxes operate between the mesoscale and the microscale, referred hereafter as submesoscale.

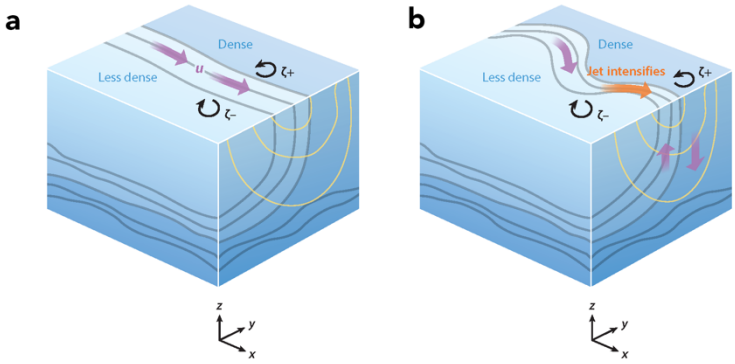

Figure 1.4. a) Schematic of an upper-ocean front, showing isopycnals (Gray lines) separating less dense water from more dense water. The front, which is within the mixed layer, overlies a more stratified region beneath. The flow in geostrophic and thermal wind balance is along the isopycnals, as indicated by u, and its isotachs (shown in yellow). Such a frontal jet generates positive (ζ+, cyclonic) and negative (ζ−, anticyclonic) vorticity on either side. In panel a, the jet is more or less linear. Panel b shows the front after the onset of baroclinic instability, which causes it to meander and lose geostrophic balance. An ageostrophic secondary circulation with up- and downwelling is generated to restore the balance. The vertical motion becomes particularly large when the magnitude of the vorticity associated with the front is of the order of the planetary vorticity f [i.e., Ro = O(1)] and submesoscale dynamics come into play. Depending on the depth and strength of the vertical motion and the depth of the underlying nutrient-replete layers, frontal upwelling can transport nutrients into the surface euphotic layer for phytoplankton production.

The development of fast, high-resolution satellite radiometers brought another physical source of biological-biogeochemical variability to light: the submesoscale frontal dynamics (Thomas et al., 2008; Ferrari, 2011). It is characterized by horizontal scales below the local Rossby radius of deformation O(1-10 km); vertical scales thinner than the main pycnocline O(100 m); and time scales of days, making them particularly difficult to sample and model. These small-scale processes arise from the squeeze of previous lateral density gradients by large and mesoscale

straining which may intensify the along-front velocity leading to the loss of the geostrophic balance. Cross-front vertical overturning circulations are then developed to restore the geostrophy by flattering the isopycnals (restratification), the so-called Ageostrophic Secondary Circulation (ASC). To do this effectively, ASC develops vertical velocities, upward on the light (warm) side and downward on the heavy (cold) side (Fig. 1.4) (Hoskins and Bretherton, 1972; Hoskins, 1982; Mahadevan and Tandon, 2006; Thomas et al., 2008; Klein and Lapeyre, 2009; McWilliams, 2016).

The response of phytoplankton to submesoscale dynamics will depend on what factor exert the main control over phytoplankton growth; light or nutrients (Mahadevan, 2016; Lévy et al., 2018). The vertical velocities associated with the upward branch of the ASC may enhance the nutrient fluxes into the euphotic zone stimulating phytoplankton growth (Mahadevan and Archer, 2000; Pidcock et al., 2010; Ramachandran et al., 2014). Likewise, deep phytoplankton organisms may be upwelled alleviating light limitation (Lévy et al., 2001; Taylor and Ferrari, 2011). On the other hand, downwelling velocities in the opposite branch of the ASC may sink surface phytoplankton communities moving them out of well sunlit and nutrient-rich upper layers (Niewiadomska et al., 2008; Lathuiliere et al., 2011).

1.1.4. Phytoplankton in the future ocean

Climate Change and its anthropogenic origin are unequivocal (IPCC, 2014; 2021). The humankind has been releasing an unprecedented amount of greenhouse gases, mostly carbon dioxide (CO_2), into the

atmosphere over the last 200 years as results of industrial processes such as fossil fuel combustion, cement production or other land uses (Fig. 1.5) (Le Quéré et al., 2018, Ciais et al., 2013). This has provoked a fast increase of the CO_2 levels in the atmosphere from the ~280 ppm of the pre-industrial era (Joos and Spahni, 2008) up to the 413.30 ppm registered by Mauna Loa Observatory (NOAA, Hawaii) at the writing of this dissertation (September, 2021; current monthly CO_2 atmospheric concentration may be consulted in https://www.co2.earth). This is the highest CO_2 atmospheric concentration in at least the last 800.000 years, and the faster growth rate in the past 55 million years (Doney and Schimel, 2007; Lüthi et al., 2008; Gingerich, 2019). Such anomalous high concentration of greenhouse gases in the atmosphere is bound to have profound impacts on ocean biogeochemistry and ecosystems (Fig. 1.6).

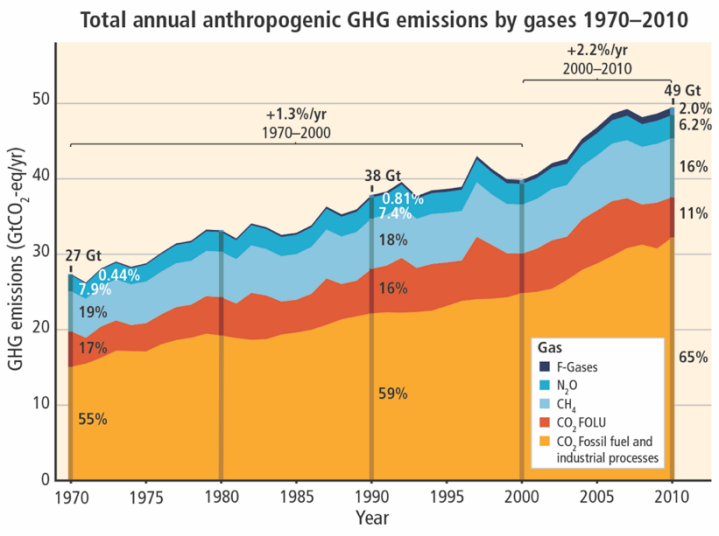

Figure 1.5. Total annual anthropogenic greenhouse gas (GHG) emissions (gigatons of CO_2-equivalent per year, Gt CO_2-eq·yr^{-1}) for the period 1970 to 2010 by gases: CO_2 from fossil fuel combustion and industrial processes; CO_2 from Forestry and Other Land Use (FOLU); methane (CH_4); nitrous oxide (N_2O); fluorinated gases covered under the Kyoto Protocol (F-gases). Taken from IPCC (2014).

Roughly the third part of the anthropogenic emission have been absorbed by world's oceans thereby buffering the increase of atmospheric CO_2 considerably (Sabine et al., 2004; Khatiwala et al., 2009, 2013). Nevertheless, there is a cost for ocean reducing atmospheric CO_2. The balance between water and atmospheric CO_2 is controlled by air-sea gas exchange, thus increase atmospheric CO_2 concentrations favours its dilution in surface seawaters. Dissolved CO_2 reacts with water to form carbonic acid (H_2CO_3), which can then dissociate by losing hydrogen ions to form bicarbonate (HCO_3^-) and carbonate (CO_3^{2-}) ions (Zebee, 2001). Both dissociations contribute to increase hydrogen ion concentrations and hence to decrease pH. Or in other words, increasing ocean partial pressure of CO_2 (pCO_2) triggers Ocean Acidification (OA; Doney et al., 2009, Gattuso, 2011). Furthermore, enhanced hydrogen ion availability reduces CO_2^{-3} concentration because of its consumption with H^+ which cause a decline in calcium carbonate saturation state (Ω), a key feature that controls ocean ability to store atmospheric CO_2 over long timescales (Feely et al., 2004). Since pre-industrial era surface ocean pH has fallen 0.1 units (Caldeira and Wickett, 2003; Lauvset et al., 2015) and calcite compensation depth has shallowed ~300 m (Sulpis et al., 2018). Ocean warming on the other hand is a direct effect of increasing Earth radiative imbalance induced by the greenhouse effect (Laffoley, 2016). Due to its higher volumetric heat capacity compared to air or land, oceans are heating up at lower rates than continental land masses and the atmosphere (Rhein et al., 2013). Nonetheless, between 1993 and 2017 the ocean surface (0-700 m) and interior (700 - 2000 m) has uptake 6.28 $\pm$ 0.48 ZJ yr^{-1} and 3.86 $\pm$ 2.09 ZJ yr^{-1}, respectively (Bindoff et al., 2019).

A great effort is being made by the research community to understand the potential net consequences of climate change on phytoplankton communities (Riebesell and Gattuso, 2015; Behrenfeld et al., 2016; Hutchins and Fu, 2017; Doney et al., 2020). Theoretically, enhanced CO_2 concentrations in seawaters should alleviate current CO_2 limitation of photosynthesis and hence boost ocean primary production (Beardall and Raven, 2004a; Reinfelder, 2011; Mackey, 2015). Ocean acidification experiments carried out in the last decades, however, throw contradictory results. Some authors report negative or non-effects of ocean acidification on primary production (Hare et al., 2007; Tanaka et al., 2013; Maugendre et al., 2017) yet increasing primary production rates have been also observed (Riebesell et al., 2007; Tortell et al., 2008; Engel et al., 2013; Eberlein et al., 2017). Ocean warming may contribute to enhance primary production as well since all metabolic processes depends on temperature (Chevin et al., 2010; Thomas et al., 2012; Pörtner et al, 2014).Nevertheless, indirect effects of ocean warming are predicted to have a more profound impact on primary productivity. Heterogeneous heating up of the water column, i.e., faster warming of the surface layer than of the ocean interior, may reinforce ocean stratification causing a decrease in nutrient fluxes from deeper layers into the euphotic zone or change light regimes, limiting primary production (Pörtner et al., 2014; Bindoff et al., 2019).

As an ocean feature, there is significant potential for climate change to produce significant effects on meso-submesoscale dynamics and thus on their effects on phytoplankton communities. Bakun (1990) hypothesized that as consequence of the intense warming of landmasses respect to ocean surface, coastal wind would increase in the next decades alongside

global warming, later supported by several studies (e.g.,Demarcq, 2009; Sydeman et al., 2014; Wang et al., 2015). Hence, since Eddy Kinetic Energy (EKE) depends on wind forcing (Yu and Metzger, 2019) it could be expected that mesoscale eddies become more common or intense in the next decades. This hypothesis has been recently supported by Martínez-Moreno et al. (2021), who reported a 2-5 % increase of eddy activity per decade in eddy-rich regions as boundary currents. Submesoscale vertical activity, however, may be reduced due to the decrease in the MLD (Richards et al., 2021). Shallower mixed layer would lead to a reduction of Mixed Layer Instability, a key processes in frontogenesis (Fox-Kemper et al., 2008). Phytoplankton thriving in a future warmed and acidified ocean could therefore be patchily fertilized by increased mesoscale and submesoscale variability inducing nutrient fluxes into the euphotic zone.

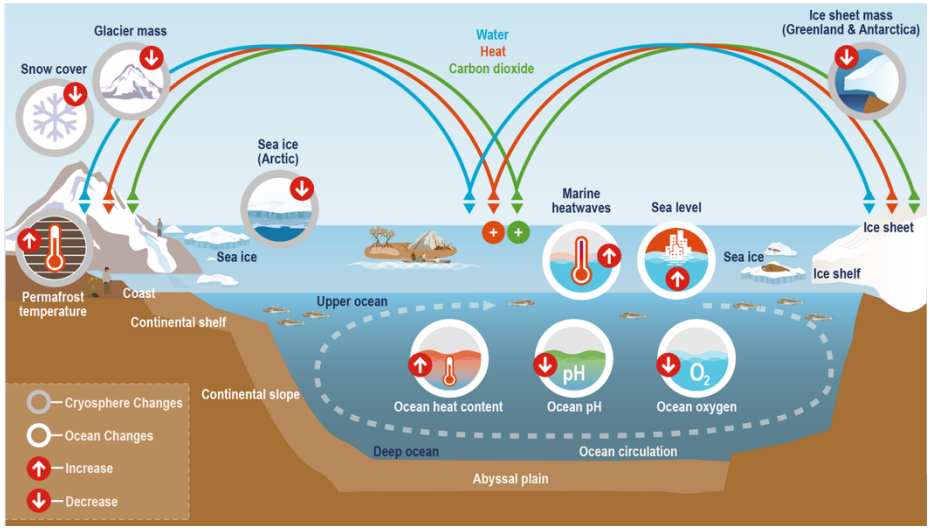

Figure 1.6. Schematic illustration of key components and changes of the ocean and cryosphere, and their linkages in the Earth system through the movement of heat, water, and carbon dioxide. Taken from Abram et al. (2019).

1.2. Thesis objectives

The overreaching objective of this thesis is to study the spatiotemporal variability of phytoplankton community structure and primary production induced by meso-submesoscale processes at submesoscale range. The phytoplankton is the cornerstone of the marine food webs, the ocean biogeochemical cycles, the ocean carbon pump, and the ocean regulation of the Earth climate. Thus, the study of the drivers involved in phytoplankton dynamics have attracted the interest of marine scientist since the beginning of the oceanography. Alongside with the development and improvement of satellite imagery, the scales of the processes dominating phytoplankton distribution have been shrinking from large-scale currents, to mesoscale processes as eddies and in the last decades to the submesoscale processes. However, despite the fact that submesoscale processes are currently considered to be the principal driver governing phytoplankton distribution and carbon fluxes, due to the inherent complexity of sampling at such high-resolution range, our knowledge about submesoscale-influenced phytoplankton spatial variability mostly constrained to the results reported by theoretical and modelling studies. Even less information is available about their temporal variability. With the aim to expand the knowledge about short-term variability of phytoplankton communities, several specific objectives were tackled to answer the following questions raised from Section 1.1:

I. *How phytoplankton organisms distribute across mesoscale eddies at submesoscale range and what drivers govern their distribution?*

II. *Does the interaction of mesoscale processes impact phytoplankton distribution?*

III. *How submesoscale frontal dynamics affect phytoplankton spatiotemporal variability?*

IV. *Which role plays temporal changes in phytoplankton variability?*

V. *Will ocean acidification impact phytoplankton productivity under nutrient fertilization?*

VI. *What are the potential biogeochemical implications?*

Question I-II are answered in **Chapter 2**, which describe the results from an oceanographic cruise that crossed a cyclonic eddy interacting with two anticyclonic eddies and an upwelling filament. The section consisted in 20 stations separated four nautical miles from each other. Physical, biogeochemical, and biological samples were taken at each station. In order to know what drivers govern submesoscale plankton distribution, distanced-based redundancy analysis were performance.

This work has resulted in the following publication:

Drivers of Plankton Distribution Across Mesoscale Eddies at Submesoscale Range, published in **Frontiers in Marine Science** as part of the research topic *"Small Scale Spatial and Temporal Patterns in Particles, Plankton and Other Organisms"*.

As suggested by modelling and theoretical studies, physical motions associated with submesoscale frontal zones may affect phytoplankton distribution and variability. **Chapter 3** presents novel results about the development and decay of a submesoscale front south of Gran Canaria. The front was sampled at spatiotemporal scales not considered in regular oceanographic cruises in order to address question IV and V.

This work has resulted in the following publication:

Shor-Term Spatiotemporal Variability in Picoplankton Induced by a Submesoscale Front South of Gran Canaria (Canary Islands), published in **Frontiers in Marine Science** as part of the research topic *"Island Dynamical Systems: Ocean and Biogeochemical Processes"*.

We are currently experiencing the effect of the climate change and will continue to do so at least to the mid-century according to all emission scenarios considered by the Intergovernmental Panel on Climate Change (IPCC, 2021). With the aim of contribing to increase the knowledge about the potential impacts of climate change over phytoplankton communities, we conducted a mesocosms experiment in the east coast of Gran Canaria. Our hypothesis was that ocean acidification under nutrient fertilization such as occurred in the cores of cyclonic eddies increases primary productivity in oligotrophic waters. The result of this experiment is compiled in **Chapter 4** which tries to solve questions VI and VII.

This work has resulted in the following publication:

High CO_2 Under Nutrient Fertilization Increases Primary Production and Biomass in Subtropical Phytoplankton Communities: A Mesocosm

Approach, published in **Frontiers in Marine Science** as part of the research topic *"Impacts of CO_2 perturbations on the Ecology and Biogeochemistry of Plankton Communities During a Simulated Upwelling Event: A mesocosms Experiment in Oligotrophic Subtropical Waters"*.

The general discussion of the thesis works, and the general conclusions extracted are presented in **Chapter 5**.

Chapter 6 corresponds to a summary of the thesis in Spanish language.

Chapter Two

Drivers of Plankton Distribution Across Mesoscale Eddies at Submesoscale Range

Frontiers in Marine Science, 21 August 2020
doi:10.3389/fmars.2020.00667

Nauzet Hernández-Hernández [1], *Javier Arístegui* [1*], *María F. Montero* [1], *Esther Velasco-Senovilla* [1], *Federico Baltar* [3], *Ángeles Marrero-Díaz* [2], *Antonio Martínez-Marrero* [1], *Ángel Rodríguez-Santana* [2]

[1] Instituto de Oceanografía y Cambio Global, IOCAG, Universidad de Las Palmas de Gran Canaria, Las Palmas, Spain

[2] Departamento de Física, Universidad de Las Palmas de Gran Canaria, Las Palmas, Spain

[3] Department of Limnology & Bio-Oceanography, University of Vienna, Vienna, Austria

2.1. Abstract

Cyclonic and anticyclonic eddies are common mesoscale features in the flow past the Canary Islands throughout the year. While drifting southwards, eddy pairs interact among them but also with upwelling filaments and eddies generated at the coastal jet of the nearby African

upwelling system. These interactions force the generation of frontal zones where ageostrophic secondary circulation (ASC) may occur. With the aim of contributing to understand how meso-submesoscale interactions modulate plankton distribution, we carried out an interdisciplinary cruise across a mesoscale eddy field. The sampled region was characterized by the presence of a cyclonic eddy interacting with two anticyclonic eddies and an upwelling filament. High resolution sampling allowed us to assess the upwelling/downwelling processes associated with eddy pumping and ASC, the injection of nutrients into the euphotic zone, and the subduction of particles related to these processes. The planktonic community, which included heterotrophic bacteria, cyanobacteria-like *Prochlorococcus* and *Synechococcus*, pico and nanoautotrophic eukaryotes and heterotrophic nanoflagellates, showed a heterogeneous distribution in response to meso-submesoscale processes. Redundancy Analysis and plankton distribution suggest that while the distribution of small organisms (picoplankton) is modulated by a combination of physical and biogeochemical drivers, the distribution of larger autotrophic and heterotrophic nanoflagellates is modulated by nutrient inputs and grazing, respectively. These observational results provide new insights in the study of the impact of mesoscale structures in the dynamics of nutrients, chlorophyll and planktonic communities, valuable to validate theoretical and modelling studies.

2.2. Introduction

Mesoscale eddies may originate nearly everywhere in the World Ocean (Chelton et al., 2007, 2011), being one of the key processes driving nutrient supply into the euphotic zone of the oceans (McGillicuddy et al.,

2003b; Klein and Lapeyre, 2009), and consequently affecting phytoplankton growth and its distribution at global scale (McGillicuddy et al., 2007; Lévy et al., 2018). Several processes, known as the "Oceanic Vertical Pump", have been proposed as responsible of eddy-related nutrient fluxes (Klein and Lapeyre, 2009). Of particular interest are two mechanisms: "eddy pumping" at the core of the eddies (McGillicuddy, 2016 and references therein), and frontogenesis, resulting from eddy-eddy interaction (Mahadevan and Tandon, 2006; Capet et al., 2008b; McWilliams, 2016).

Eddy pumping is used to define the upwelling and downwelling generated during eddy intensification. When cyclonic (anticyclonic) eddies intensify, isopycnals are uplifted (depressed) inducing to upwelling (downwelling) at the eddy center, with associated vertical velocities up to 1 $m \cdot d^{-1}$ (Gaube et al., 2014). This may lead to a surface enhancement of chlorophyll in cyclones and a depression and downward transport of chlorophyll in anticyclones (Falkowski et al., 1991; Mcgillicuddy Jr et al., 1998; Siegel et al., 2008, 2011). On the other hand, eddy-eddy interactions may lead to frontogenesis, resulting on convergent strain fields that will act destroying the thermal wind balance, establishing an ageostrophic secondary circulation (ASC) in order to restore geostrophy (Mahadevan, 2016; McWilliams, 2016). Vertical velocities originated by frontogenesis may be as high as 100 $m \cdot d^{-1}$ (Mahadevan and Tandon, 2006). Nagai et al. (2008) modelled the distribution of chlorophyll associated with frontal ASC predicting a subduction in the cold (cyclonic) side (Fielding et al., 2001; Omand and Mahadevan, 2015) and chlorophyll enhancement in the warm (anticyclonic) side (Hosegood et al., 2017).

Past studies reporting the effect of the "Oceanic Vertical Pump" over phytoplankton communities point out that the whole phytoplankton community does not respond in the same way against the same stressor (Benitez-Nelson et al., 2007; Nencioli et al., 2008; Bibby and Moore, 2011; Chenillat et al., 2015). Rodríguez et al. (2001) showed that the size structure of the phytoplankton community is controlled by the strength of vertical velocities. Their observations indicate that the relative proportion of large cells increases with the magnitude of the upward velocity. Sangrà et al. (2014) also observed in a not nutrient-limited environment that phytoplankton size spectra strongly correlate with turbulence, being the larger phytoplankton size classes more abundant in high-turbulence environments. In a study along the Kuroshio Front, Clayton et al. (2014) described the complexity of the phytoplankton community structure, shaped by a combination of the large-scale biogeographical variability of the region, mesoscale mixing of populations and finer scale modification of the light and nutrient environment. However, none of these studies addresses the variability of the phytoplankton community composition at submesoscale levels, in spite of the generally accepted view that processes at small scales govern carbon fluxes in the ocean (Lévy et al., 2001; McGillicuddy, 2016).

With the aim of contributing to understand the impact of meso-submesoscale processes over plankton communities, we conducted an interdisciplinary survey across a highly variable mesoscale field south of Gran Canaria Island (Canary Island). The main goal of the study was to understand how physical and biological factors, resolved at a resolution close to submesoscale (~1 km) could affect the distribution of pico- and nanoplankton, the main components of planktonic communities in the

Canary Islands waters (Arístegui et al., 2004). This region spans the coastal transition zone between the rich eutrophic waters of the NW Africa upwelling system and the poor oligotrophic waters of the North Atlantic Subtropical Gyre (Arístegui et al., 2009). It is almost unique in terms of the high mesoscale and submesoscale variability resulting both from the topographic perturbation of the prevailing winds and currents by the islands of the archipelago and from baroclinic instabilities developed along the offshore boundary region of the NW African coastal upwelling system. Mesoscale eddies are continuously shed downstream off the islands (Arístegui et al., 1994, 1997; Piedeleu et al., 2009; Barceló-Llull et al., 2017a), being the origin of the main pathway of long-lived eddies of the northeast subtropical Atlantic, coined as the "Canary Eddy Corridor" by Sangrà et al. (2009). On the other hand, upwelling filaments and eddies, resulting from instabilities along the coastal upwelling jet, may exchange chemical and biological properties between the shelf waters and the open ocean, contributing largely to the coastal-ocean export of organic matter (García-Muñoz et al., 2004, 2005; Pelegrí et al., 2005; Álvarez-Salgado et al., 2007; Santana-Falcón et al., 2017). Eventually, upwelling filaments may interact with island-generated eddies leading to a complex hydrographic environment that shapes the distribution and activity of planktonic communities (Barton et al., 2004; Arístegui and Montero, 2005; Sangrà et al., 2005). The almost permanent occurrence of several kind of meso-submesoscale features, as well as the interaction among them, makes the Canary region a perfect natural oceanographic laboratory to study the coupling between physical and biogeochemical processes.

2.3. Methods

2.3.1. Sampling and hydrographic data

The data for this study were collected during the cruise "RODA I" (11th August – 7th September 2006) on board of the B.I.O Hespérides. In order to map the hydrographic field to search for mesoscale features (Fig. 2.1.a), a 70 x 80 nm grid was first surveyed downstream of Gran Canaria (11th - 14th August), by means of 62 Expendable Bathythermographers (XBT's) casts down to 1000 m (Fig. 2.1.b). After locating the eddies' emplacement, a high-resolution physical biogeochemical section was sampled (14th - 16th August) crossing a cyclonic eddy interacting with two anticyclonic eddies and an upwelling filament. The section consisted in 20 stations (named 64 to 83) separated 4 nautical miles from each other (Fig. 2.1.b).

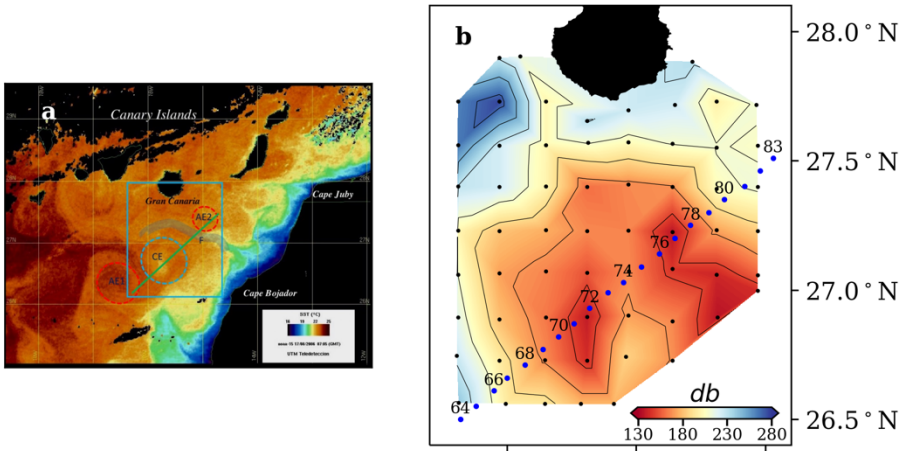

Figure 2.1. (a) Sea surface temperature (SST) image from NOAA-15 for 15 August 2006. Study area (blue box), showing mesoscale and submesoscale features sampled during the cruise: upwelling filament (F), cyclonic eddy (CE) and anticyclonic eddies (AE1 and AE2). (b) Topography of the 16 °C isotherm obtained from the XBT grid. Black dots indicate XBT stations; blue dots indicate CTD stations along the studied section. Labels are only included in the even stations.

At each station, hydrographic casts were performed down to 1000 m using a SeaBird 911 Plus CTD system mounted on a General Oceanics rosette sampler equipped with 24 Niskin bottles of 12L. A Wet Lab ECO-AFL/FL fluorescence sensor and a Sea Tech transmissometer were additionally equipped in the rosette and connected to the CTD probe. All CTD sensors were previously calibrated in the factory. Chlorophyll *a* (Chl *a*) was also inferred from the fluorescence sensor calibrated with chlorophyll reference patterns in the factory. Water samples were collected for inorganic nutrients and planktonic organisms at 5, 25, 50, 75, 100, 150 and 200 m, plus an additional sample at the depth of the deep chlorophyll maximum (DCM).

The geostrophic velocity (V_g) field, relative to 1000 dbar, was estimated from potential temperature (T_θ) and practical salinity (S). Potential temperature anomaly (ΔT_θ) was calculated using as reference values the T_θ profile at station 83 (outside eddy AE2), and then subtracted from each of the temperature profiles. The Mixed Layer Depth (MLD) was inferred by means of the de Boyer Montégut et al. (2004) approximation.

2.3.2. Inorganic nutrients

Triplicate samples for nitrate and nitrite determination were poured directly from the Niskin bottles into 15 mL polyethylene tubes (Van Waters and Rogers Co., VWR) and preserved frozen at -20 °C until their analysis. Nitrate + nitrite (NO_x) were colorimetrically measured using a Bran+Luebbe Autoanalyzer AA3 model following the Hansen and Koroleff (1999) protocol for automated seawater nutrients analysis.

Detection limit for NO_x was 0.02 μM. Instrument precision (0.008 μM for NO_x) was calculated from the standard deviation of replicate samples.

Table 2.1. Integrated (0–200 m) biomass concentrations (mg C m^2; $x10^3$) for Prochlorococcus (Pro), Synechococcus (Syn), picoeukaryotes (PEuk), nanoeukaryotes (NEuk), heterotrophic bacteria (HB), and heterotrophic nanoeukaryotes (HNF) at every station.

Station	Pro	Syn	PEuk	NEuk	HB	HNF
64	334.83	34.383	49.892	736.046	661.519	593.482
65	574.23	56.333	73.374	785.963	1358.828	604.955
66	424.76	39.652	167.522	1068.997	2525.68	786.17
67	241.89	39.862	110.502	901.381	686.436	702.452
68	176.116	43.465	142.39	918.386	591.305	740.412
69	92.503	11.328	57.641	684.336	506.492	579.007
70	98.385	11.416	72.033	1147.113	475.885	950.37
71	48.799	27.638	16.407	1146.802	636.875	963.38
72	154.056	29.138	84.533	1250.464	698.072	1050.256
73	314.795	42.327	136.298	1005.244	995.558	819.515
74	406.545	66.544	122.003	1255.191	1121.546	998.722
75	244.266	33.667	58.61	785.925	1095.068	754.185
76	309.07	40.824	88.703	1307.702	1701.209	1005.162
77	467.478	68.324	70.142	1270.363	1071.691	833.153
78	232.152	32.571	23.191	870.417	989.976	677.854
79	165.025	40.034	27.779	740.15	1147.866	652.27
80	191.887	56.646	43.179	662.869	1140.08	517.792
81	222.625	63.377	92.168	664.548	1218.129	556.902
82	381.959	53.109	67.812	966.238	1073.152	776.01
83	390.556	70.626	82.07	824.713	1103.313	641.42

2.3.3. Cell abundances and biomass conversion

Picoplankton (0.2 - 2 μm) was enumerated by flow-cytometry (Becton–Dickinson FACScalibur with 488 nm argon ion laser). Duplicate samples were collected in sterile cryovials (2 mL), immediately fixed with paraformaldehyde (2 % final concentration), refrigerated at 4 °C for half an hour, and quickly frozen in liquid nitrogen (-196 °C) until their analysis on board. For the enumeration of total heterotrophic bacterioplankton (HB; which includes also Archaea), as well as the proportion of high DNA (HNA) and low DNA (LNA) bacteria (Gasol et al., 1999), the samples were stained with SYTO-13 (Molecular Probes Inc.), using a dilution of the stock solution (1:10) to a final concentration of 2.5 μM; and their signature was identified in a plot of side scatter vs. green fluorescence. The identification and enumeration of autotrophic picoplankton – the cyanobacteria *Prochlorococcus* (Pro) and *Synechococcus* (Syn), and picoeukaryotes (PEuk) - in unstained samples was based on the analysis of multiple bivariate scatter plots of side scatter, and red and orange fluorescence. The analyses were run at low speed for the HB and at medium or high speed for the autotrophic picoplankton, until 10,000 events were acquired. A suspension of yellow-green 1 μm latex beads (10^5 and 10^6 beads mL^{-1} for autotrophs and bacterioplankton, respectively) was added as an internal standard (Polyscience Inc). The flow rate was determined volumetrically after every 10 samples run.

Autotrophic (NEuk) and heterotrophic (HNF) nanoplankton (2 - 20 μm) were analyzed by epifluorescence with an inverted microscope (ZEISS AXIOVERT 35) with 1000x resolution. Samples (100 mL) were

preserved with glutaraldehyde (1 % final concentration) and stored under cold (4 °C) and dark conditions during few days. Subsamples (45 mL) were then filtered through 0.6 µm black polycarbonate filters and stained with DAPI (4,6-diamidino-2-phenylindole; Porter and Feig, 1980) at a final concentration of 5 $\mu g \cdot L^{-1}$ (Sieracki et al., 1985). To differentiate between HNF and NEuk, the samples were analyzed under UV, green and blue light filters. The enumeration included at least 100 cells of each group per sample.

Plankton abundances were transformed to biomass following the conversion factors obtained by Montero et al. (unpublished) for coastal and oceanic waters of the Canary Islands region. To estimate picoplankton cell biovolumes, more than 60 experiments of sequential filtration (through seven polycarbonate filters from 0.2 to 3 µm) were performed, with water from the surface and the deep chlorophyll maximum around Gran Canaria. Average biovolumes from cell counts obtained by Flow Cytometry were calculated from sigmoidal fits assuming a spherical shape. For nanoplankton, 140 samples were counted and measured by epifluorescence microscopy from three size classes (2 - 6, 6 - 11 and 11 - 20 µm). Average biovolumes were derived from mathematical equations, according to the shape of the cell. The following conversion factors were applied: 18 fg $C \cdot cell^{-1}$ for HB, 43 fg $C \cdot cell^{-1}$ for Pro, 120 fg $C \cdot cell^{-1}$ for Syn, 500 fg $C \cdot cell^{-1}$ for PEuk, and 3100 fg $C \cdot cell^{-1}$ for average NEuk and HNF.

Table 2.2. Integrated (0–200 m) and averaged values for nitrate + nitrite (NO_x), and average values for across-section geostrophic velocities (V_g) and potential temperature (T_θ) at every station

Station	NO_x(μM)	V_g ($m \cdot s^{-1}$)	T_θ (°C)	MLD (m)
64	2	0.09	20.62	16.61
65	1.6	0.19	20.45	15.1
66	3.4	0.47	19.92	26.17
67	8.43	0.14	18.59	22.65
68	1.76	0.09	18.01	18.63
69	10.06	0.18	17.59	9.06
70	10.19	0.17	17.8	11.58
71	10.32	0.02	17.7	8.05
72	8.39	0.12	17.94	14.09
73	10.32	0.18	18.33	16.61
74	1.88	0.23	18.24	15.01
75	7.76	0.04	17.86	22.65
76	5.14	0.2	17.93	20.64
77	8.49	0.2	18.5	22.65
78	2.6	0.15	18.66	15.1
79	1.85	0.39	19.25	16.61
80	1.08	0.04	19.01	14.09
81	0.88	0.33	19.38	31.21
82	2.59	0.03	19.3	18.63
83	6.12	0.02	18.84	19.13

2.3.4. Data analysis

In order to elucidate the influence of the physical and biogeochemical variables (V_g, T_θ, MLD, NO_x and HNF; environmental variables hereafter) on the distribution of the planktonic groups (Pro, Syn, PEuk, NEuk, HB and HNF), a correlation analysis was performance following

Legendre & Legendre, (2012). Note that HNF is included in both environmental variables and planktonic groups since grazing by HNF may modulate other planktonic groups distribution. For statistical analysis, all plankton biomasses and nutrient concentrations were depth-integrated from 0 to 200 m at every station (Table 2.1 and 2.2). Since both T_θ and V_g are not accumulative magnitudes, they were depth-averaged instead (Table 2.2). To select the suitable correlation analysis, data gradient linearity was first tested by means of a Detrended Correspondence Analysis (DCA). Since all DCA values were below 3 (in fact, <0.4), which indicates linear gradient of the data set, a Distance Based Redundancy Analysis (db-RDA) was computed. Plankton data matrix was transformed using the Hellinger's method, while environmental variables remained untransformed. Absence of multicollinearity was inferred by means of Variance Inflation Factors (VIF's). Monte Carlo permutation significance test was conducted to obtain the p-value and the adjusted correlation coefficient (R^2_{adj}) was calculated. RDA results were graphically represented in non-scaled correlation triplots. All statistical analyses were conducted in R software using vegan package (http://www.r- project.org).

2.4. Results

2.4.1. Signature of meso-submesoscale features in the hydrographic field

Fig. 2.1.a shows a satellite image of sea surface temperature (SST) at the time of the study, where the eddy field south of the Canary Islands and several offshore filaments stretching from the NW African upwelling

region are observed. Four different mesoscale-submesoscale features were sampled during our cruise (blue box in Fig. 2.1.a): A cyclonic eddy (CE) in the centre of the box, the margins of two anticyclonic eddies (AE1, AE2) at the southwest and northeast position of the CE, respectively, and the offshore extension of an upwelling filament (F) between CE and AE2. Fig. 2.1.b represents the 16 °C isotherm topography as obtained from the XBT grid and shows the position of the high-resolution biogeochemical section (stations 64-83) crossing all the mentioned features, with the isotherms' topography in AE1 being deeper than in AE2. In Fig. 2.2, the CE is clearly identified by the doming of isotherms and isopycnals at stations 67-75, being the eddy centre located at station 70. Although the XBT grid did not cover the whole extension of the two AE, the downwelling of surface warm and high salinity water at stations 64-67 and 81-83, as well as other signatures (see below), indicate the presence of AE1 and AE2, respectively.

The representation of the potential temperature anomaly (ΔT_θ) shows that the CE introduces colder waters (about -4 °C) in the upper layers (Fig. 2.3.a). The CE radius, as calculated from the vertical anomaly section, is about 40 km, which is of the order of the climatological first baroclinic radius of deformation (R_d) for the region (Chelton et al., 1998), being thus a mesoscale structure. At the northern part of the section, the 21-23 °C isotherms define a bowl-shape structure centered at station 81 (Fig. 2.2.a), introducing positive ΔT_θ of about + 2 °C (Fig. 2.3.a). This relatively shallow warm core structure is associated with the above-mentioned submesoscale anticyclonic eddy (AE2) of 20 km radius. Between the CE and AE2, the offshore branch of an upwelling

filament is observed centered at station 77. The width of the filament is about 20 km, well below the R_d, being thus a submesoscale structure. Finally, at the southern end of the section there is a strong frontal region between station 65 and 68 resulting from the interaction of the CE with AE1, as observed in the SST field (Fig. 2.1.a), with a positive ΔT_θ of about + 3 - 4 °C in the 50 - 100 m depth range (Fig. 2.3.a). The width of this frontal structure is about 35 km, well below R_d, being also a submesoscale structure. AE1 shows signatures of an intrathermocline eddy, characterized by a biconvex shape of the isopycnals and by a homogeneous layer of subtropical mode water embedded within (36.9 psu in 64-69 stations, Fig. 2.2.b) similar to the PUMP eddy described by Barceló-Llull et al. (2017b) in the same region. Along the south-north (left-right) section (Fig. 2.3.b) the frontal region between AE1 and CE (stations 65 and 68) originates a strong jet, with south-eastward V_g of up to 1 $m \cdot s^{-1}$. The subsurface maximum of the velocity field can be associated with the biconvex shape of the isopycnals in AE1. The estimated Rossby number (R_o) for this feature is 0.48, which represents a typical value for submesoscale processes (Mahadevan, 2016). On the other hand, relatively high positive and negative V_g regions are found at the boundaries of AE2, between stations 79 - 80 and 81 - 82, respectively; both reaching values up to 0.5 $m \cdot s^{-1}$.

2.4.2. Biogeochemistry

The NO_x (nitrate + nitrite) distribution (Fig. 2.4.a) presents low values (<1 μM) in the upper 50 m at all stations, except in the core of the cyclonic eddy (stations 69 - 73), where the uplifting of colder deep waters brings NO_x concentrations of about to 2 - 4 μM to the upper 50 m. The

lowest NO_x concentrations in the upper 100 m layer are found at the CE boundaries (stations 68 and 74) and in the convergence regions of AE1 and AE2, due to downwelling of surface water.

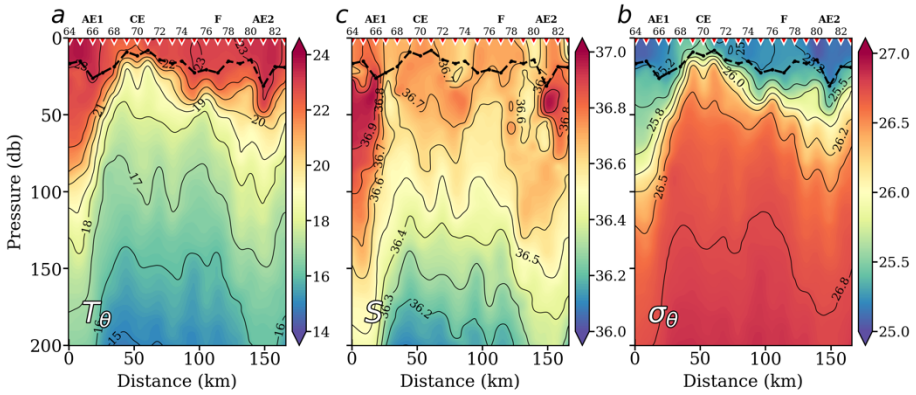

Figure 2.2. Vertical sections of potential temperature (T_θ) in °C (**a**), potential density (σ_θ) in kg·m^{-3} (**b**), and practical salinity (S) (**c**). Inverted red triangles on the top axis indicate stations position. The locations of the anticyclonic eddies (AE), the cyclonic eddy (CE), and the filament (F) are also indicated on the top axis. The bold black line shows the depth of the mixed layer (MLD).

Chlorophyll *a* (Chl *a*) (Fig. 2.4.b) presents the typical subtropical ocean distribution, with low values in surface waters and a maximum at depth (deep chlorophyll maximum, DCM). The DCM is closely related to the physical structure of the water column, being shallower and more intense in the center of the cyclonic eddy (where NO_x concentrations are higher) and deeper and weaker at stations associated with downwelling of surface water (AE1, AE2). In general, the DCM is placed below the seasonal thermocline along the section, between 50 and 80 m depth.

Transmittance (Tr), as a proxy of accumulation of organic and mineral particles (Fig. 2.4.c), is higher (less particles) in deep waters below the DCM. Lower Tr values (more particles) are found in surface waters and coinciding with the DCM (Fig. 2.4.b). The low Tr at surface waters between stations 74 and 76 is probably due to the accumulation of

mineral and organic (low chlorophyll) particles at the intense frontal region between the CE and the F.

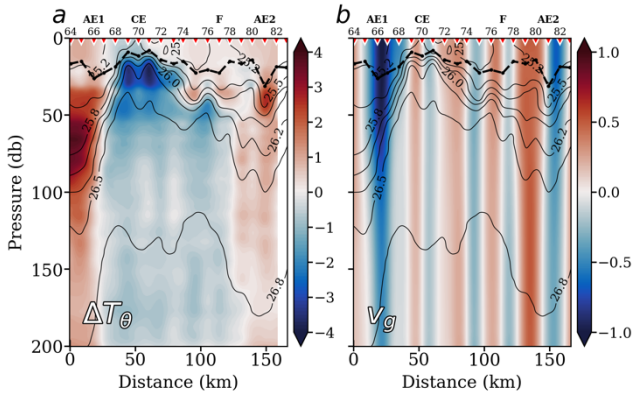

Figure 2.3. Vertical sections of potential temperature anomaly (ΔT_θ) in °C (**a**) and across section geostrophic velocity (V_g), relative to 1000 dbar, in $m \cdot s^{-1}$ (**b**), both with the isopycnals superimposed. Inverted red triangles on the top axis indicate stations position. The locations of the anticyclonic eddies (AE), the cyclonic eddy (CE), and the filament (F) are also indicated on the top axis. The bold black line shows the depth of the mixed layer (MLD). In the V_g plot, positive values indicate north-westward currents, while negative values indicate south-eastward currents.

2.4.3. Plankton community distribution

The biomass concentrations of Pro and Syn are shown in Fig. 2.5.a and b, respectively. Both cyanobacteria groups present a rather similar distribution pattern with higher concentrations between stations 64 - 67; 72 - 77 and 81 - 83. However, maximum values of Pro are found below the MLD, while Syn highest concentrations are found above it. Cyanobacteria concentrations are lowest in the core of the CE (stations 69 - 71). PEuk biomass matches the pattern of distribution of the DCM (Fig. 2.5.c). High concentrations are observed below the seasonal thermocline with highest biomass at the margins of the CE. At the core of the CE and in the F region, where the isopycnals rise and NO_x concentrations are higher, PEuk drop in biomass, being replaced by

larger autotrophic eukaryotes (NEuk; Fig. 2.5.d), which are the main contributors to the DCM in these areas (Fig. 2.4.b).

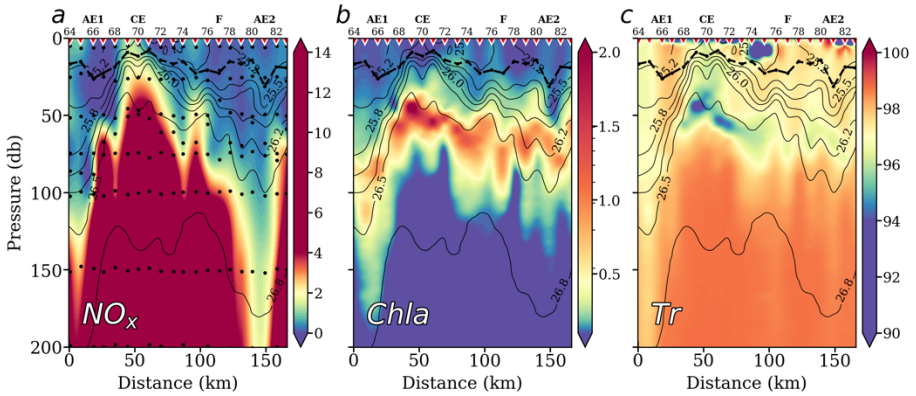

Figure 2.4. Vertical distribution of nitrate + nitrite concentrations (NO_x) in µM (**a**), chlorophyll a (Chl *a*) in $mg \cdot L^{-1}$ (**b**), and Transmittance (Tr) in % (**c**), with isopycnals superimposed. Inverted red triangles on the top axis indicate stations position. The locations of the anticyclonic eddies (AE), the cyclonic eddy (CE), and the filament (F) are also indicated on the top axis. The bold black line shows the depth of the mixed layer (MLD). Black dots indicate sampled depths.

The highest bacteria accumulations (Fig. 2.6.a) are found at the frontal regions of CE, where isopycnals depress (Figs. 2.3 and 2.4). The ratio of HNA/LNA bacteria (Fig. 2.6.b) is lower outside the CE region, and particularly low (<0.5) in the whole water column (down to 1000 m; data not shown) at the frontal region between the CE and AE1, where water transmittance is lower (Fig. 2.4.c). The lowest HB biomasses, but with highest HNA/LNA ratios, are observed at the core of the CE, where HNF concentrations are enhanced (Fig. 2.6.c), suggesting a prey-predator relationship (see below).

Distance based redundancy analysis correlates phytoplankton groups with physical and biogeochemical variables. These correlations are presented in ordination triplots (Fig. 2.7), where angles between vectors reflect the correlations (Table 2.3). Specifically, the correlation (R^2) is

equal to the cosine of the angle between vectors. This means that vector pairs describing an angle of 90° are uncorrelated since the cosine of 90° is equal to 0, while vector pairs angles of 50° (or lower) would be highly correlated as cosine of 50° is 0.65 (>0.65).

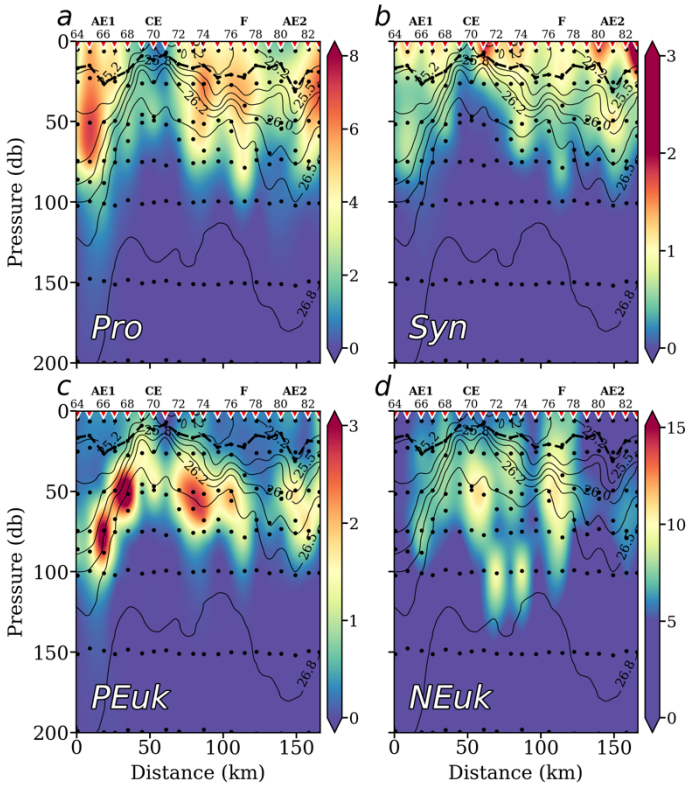

Figure 2.5. Vertical distribution of cyanobacteria-like *Prochlorococcus* (Pro) (**a**), *Synechococcus* (Syn) (**b**), autotrophic picoeukaryotes (PEuk) (**c**), and nanoeukaryotes (NEuk) (**d**) biomass concentrations in mg C·m^{-3}, with isopycnals superimposed. Inverted red triangles on the top axis indicate stations position. The locations of the anticyclonic eddies (AE), the cyclonic eddy (CE), and the filament (F) are also indicated on the top axis. The bold black line shows the depth of the mixed layer (MLD). Black dots indicate sampled depths. Note the different scales for the plots.

In our case, phytoplankton groups and the physical and biogeochemical variables present statistically significant correlation ($R^2_{adj} = 0.41$, p-value = 0.006) being a significant percentage (55.7 %) of the plankton

variability explained by these variables. Positive correlations (angles lower than 50°, i.e., >0.65) are observed between (i) NEuk, HNF and NO_x concentrations; (ii) total HB, HNA, LNA, T_θ and MLD; and (iii) PEuk, V_g and MLD. Conversely, there are negative correlations between (i) all prokaryotic groups (HB, Syn and Pro) and HNF; and (ii) nanoplankton (NEuk and HNF) with T_θ and MLD.

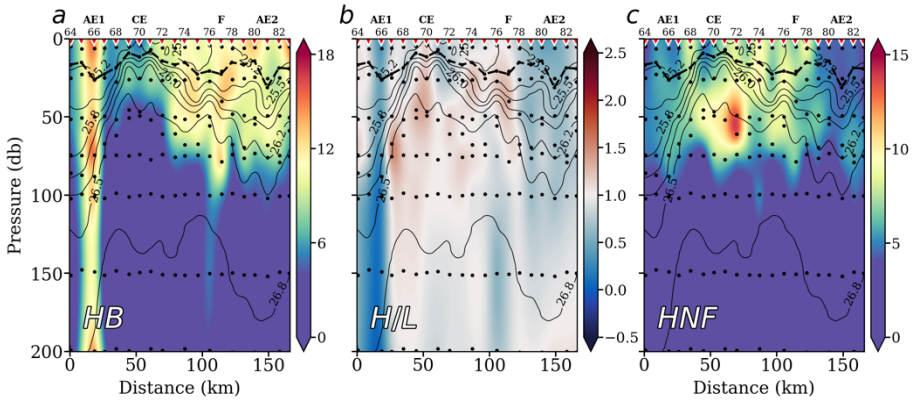

Figure 2.6. Vertical distribution of heterotrophic bacteria (HB) biomass concentration in mg C·m^{-3} (a), the ratio HNA/LNA (b), and heterotrophic nanoeukaryotes (HNF) biomass concentration in mg C·m^{-3} (c); all with isopycnals superimposed. Inverted red triangles on the top axis indicate stations position. The locations of the anticyclonic eddies (AE), the cyclonic eddy (CE), and the filament (F) are also indicated on the top axis. The bold black line shows the depth of the mixed layer (MLD). Black dots indicate sampled depths. Note that scales are different for the HB and NEuk plots.

2.5. Discussion

2.5.1. Meso-submesoscale interactions and their effects on biogeochemistry

Our results show the presence of four different meso-submesoscale structures interacting among them. The main structure is a mesoscale CE characterized by a shoaling of the isopycnals and the nitracline in its core and the consequently increase in Chl *a*. The doming of the seasonal pycnocline produces the upwelling of nutrients into the euphotic zone,

hence increasing Chl *a* in the core of the eddy at about 50 m depth. This process, referred as 'eddy pumping' (Sangrà et al., 2007; McGillicuddy, 2016), is characteristic of young eddies south of the Canary Islands in their early stages of generation (Arístegui et al., 1997; Sangrà et al., 2009).

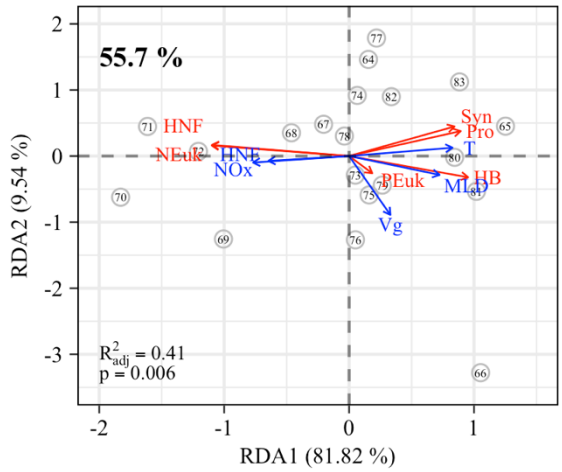

Figure 2.7. Results of the correlation plot of db-RDA, for the integrated biomasses of the different plankton groups (red arrows: Pro, *Prochlorococcus*; Syn, *Synechococcus*; PEuk, picoeukaryotes; NEuk, nanoeukaryotes; HB, heterotrophic bacteria; HNF, heterotrophic nanoflagellates) and the physical biogeochemical variables (blue arrows: T, potential temperature; MLD, mixed layer depth; V_g, geostrophic velocity; NO_x, nitrate + nitrite; HNF, heterotrophic nano flagellates). Stations are indicated by open dots. Note that distances among stations are not approximated to ecological distances. The explained variance for canonical axes RDA1 and RD2 is given on the axis. The percentage on the upper left corner refers to the explained constrained variance by all canonical axes. The adjusted correlation coefficient (R^2_{adj}) and the Monte Carlo permutation test p-value are also shown in the lower left corner.

At stations 65 - 68, the CE interacts with AE1 in its south-western boundary, resulting in a strong submesoscale frontal zone. The convergence of two water masses with different densities in a mesoscale flow field, as observed in this frontal zone, may lead to a loss of the geostrophic balance and the subsequently Ageostrophic Secondary Circulation (ASC) (Hoskins, 1982; Capet et al., 2008a; McWilliams,

2016). Despite vertical velocities were not measured, several observations give evidence of the presence of ASC in this frontal zone. The high R_o (0.48) associated with the front is an indicator of high relative vorticity, which generates losses in the geostrophic balance (Mahadevan and Tandon, 2006; Mahadevan, 2016). Moreover, Barceló-Llull et al. (2017a) obtained, in an intrathermocline eddy similar to AE1, maximum values of vertical velocity (w) of −6.4 $m \cdot day^{-1}$ (downwelling) in the western edge of the eddy and 3.4 $m \cdot day^{-1}$ (upwelling) in the eastern edge, between 160 and 185 m depth; showing a dipolar shape, with gradual changes with depth. Figure 2.4.a shows that the upward vertical advection of nitrate into the euphotic zone crosses the isopycnals at the frontal regions of CE, suggesting diapycnal mixing (Mahadevan and Archer, 2000; Spall and Richards, 2000; Lévy et al., 2001; Klein and Lapeyre, 2009). To conserve potential vorticity, the implied ASC provides downwelling on the cyclonic (dense) side of the front and upwelling on the anticyclonic (less dense) side (Nagai et al., 2008), as suggested from the nitrate field (Fig. 2.4.a). This leads to a patchy distribution of Chl *a* (Fig. 2.4.b), as well as of the PEuk and NEuk organisms responsible of the DCM along the front (Figs. 2.5.c and d).

One prominent characteristic of the AE1 - CE frontal zone is the high horizontal V_g, which reaches up to 1 $m \cdot s^{-1}$, a value five times higher than the average V_g (0.2 $m \cdot s^{-1}$) reported for the Canary Current (Sangrà, 1995; Pelegrí et al., 2005), and of the same order of magnitude of the highest ones registered in the ocean. Strong horizontal velocities (up to ~0.5 $m \cdot s^{-1}$) are also observed at the frontal regions of AE2, giving evidence of the anticyclonic nature of the eddy. These strong horizontal velocities associated with frontal zones would transport and redistribute small

particles and organisms around the eddy field south of the islands, being responsible of the patchy distribution of organic matter and plankton observed in the Canary region (Arístegui et al., 2003; Arístegui and Montero, 2005; Baltar et al., 2009).

The filament (F) crossing our sampling region (Fig. 2.1.a) stems from the coastal jet of the upwelling system. It recirculates around the cyclonic eddy, although its signature is rather weak along our grid of study. In fact, although there are clear evidences of its presence from the T_θ, S and σ_θ fields, there is no evidence of a larger transport of Chl *a*, in spite that NEuk present relatively higher biomasses down to 50 m near the core of F (station 77), coinciding with relatively higher nitrate concentrations close to the uplifted pycnocline (Figs. 2.4.a and 2.5.d). This agrees with previous studies of filaments in this region that show a sharp demise in planktonic biomass along the offshore extension of the filaments (Arístegui et al., 2004; Baltar et al., 2009).

2.5.2. Drivers of plankton distribution and community structure

Although Syn and Pro share similar patterns of distribution, with higher concentrations in AE1 and AE2 and lower in the core of CE, Syn presents maximum concentrations in shallower waters than Pro, each one dominating different niche. This has been previously attributed to differences in light harvesting between the two groups (Bouman et al., 2006; Biller et al., 2015; Mackey, 2015; Grébert et al., 2018). RDA analysis shows a strong negative correlation between the two cyanobacteria groups and NO_x, indicating that either they are outcompeted by eukaryotes when nutrient concentrations are higher, or

that picocyanobacteria rely mainly on dissolved organic matter for their growth (Berman and Bronk, 2003; Mulholland and Lee, 2009; Znachor and Nedoma, 2010; Duhamel et al., 2018). Strong vertical velocities associated with eddy pumping and ASC in CE could have contributed to displace the smaller picoplanktonic cells (Pro, Syn and HB) to the frontal regions of the eddy, where they accumulate (McGillicuddy et al., 2003b; Guidi et al., 2012; Omand and Mahadevan, 2015). In particular, HB present high biomasses in the water column (down to at least 1000 m; data not shown) at the strong frontal zone between AE1 and CE, presumably due to aggregation to sinking particles. Past studies in the Canary region have shown that HB accumulate in frontal zones between eddies, where dissolved and particulate organic matter are concentrated (Arístegui et al., 2003; Arístegui and Montero, 2005; Baltar et al., 2009). However, there is not a clear explanation of why LNA bacteria prevail over HNA bacteria in this frontal region, except that there could be preferential grazing pressure over HNA bacteria. Syn, Pro and HB also present strong negative relationship with HNF, suggesting that grazing of bacteria and cyanobacteria by HNF, commonly reported in the literature (e.g., Massana et al., 2009; Baltar et al., 2016; Yang et al., 2018; Livanou et al., 2019), could have also contributed to determine their distribution across the eddy field.

Like in other oceanic regions (Zubkov et al., 2000a, 2000b), PEuk accumulate below the thermocline, close to the nitracline, being the principal contributor to the DCM across the section. Painter et al. (2014) observed that nitrate uptake rates by PEuk are 10-fold higher in the DCM than in surface waters, contributing to higher growth rates. They argued that PEuk are well adapted to low light regimes, granting them the

benefit to thrive at deeper layers than other phytoplankton groups. RDA shows a strong inverse correlation between PEuk and the MLD, indicating that the deeper the mixed layer is (and hence the DCM) the greater the contribution of PEuk to the DCM.

There are two exceptions where PEuk dominance at the DCM is replaced by NEuk: the cores of the CE and the F, where the uplifting of isotherms brings high nutrient concentrations to the upper 50 m, with higher irradiances benefiting the growth of larger eukaryotic cells. Indeed, larger cells of micro- and nanoplankton have an advantage over smaller cells in utilizing nutrient pulses (Marañón et al., 2013; Marañón, 2015). Moreover, the greater motility of larger flagellate cells allows NEuk to withstand at some extent physical forcing, maintaining their position in the core of these features, in spite of advection. The strong positive relationship with NO_x and negative relationship with T_θ, obtained by RDA, support the notion that upwelling of cold-nutrient rich water drives NEuk distribution.

HNF display biomass maxima at the same stations than NEuk, also presenting strong positive correlations with NO_x and negative with T_θ and all prokaryotic groups (Pro, Syn and HB). It is well known that nanoflagellates prey over small picoplankton (Christaki et al., 2005; Tsai et al., 2018). However, the fact that HNF correlates inversely with nutrients could also indicate that a large part of these organisms may behave as mixotrophs (Stoecker et al., 2017 and references therein).

Collectively, the distribution of small prokaryotic picoplankton would be modulated by physical forcing, displacing the organisms away from

highly advective regions (like the core of CE and F), but also by grazing of HNF and the availability of organic matter at the frontal regions between mesoscale features. The PEuk distribution would depend mainly on the competition with NEuk on light availability and nutrients, but also on grazing by HNF. Conversely, the distribution of larger flagellated organisms, with a moderate capacity to withstand water advection, would be driven by their metabolic requirements: nutrient concentration (NEuk) and prey availability (HNF).

2.6. Conclusions

The small-scale resolution of our sampling provides new insights in the study of the impact of mesoscale and submesoscale features in the dynamics of nutrients, chlorophyll and planktonic communities. We were able to assess the upwelling/downwelling processes at submesoscale resolution, associated with eddy pumping and with the ageostrophic secondary circulation, which dominates small-scale circulation patterns at the frontal regions between adjacent structures.

We found that autotrophic and heterotrophic pico- and nanoplanktonic organisms presented a heterogeneous distribution in response to nutrient inputs caused by meso- and submesoscale processes, but also due to potential motility and grazing pressure. Redundancy Analysis suggests that the distribution of motile organisms like the nanoplanktonic NEuk and HNF are driven by nutrient supply and prey availability, respectively. Due to their mobility, these organisms may maintain their position at the core of the eddy. On the contrary, the distribution of small picoplanktonic organisms is modulated by physical (vertical and

horizontal velocities) and biogeochemical (nutrient/organic matter availability or grazing pressure) drivers, or a combination of both.

We are aware that this study is limited to a single section and therefore our conclusions may be interpreted with caution. However, our results strongly suggest that the structure of the planktonic community, and hence its contribution to primary productivity and flux of carbon to the deep ocean, will be modified along the life cycle of eddies through their interaction with other mesoscale and submesoscale features, from their generation state to their final fading, as the relative impact of physical and biogeochemical processes vary.

2.6.1. Author contributions

JA conceived and designed the cruise. JA and FB carried out sampling. NH-H, JA, MM, EV-S, ÁM-D, AM-M, and ÁR-S analyzed the data. NH-H performed the statistics. JA and NH-H wrote the manuscript with inputs from all co-authors. All authors contributed to the article and approved the submitted version.

2.6.2. Funding

This work was a contribution to projects RODA (CTM2004-06842-C03/MAR), PUMP (CTM2012-33355), FLUXES (CTM2015-69392-C3-1-R), and e-IMPACT (PID2019- 109084RB-C2), funded by the Spanish "Plan Nacional de I + D," CEI2019-01, funded by the ULPGC, and to project TRIATLAS (AMD-817578-5) financed by the European Commission (H2020). NH-H was supported by a grant

(TESIS2015010036) of the Agencia Canaria de Investigación, Innovación y Sociedad de la Información (ACIISI).

2.6.3. Acknowledgments

We thank to the officers and crew of the BIO Hespérides, Minerva Espino, and the staff of the Unit of Marine Technology (UTM) of the Spanish Research Council (CSIC) for their invaluable help at sea. This manuscript is in memoriam of Dr. Pablo Sangrà, who passed away when we were working together on a preliminary draft of the manuscript.

Chapter Three

Short-Term Spatiotemporal Variability in Picoplankton Induced by a Submesoscale Front South of Gran Canaria (Canary Islands)

Frontiers in Marine Science, 17 March 2021
doi: 10.3389/fmars.2021.592703

Nauzet Hernández-Hernández[1]*, Yeray Santana-Falcón*[1,2]*, Sheila Esreada-Allis*[3] *and Javier Arístegui*[1]

[1] Instituto de Oceanografía y Cambio Global, IOCAG, Universidad de Las Palmas de Gran Canaria ULPGC, Las Palmas, Spain

[2] CNRM, Université de Toulouse, Météo-France, CNRS, Toulouse, France

[3] Physical Oceanography Department, CICESE, Baja California, Mexico

3.1. Abstract

The distribution and variability of phytoplankton in the upper layers of the ocean are highly correlated with physical processes at different time and spatial scales. Model simulations have shown that submesoscale features play a pivotal role on plankton distribution, metabolism and carbon fluxes. However, there is a lack of observational studies that provide evidence for the complexity of short-term phytoplankton distribution and variability inferred from theoretical and modelling

approaches. In the present study, the development and decay of a submesoscale front south of Gran Canaria Island is tracked at scales not considered in regular oceanographic samplings in order to analyse the picoplankton response to short-term variability. Likewise, the contribution of each scale of variability to the total variance of the picophytoplankton community has been quantified. We observe statistically different picophytoplankton assemblages across stations closer than 5 km, and between time periods shorter than 24 h, which were related to high physical spatiotemporal variability. Our results suggest that both temporal and spatial variability may equally contribute to the total variance of picoplankton community in the mixed layer, while time is the principal contributor to total variance in the deep chlorophyll maximum.

3.2. Introduction

As higher plants, unicellular marine primary producers' growth mainly depends on nutrient and light availability. Access to these resources may be limited in the highly dynamic oceanic environments, which are dominated by physical processes that generally alter resource availability. Indeed, a large number of studies has indicated that the distribution and variability of phytoplankton and other biogeochemical parameters like nutrients and organic matter in the upper layers of the ocean are highly correlated in time and space with physical processes (Abraham, 1998; Mahadevan and Campbell, 2002; Lévy and Klein, 2004; Niewiadomska et al., 2008; Omta et al., 2008; Lehahn et al., 2017).

Mesoscale motions have commonly been assumed to be the most important factor modulating the distribution of biogeochemical properties at the upper levels of the ocean (Falkowski et al., 1991; Oschlies and Garçon, 1998; McGillicuddy et al., 2007; Johnson et al., 2010). However, recent theoretical studies (Lévy et al., 2001; Mahadevan and Campbell, 2002; Mahadevan and Tandon, 2006; Klein and Lapeyre, 2009) have highlighted the role played by smaller processes that operate below the local Rossby radius of deformation, referred to here as submesoscale. An estimated 50% of the total variance of vertical velocities in the upper layer of the ocean may be explained by submesoscale processes (Klein and Lapeyre, 2009). These small-scale motions arise from the disruption of the geostrophic balance by mesoscale straining being common in fronts and eddies edges. Vertical motions associated with ageostrophic secondary circulation (ASC) are originated at both sides of the fronts (upward on the warm side and downward on the cold side) leading to small-scale fluxes of biogeochemical properties like nutrients (Mahadevan and Tandon, 2006; Lévy et al., 2012a). Diapycnal mixing has been shown to be a dominant component of the vertical velocity in submesoscale fronts and filaments by destroying the thermal wind and driving intense ASC in the upper layers (Estrada-Allis et al., 2019). Thus, intensification of diapycnal mixing may enhance vertical transport of nutrients (Arcos-Pulido et al., 2014; Corredor-Acosta et al., 2020; Tsutsumi et al., 2020) as well as upwelling/downwelling of phytoplankton communities from sub-surface layers into the euphotic zone and vice versa. These physical cells act to restore the geostrophy by means of restratification in a process known as frontogenesis (Hoskins and Bretherton, 1972; Hoskins, 1982; Capet et

al., 2008a; McWilliams, 2016). The importance of submesoscale lies in that their spatiotemporal scales are similar to those in which biological process acts, i.e., from 0.1 to tens of kilometers and of the order of 0(1–10) days. Phytoplankton productivity and growth may thus be influenced by those changes in nutrient and light availabilities (Allen et al., 2005; Lévy et al., 2009; Lathuiliere et al., 2011; Taylor and Ferrari, 2011; Shulman et al., 2015; Liu and Levine, 2016; Taylor, 2016; Hosegood et al., 2017). Additionally, submesoscale motions may also induce shifts on phytoplankton community structure (D'Ovidio et al., 2010; Lévy et al., 2018) affecting food web dynamics and, ultimately, the carbon cycle (Mayot et al., 2017).

The study of the mechanisms controlling frontogenesis and the associated ASC is a relevant topic due to its potential impact, not only on the short-term modulation of nutrients, organic matter or light, and hence on phytoplankton communities (Mahadevan and Campbell, 2002; Klein and Lapeyre, 2009; Lévy et al., 2009, 2012a), but also because of its role in global ocean circulation (D'Asaro et al., 2011; Taylor and Ferrari, 2011; Lévy et al., 2012b), heat transport (Siegelman et al., 2020) or fish and marine mammal distribution (Snyder et al., 2017; Siegelman et al., 2020). However, due to the inherent complexity of sampling at such high-resolution levels, only a few studies have reported in situ data of submesoscale spatial phytoplankton distribution across a frontal region yet (Martin et al., 2005; Taylor et al., 2012; Clayton et al., 2014; Cotti-Rausch et al., 2016; Mousing et al., 2016; Hernández-Hernández et al., 2020). Therefore, our knowledge about submesoscale-influenced phytoplankton distribution and variability mostly constrained to the

information extracted from theoretical and modelling studies (Lévy et al., 2001, 2012a; Li et al., 2012; Liu and Levine, 2016; Taylor, 2016).

In this study we provide physical and biogeochemical observations on the development and decay of a submesoscale wind-shear front formed on the wake of Gran Canaria Island. Our overarching objective is to discuss how short-term front-generated physical variability affects the distribution and community structure of picophytoplankton organisms, which are major contributors to total phytoplankton biomass and primary production in the subtropical waters surrounding the Canary archipelago (Zubkov et al., 2000a, 2000b; Arístegui et al., 2009). For that aim, we first study the spatiotemporal evolution of the front and biogeochemical parameters. We then statistically examine the effect of the front over the phytoplankton distribution and community structure via Metric Multidimensional Scaling Analysis. We finally compare the variance induced by the spatial and temporal variabilities to determine which source of variability has major influence over picoplankton community variability.

3.3. Materials and methods

3.3.1. Hydrography, wind, and sampling design

Data reported in this paper were collected from 9 to 12 of May of 2011 on board R/V *Atlantic Explorer* from a section across a wind-shear convergent front (Figs. 3.1.a and b). In order to assess both spatial and temporal variability at submesoscale range (horizontal scale of O (1-10 km), vertical scale of O (100 m) and temporal scale of O (1 day)), a section consisting in 6-7 oceanographic stations (Figs. 3.1.a and b),

separated ~4 km (25 km in total), was entirely sampled every 24 h, during a 96 h period. Unfortunately, intense wind speed (Fig. 3.1.c) did not allow the sampling of the section at 48 h (May 11th). At each station, conductivity-temperature-depth (CTD) casts were made from surface to 300 m using a SeaBird SBE25 CTD sensor additionally equipped with a Wet Lab ECO-AFL/FL Fluorometer. The CTD was mounted onto an oceanographic rosette implemented with six Niskin bottles of 12 L. Discrete water samples were collected for chlorophyll *a* (Chl *a*), nutrients and picophytoplankton abundances at six levels, from surface to 150 m, including the deep chlorophyll maximum (DCM). TEOS-10 algorithms were used to calculate all physical derived variables. Mixed layer depth (MLD) was calculated following de Boyer Montégut et al. (2004). Wind velocities and directions every 10 minutes were obtained from the Meteorological Station based on the Gando Airport, at the wind-exposed eastern coast of the Gran Canaria Island. Raw wind data was averaged every 4 hours for plotting (Fig. 3.1.c).

3.3.2. Satellite-derived data

Satellite-derived wind velocities and directions components displayed in Fig. 3.1.a and b were obtained from the scatterometer mounted on the polar-orbiting satellite MetOp-A (Meteorological Operational satellite) of the European Space Agency (ESA) and provided by Copernicus Marine Environment Monitoring Services (CMEMS). Sea surface temperature (SST) and salinity (SSS) from the CMEMS's product, Atlantic -Iberian Biscay Irish- Ocean Physics Reanalysis accessible through *https://resources.marine.copernicus.eu*, was used to track the frontal evolution during the cruise. Both data sets present daily temporal

resolution, while offering a horizontal resolution of 12.5 x 12.5 km and 8 x 8 km for wind and temperature and salinity, respectively.

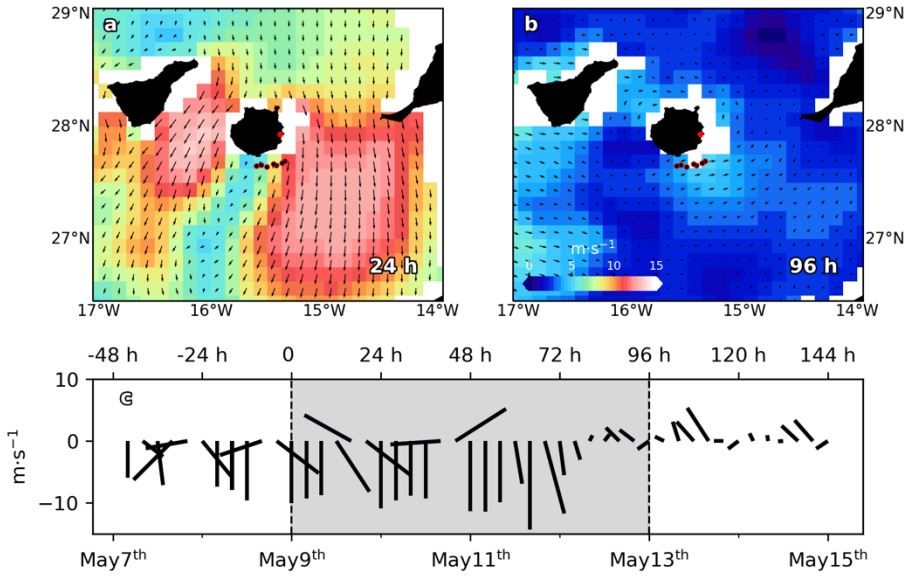

Figure 3.1. Sea surface winds (m·s^{-1}) and direction (black arrows) from scatterometer on the Meteorological Operational satellite MetOp-A (European Space Agency, esa), for **(a)** May 10th 2011 (24 h) and **(b)** May 13th 2011 (96 h). Black dots with red borders indicate stations positions. Red dot indicates Gando airport location. **(c)** Wind speed (m·s^{-1}) time series from May 7th to May 15th. Dashed vertical lines delimit sampling period. Negative (positive) values correspond with north (south) and east (west) wind directions.

3.3.3. Vertical motions

Vertical velocities associated with diapycnal mixing were calculated under the assumption of negligible viscous forces and important rotation effects. In this case, the ageostrophic Coriolis forcing can be balanced by vertical mixing, and it holds by the scaling of Garrett and Loder (1981), w_{GL} hereinafter):

$$w_{GL} \sim \frac{-1}{\rho^2} \frac{\partial}{\partial x}\left(A_v \frac{\partial b}{\partial x}\right)$$

where x is the cross-frontal direction, A_v is the vertical eddy viscosity, and b is the buoyancy in terms of density (ρ), mean density (ρ_o), and gravitational acceleration (g), such as $b = -g\ (\rho/\rho_o)$.

Though vertical velocities from w_{GL} must not be taken as total vertical velocity, it allows us to compare the magnitude of the diffusive flux and vertical advective flux, i.e., the magnitude of the vertical velocity due diapycnal mixing. Modelling studies have shown that w_{GL} resembles the shape of the total vertical velocity near the surface while differs in its magnitude (Mahadevan and Tandon, 2006; Gula et al., 2014).

3.3.4. Chlorophyll *a*

For Chl *a* analysis, 500 mL of water were filtered through 25 mm Whatman GF/F glass-fiber filters, and then stored frozen at -20 °C until their analysis in the land-based laboratory. Pigments were extracted overnight in 10 mL of 90% cold acetone. Chl *a* was measured fluorometrically, before and after acidification (by adding two drops of 37% HCl) by means of a Turner Designs bench fluorometer previously calibrated with pure Chl *a* (Sigma Co.) following Holm-Hansen et al. (1965). Chl *a* data were used to calibrate the Wet Lab ECO-AFL/FL Fluorometer mounted on the oceanographic rosette and connected to the CTD probe.

3.3.5. Inorganic nutrients

Seawater samples for nitrate + nitrite (NO_x^-) determination were collected in 15 mL polyethylene tubes (Van Waters and Rogers Co., VWR) and preserved frozen at -20 °C until their analysis in the land-

based laboratory. Nitrite was colorimetrically measured using a Bran+Luebbe Autoanalyzer AA3 model following Hansen and Koroleff (1999) protocol for automated seawater nutrient analysis.

Vertical nutrient fluxes were assessed by following Fick's law:

$$F_{NO_x^-} = -k_z \frac{\partial NO_x^-}{\partial z}$$

where k_z is the vertical eddy diffusivity. Notice that the nature of our survey does not allow us for a direct analysis of the kinetic energy dissipation rates from microstructure profilers to obtain kz (e.g., Arcos-Pulido et al., 2014; Tsutsumi et al., 2020). Notwithstanding, the increasing interest of the impact of mixing and turbulence in the biological marine systems, prompted a series of studies that compares k_z from microstructure data and fine-structure parameterizations with a reasonable degree of agreement (e.g., Inoue et al., 2007; Arcos-Pulido et al., 2014).

Here, we calculate k_z based on the parameterization of Zhang et al., (1998) validated in Inoue et al. (2007) and Arcos-Pulido et al. (2014), in which both turbulence and double diffusion mixing process are combined to obtain k_z. The approach of Zhang et al. (1998) is valid in a salt-fingering regime as dominance of Turner angles higher than 45° indicates (Fig.S2). The reader could refer to Arcos-Pulido et al. (2014), for a full derivation of the parameterization used here.

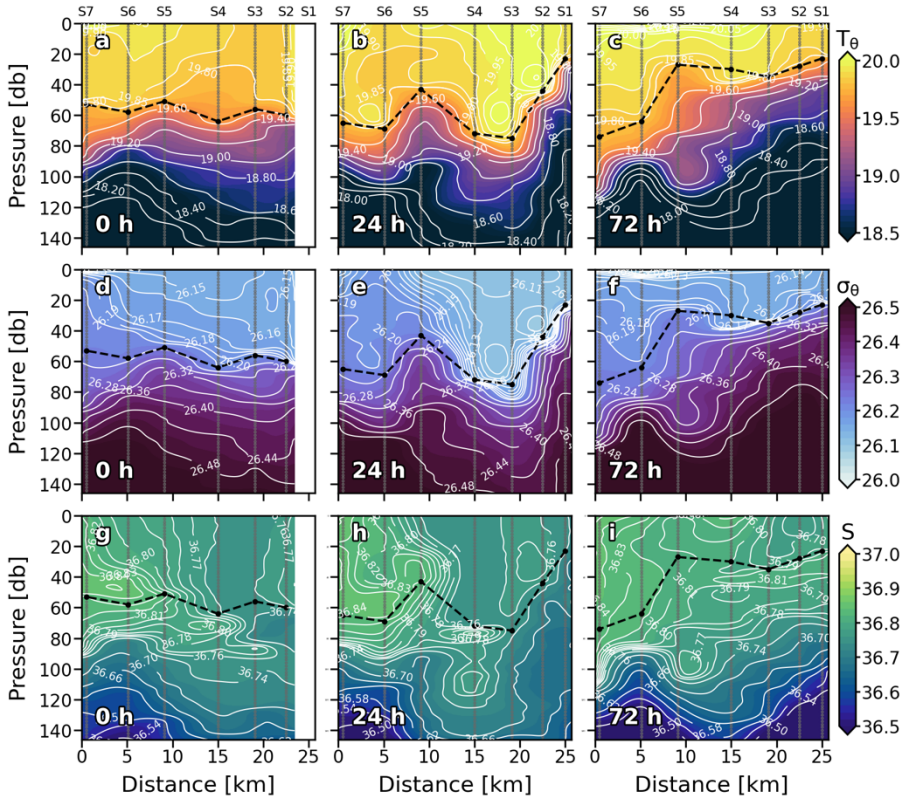

Figure 3.2. Vertical sections of potential temperature (T_θ) (°C) (**a**, **b** and **c**), potential density (σ_θ) (kg·m^{-3}) (**d**, **e** and **f**) and salinity (S) (**g**, **h**, and **i**) for every sampling day. Stations are indicated in the upper part of the plot. Isopycnal field is superimposed as solid white lines. Dashed black line indicates the mixed layer depth. Sampling depths are represented by grey dots.

3.3.6. Picoplankton abundances and biomass conversion

Cyanobacteria-like *Prochlorococcus* (Pro) and *Synechococcus* (Syn), as well as photosynthetic picoeukaryotes (Euk), were counted with a FACSCalibur (Becton and Dickinson) flow cytometer. Seawater samples (1.8 mL) were collected on 2 mL cryotubes (VWR) and fixed with 20% paraformaldehyde to 2% of final concentration. Fixed samples were stored at 4 °C for 20 minutes and then frozen and preserved in liquid nitrogen (-196 °C) until their analysis. 200 µL of sample were transferred

to a flow cytometer tube and inoculated with 4 µL of yellow-green 1 µm ø latex beads suspension, as an internal standard (Polyscience Inc.). Samples were run at 60 $\mu L \cdot min^{-1}$ for 150 seconds approximately. Groups were identified comparing red (FL3-H) fluorescence versus both orange (FL2-H) fluorescence and side scatter (SSC-H) in bivariate scatter plots.

Table 3.1. Values of nutrient gradients (g_{NOx}; $mmol \cdot m^{-3}$), vertical eddy diffusivity (K_z; $m^2 \cdot s^{-1}$) and nutrient fluxes (F_{NOx}; $mmol \cdot m^{-2} \cdot d^{-1}$) right below the MLD. All values may be found in table S1.

Day	Station	g_{NOx} ($mmol \cdot m^{-4}$)	K_z ($m^2 \cdot s^{-1}$, $x10^5$)	F_{NOx} ($mmol \cdot m^{-2} \cdot d^{-1}$)
	1			
	2			
	3	-0.117	3.85	0.013
0 h	4	-0.116	1.71	0.007
	5	-0.324	3.78	0.039
	6	-0.429	3.87	0.057
	7	-0.691	4.69	0.108
	1	-0.301	3.52	0.033
	2	-0.120	4.25	0.013
	3	-0.128	3.19	0.010
24 h	4	-0.097	1.65	0.006
	5	-0.270	3.29	0.031
	6	-0.885	3.72	0.114
	7	-0.009	3.75	0.001
	1	-0.422	4.26	0.066
	2	-0.455	4.13	0.046
	3	-0.029	3.25	0.003
72 h	4	0.014	9.11	-0.004
	5	-0.094	3.75	0.012
	6	-0.040	3.26	0.005
	7	-0.707	2.30	0.056

Carbon biomasses were estimated using empirical conversion factors provided by M.F. Montero (Montero et al., unpublished data). They carried out more than 60 experiments of sequential filtration (through seven polycarbonate filter from 0.2 to 3 μm) with water from the surface and the DCM of the coastal waters of Gran Canaria island. Picoplankton biovolumes were calculated via sigmoidal fits of cell counts obtained by Flow Cytometry. Spherical shape was assumed for picoplankton. Abundances were then multiplied by its corresponding average carbon content (43 fg C·cell^{-1} for Pro; 100 fg C·cell^{-1} for Syn and 444 fg C· cell^{-1} for Euk) obtaining average biomass data for each group. Biomass data were integrated from 0 to 150 m, from 0 to MLD and in the DCM. Integrated biomass data were then used as input for statistical computations.

3.3.7. Statistical analysis

In order to identify potential effects of submesoscale processes over picoplankton community structure, a Metric Multidimensional Scaling Analysis (MDS) (also referred to as Principal Coordinate Analysis, PCoA) was carried out for every sampling day. Ecological distance matrices of integrated picoplankton biomass were calculated by means of Bray-Curtis dissimilarity and then used as inputs for MDS analysis. The two orthogonal axes (MDS1 and MDS2) obtained from the MDS analysis were used as axes for results' scatter plots.

Stations were grouped using K-means clustering method, which aims at partitioning the data into groups such that the sum of squares from data within the assigned cluster is minimized. The value of between-cluster

sum square (BSS) divided by the total sum of squares (TSS) was used to decide the optimal number of clusters. The number of clusters that provides higher BSS/TSS ratio was chosen. A first approximation to the optimal number of clusters was also done following the Elbow method.

To quantify the contribution of each scale of variability to the total variance of picoplankton community, a Variance Component Analysis (VCA) was conducted. Previously, the biomass dataset was Winsorized to avoid extreme values. A random effect Linear Mixed Model (LMM) was then fitted to the whole water column, mixed layer (ML) and DCM. Variance components were extracted from fitted LMM. Finally, variances were expressed as the percentage of total variance. R software (http://www.r- project.org) was used to conduct all statistical analysis.

3.4. Results

3.4.1. Spatiotemporal evolution of the front

The cruise took place during a highly variable wind regime according to data provided by the Gando Airport meteorological station (Fig. 3.1.c). During the first 48 h of the experiment, trade winds (northeast) increased from ~8 $m \cdot s^{-1}$ (0 h) to more than 14 $m \cdot s^{-1}$ (48 h). 72 h on, wind shifted its direction blowing from the south, and its speed dropped down to less than 6 $m \cdot s^{-1}$. Satellite-derived wind velocities and direction shown in Figs.1.a and b support the above data. At 24 h, intense (up to ~14 $m \cdot s^{-1}$) trade winds are observed at both flanks of the island. However, in the lee of the island winds dropped down to ~6 $m \cdot s^{-1}$. Notice that the sample section crossed the wind shear zone. Unfortunately, the studied zone was not in the satellite trajectory at 72 h. Instead, wind velocity and direction

for the day after (96 h) are plotted in Fig. 3.1.b. As Fig. 3.1.c shows, 72 and 96 h wind conditions were quite similar. At 96 h, due to weak (~5 $m \cdot s^{-1}$) northward winds, the windless zone in the lee of the island disappeared and consequently the wind shear front which crossed the section vanished.

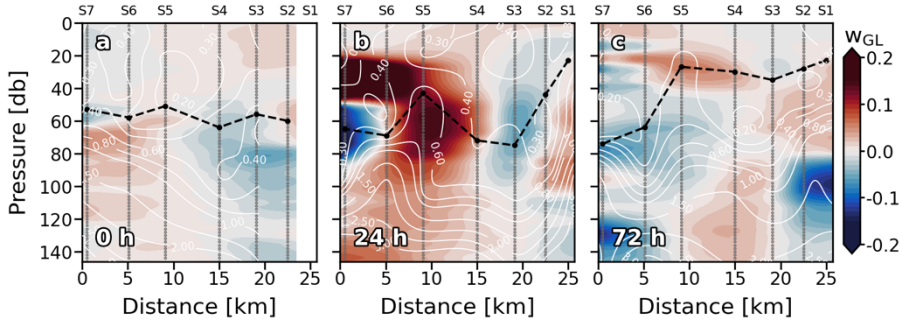

Figure 3.3. Vertical sections of vertical velocities (w_{GL}; $m \cdot day^{-1}$) for every sampling days (**a**,**b** and **c**). Stations are indicated in the upper part of the plot. Nutrient ($mmol \cdot m^{-3}$) field is superimposed as solid white lines. Sampling depths are represented by grey dots. Positive (negative) values indicate upward (downward) velocities.

Since S1 was not sampled on the first day (0), only the eastern part of the front (S2, S3 and S4) was recorded. It was characterized by doming of the isopleths inside the ML, introducing relatively colder and denser water into shallower depths (Fig. 3.2.a, d and g). Vertical isopleths at S2 (19.80 °C, 26.15 $kg \cdot m^{-3}$ and 36.77) suggest that the downward branch of the front, which would be on S1, was also affecting this station. Downward movement of the isotherms was observed at S5 and S6 (Fig. 3.2.a). Highest surface values of T_θ, σ_θ and S occurred at S7. Vertical velocities tracked pretty well with T_θ, σ_θ and S fields in the ML (Fig. 3.3.a). Negative w_{GL} (downward) were associated with the deepening of the isopleths at S5 and S6 while positive w_{GL} (upward) occurred at S2, S3 and S4 where isopleths dome. Thermo and pycnocline were situated at ~70 m remaining relatively stable along the section as well as MLD.

Wind intensification in the first 24 h (Figs. 3.1.a and c) strengthened the front that led to a reinforcement of the 19.80 °C isotherm, 26.15 kg·m^{-3} isopycnal and 36.77 isohaline, deepening from ~30 m to ~90 m and spreading from S5 and S6 to S3, S4 and S5 (Figs. 2b, 2.e and 2.h). A doming of the isopleths associated with the front affected the entire S6. Like at 0 h, w_{GL} field was consistent with the physical structure. Vertical velocities also strengthened at 24 h (Fig. 3.3.b). Downward velocities were associated with the front-related downwelling whilst upward velocities coupled with isopleths upwelling. Thermocline (pycnocline) reshaped by the downwelling produced by the front, and the upwelling produced by the doming of the isopleths, presenting a vertical zig-zag pattern along the section.

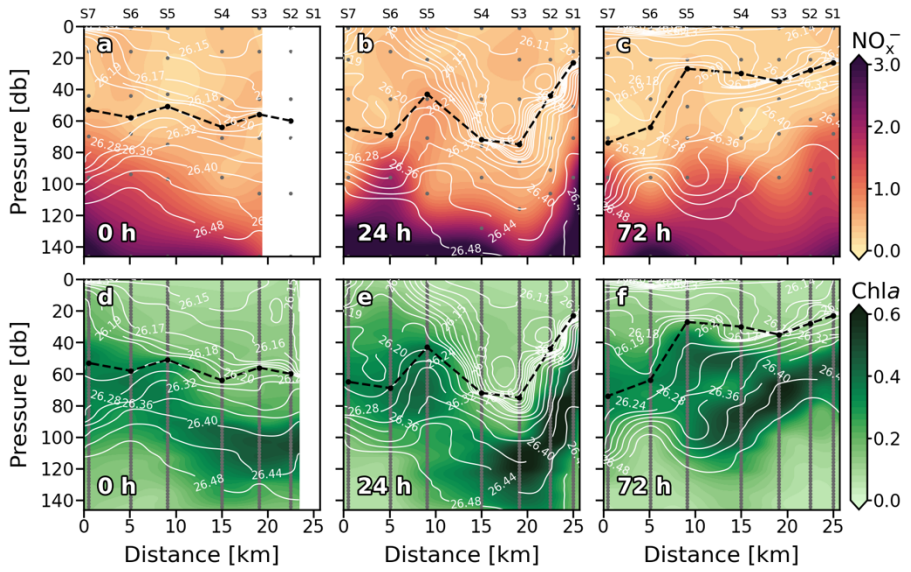

Figure 3.4. Vertical sections of nitrate + nitrite (NO_x^-) (mmol·m^{-3}) (**a**, **b** and **c**), and chlorophyll *a* (Chl *a*) (mg·m^{-3}) (**d**, **e** and **f**) for every sampling day. Stations are indicated in the upper part of the plot. Isopycnal field is superimposed as solid white lines. Dashed black line indicates the mixed layer depth. Sampling depths are represented by grey dots.

On day 4 (72 h), neither wind intensity nor direction were favourable for front development (Figs. 1.b and 1.c). Indeed, 19.80 °C isotherm, 26.15 $kg \cdot m^{-3}$ isopycnal and 36.77 isohaline horizontally crossed the whole section (Fig. 3.2.c, f and i). Nevertheless, a relative weak zig-zag pattern was still recognizable in the MLD similar to 24 h scenario (upwelling at S5 and S6, downwelling at S3 and S4; Figs. 3.2.b, e and h); probably a remnant of the thermocline deformation caused by the up- and downwelling fluxes driven by the front the day before. w_{GL} also maintained its bipolar structure between upwelling and downwelling stations above the MLD (Fig. 3.3.c). Below the isopleth doming observed at S5 and S6, counterpart bowl-shaped structure with negative w_{GL} highlights, both conforming a bipolar lentil-like shaped structure. Thermo and pycnocline were placed at ~ 40 m at S1, S2, S3 and S4, whilst at ~100 m at S6 and S7. The Shallowest thermo and pycnocline occurred at S5 associated with upwelling motions.

Though satellite-derived data should be used carefully in high-resolution cruises (as is the case) due to their significantly coarse horizontal resolution, a thermo-haline frontal zone is observed crossing through approximately the middle of the sampled section (Fig. S1) supporting our *in situ* observations. SST and SSS data also support the front temporal evolution, showing a moderate intense front at 0 and 24 h (Figs. S1.a and b) compared with 72 h (Fig. S1.d).

3.4.2. Biogeochemical features

Nutrients (NO_x^-) present the typical vertical distributions of oligotrophic systems throughout the cruise (Figs. 3.4.a, b and c). Low values (< 0.5

mmol·m^{-3}) were found at surface waters down to the thermocline, where NO_x^- increased into deeper waters (nitracline), reaching more than 3 mmol·m^{-3} at 150 m. Nevertheless, this typical nutrient distribution is not consistent along the sections. At 0 h (Fig. 3.4.a), the nutricline did not coincide with the thermocline along the section, being deeper at S3 and S4 (~120 m) compared with S5, S6 and S7 (~80 m). Deeper nutricline at S3 and S4 coincides with downward w_{GL} below the MLD while shallower nutricline at S5, S6 and S7 is associated with upward velocities (Fig. 3.3.a). Highest NO_x^- values were found at S5, S6 and S7 below the MLD and at S3-S4 and S6-S7 above it. Notwithstanding, while high NO_x^- in the first stations seen to be linked to high NO_x^- concentrations below the MLD at S5-S6, high values at S6-S7 are not connected with NO_x^- maximums below the MLD. The most intense upward (positive) F_{NOx} below the MLD (Table 3.1) were observed at S5 - S7 (0.039, 0.057 and 0.108 mmol·m^{-2}·d^{-1} respectively) as well as the nutrient gradients (g_{NOx}). Negative values of g_{NOx} indicates a favourable nutrient gradients for upward fluxes. Comparing NO_x^- and F_{NOx} with the w_{GL} field, it could be observed that the higher values of NO_x^- and F_{NOx} at S5 and S6 were associated with most intense w_{GL} in the MLD as well as that w_{GL} in the MLD at S7 were negative (downward) which may be the reason of the detached high NO_x^- patch observed in the surface waters of S6-S7.

The reshaping of the thermocline (pycnocline) by the reinforcement of the front at 24 h also reshaped the nutricline (Fig. 3.4.b), which shows the same zig-zag pattern observed in T_θ and σ_θ (Fig. 3.2.b). At S1 and S6, sloping of the isotherms introduced water with concentrations of about 2 mmol·m^{-3} ~ 40 m above the main thermocline reaching the

surface at S6 while deepening of the isopleths at S2-S4 sinks surface waters to ~ 90 m depth. The both, most intense positive and negative w_{GL} (Fig. 3.3.b) occurred associated with this isotherm sloping, respectively. The highest F_{NOx} and g_{NOx} were found at S6 and S1 (0.114 mmol·m^{-2}·d^{-1}) while lowest were found at S2-S4 and S7 (Table 3.1). In day four (72 h; Fig. 3.4.c), the doming of the isopleths below the MLD at S1-S2 and S7 introduced nutrient-richer waters from deeper layers into the bottom of the MLD (Fig. 3.4.b). Nevertheless, large amounts of NO_x^- inside the ML were observed at S1-S2 and S5 (Fig. 3.4.c). The highest F_{NOx} and g_{NOx} values right below to the MLD supports the upwelling of nutrients in those stations (Table 3.1), although w_{GL} did not completely agree with NO_x^- and F_{NOx}. Beside NO_x^- distribution suggest that a tongue of nutrient-richer waters outcrop from ~100 m to about 20 m at S5, upward vertical velocities only dominated on the MLD while downward velocities are presented below the MLD.

Similarly, the vertical distribution of Chl *a* follows the characteristic pattern of an oligotrophic system (Figs. 3.4.d, e and f), presenting low values (< 0.1 mg·m^{-3}) at surface waters, while a DCM was consistently observed over the nitracline. At 0 h (Fig. 3.4.d), the horizontal distribution of Chl *a* along the section revealed a discontinuity in the DCM between eastern stations (S1, S2, S3 and S4), where a deeper and more intense DCM occurred (0.4-0.5 mg·m^{-3}) and western stations (S5 and S6), as seen in nutricline (Fig. 3.4.a). This discontinuity became obvious when the front intensified at 24 h (Fig. 3.4.e). An intense DCM (~0.6 mg·m^{-3}) due to the front-driven sloping of the isotherms was placed at 40 m at S1 and at ~150 m at S3 and S4. Relatively high values of Chl *a* were also observed at 24 h in surface waters of S6 and S7, coinciding

with nutrient upwelling (Fig. 3.4.b). In the western stations, the DCM remained centred at 60 m depth. However, a slightly increase in Chl *a* (~0.45 $mg \cdot m^{-3}$) coincided with nutrient upwelling in S5. Weakening of the front at 72 h (Fig. 3.4.f) resulted in an overlap of the two DCM cores at S5 coinciding with the lentil-like shaped structure described in the section above (Figs. 3.2.c and d).

3.4.3. Picoplankton distribution and community structure

Maximum values of *Prochlorococcus* (Pro) biomass were generally distributed between subsurface waters (>20 m) and just above the DCM throughout the cruise (Figs. 3.5.a, b and c). At 0 h (Fig. 3.5.a), Pro biomass was widely distributed along the section presenting higher values in the MLD of S3, S4 and S5. On the second sampling day (Fig. 3.5.b), Pro biomass decreased, and the maximum values were associated with upwelling velocities at S4, S5 and S6 (Fig. 3.3.b). At 72 h (Fig. 3.5.c), the highest Pro biomass values were found at S2 at 60 m coinciding with positive (upward) w_{GL} and F_{NOx} (Fig. 3.3.c and Table 3.1). The highest Pro biomass values were consistently placed in nutrient upwelling zones.

Synechococcus (Syn) was generally widely distributed in the well-mixed waters above the thermocline (Figs. 3.5.d, e and f). Like Pro, Syn presented its highest biomass at S4 in the first sampling day (Fig. 3.5.d). At 24 h (Fig. 3.5.e) the general Syn biomass distribution changed, and high Syn biomass values were found below the thermocline, at the base of the front (~120 m). Deep, high Syn biomass values were also observed on day four (72 h; Fig. 3.5.f) associated with the downwelling occurred

below the MLD at S5. Nevertheless, maximum values at 72 h were found in surface waters of S1 and S2. The distribution of the Euk and the DCM resembled throughout the first 24 h (Figs. 3.5.g and h). At 72 h the relationship between Euk and DCM distribution was observed along S4-S7, while maximum values of Euk biomass were found below the DCM (MLD) in S1-S3 breaking with the observed general pattern (Fig. 3.5.i).

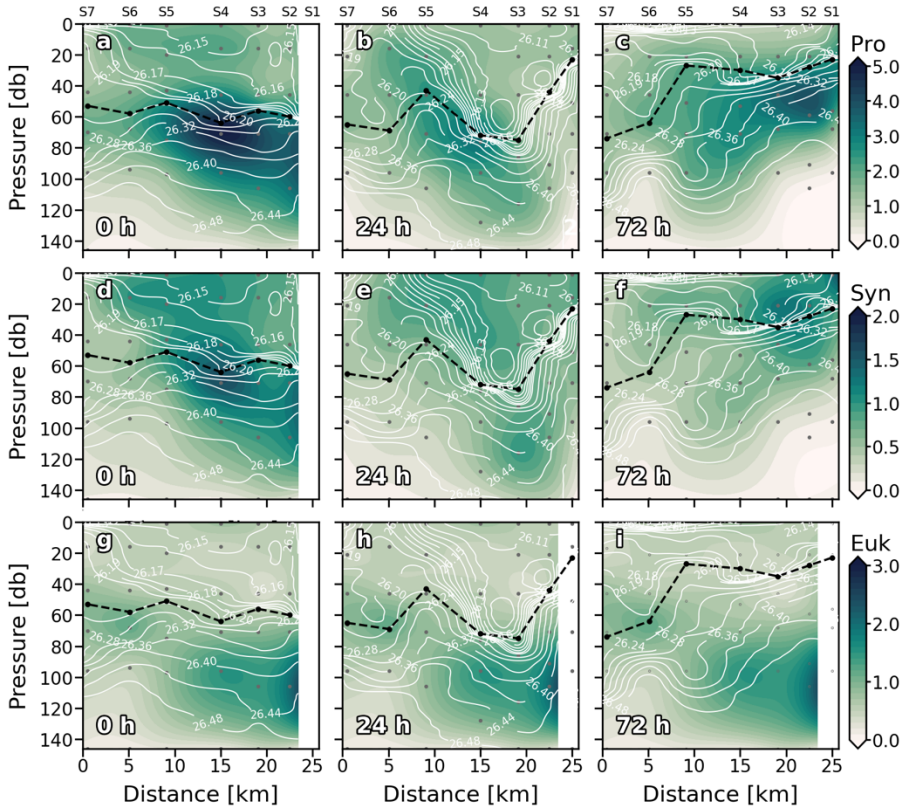

Figure 3.5. Vertical sections of phytoplankton biomass (mg C·m^{-3}) of *Prochlorococcus* sp. (Pro) (**a**, **b** and **c**); *Synechococcus* sp. (Syn) (d, e and f) and Eukaryotes (Euk) (**g**, **h** and **i**) for every sampling day. Stations are indicated in the upper part of the plot. Isopycnal field is superimposed as solid white lines. Dashed black line indicates the mixed layer depth. Sampling depths are represented by grey dots.

Water column integrated biomass values are compiled in Table. 3.2. At 0 h, all picoplankton groups present higher integrated biomass in the

eastern stations, showing cyanobacteria group differences of up to 3-fold between both ends of the section (S2 and S7). Differences of up to 2-fold between S4 and S6 separated by ~10 km in cyanobacteria's biomass can be observed. Pro is the major contributor to picoplankton community biomass along the section at 0 h (56.59 ± 2.64 %), while Syn and Euk show similar contributions to total biomass (22.68 ± 3.88 % and 20.73 ± 1.43 % respectively; Fig. 3.6.a). With the enhancement of the front on day two (24 h) the highest cyanobacteria biomasses are observed at the front-associated stations (S3 - S5) while both ends of the section show similar values (Table. 3.2). Nevertheless, differences are not as high as at 0 h. Euk presents a consistent integrated biomass along the section at 24 h. Pro still is the major contributor to the total biomass (51.32 ± 7.88 %) except in S2 where Euk and Pro show similar contribution rates (38.81 % and 38.04 % respectively; Fig. 3.6.b). At 72 h, both Syn and Euk present similar integrated values among the stations. Pro keeps showing higher values in front-affected stations (S2-S5) as well as in the major contribution percentages to total biomass (48.16 ± 2.51%; Fig. 3.6.c).

3.4.4. Front effects over the community structure

Metric Multidimensional Scaling Analysis sorts stations according to differences in picoplankton community structure. Therefore, closer stations present similar picoplankton community assemblages and *vice versa*. At 0 h, three stations groups were obtained from K-means clustering method (Fig. 3.7.a): (1) S2, S3, and S4 where front-driven up motions occurred; (2) S5 and S6, that were situated at the western boundary of the front; and (3) S7, the farthest from the front. At 24 h

(Fig. 3.7.b), three groups were also observed: (1) S1, S2, and S7, that represent the eastern and western boundaries of the front; (2) S3, S4, and S5 situated at the upwelling front; and (3) S6, where the downwelling front occurs. The vanishing of the front at 72h also lead to the vanishing of community structure heterogeneity and no significant differences were observed among station in community structure (Fig. 3.7.c). The selection of three groups at 0 h and 24 h was supported by high BSS/TSS ratio (91.7 % and 85.1 % respectively). At 72 h the BSS/TSS ratio is not displayed since there were no differences among stations.

Table 3.2. Integrated biomass (mg C·m^{-2}) between surface and 150 m depth of Eukaryotes (Euk), *Prochlorococcus* sp. (Pro) and *Synechococcus* sp. (Syn) for the three sampling days (0 h, 24 h, 48 h) and for every station.

St	0 h			24 h			72 h		
	Euk	**Pro**	**Syn**	**Euk**	**Pro**	**Syn**	**Euk**	**Pro**	**Syn**
1				73.60	107.20	62.33	55.87	168.05	63.11
2	162.19	350.75	134.90	119.36	117.14	71.48	80.69	209.60	73.02
3	112.82	324.36	121.75	90.82	213.89	111.08	85.67	219.19	85.54
4	115.44	394.43	142.35	70.79	267.73	100.08	126.79	250.77	75.48
5	88.29	245.33	91.97	87.65	235.60	74.18	87.11	229.61	64.97
6	84.31	196.21	71.29	91.91	187.65	64.70	58.86	146.51	50.88
7	78.18	146.87	49.74	69.87	106.63	37.49	71.45	133.94	39.95

3.4.5. Spatial vs. temporal variability

The contributions of every source of variability to total variance are compiled in table 3.3. Depending on the phytoplankton group, two behaviours may be observed in the entire water column. Cyanobacteria-like Pro and Syn present higher space variability (i.e., among station in

the same day), while Euk presents higher temporal variability. This pattern is not observed in the DCM, where all phytoplankton groups show higher temporal than spatial variability. Inside the mixed layer, phytoplankton groups present almost equally spatiotemporal variability. Chl *a* shows higher temporal variability in all cases.

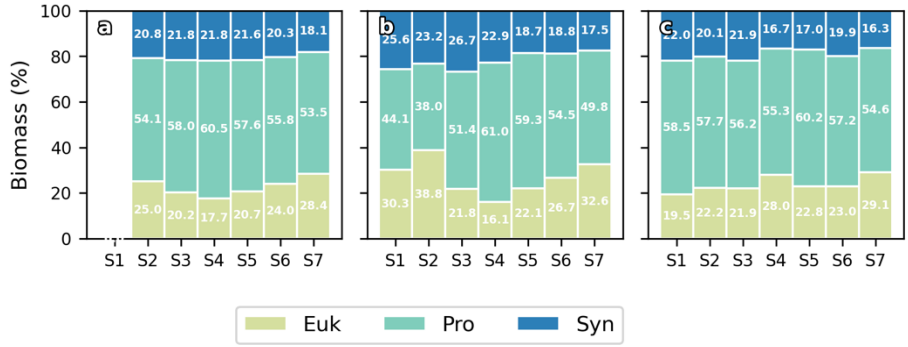

Figure 3.6. Bar plots of contribution (%) of Eukaryotes (Euk), Prochlorococcus sp. (Pro) and Synechococcus sp. (Syn) to total integrated biomass at 0 h (a), 24 h (b), and 72 h (c) for every station.

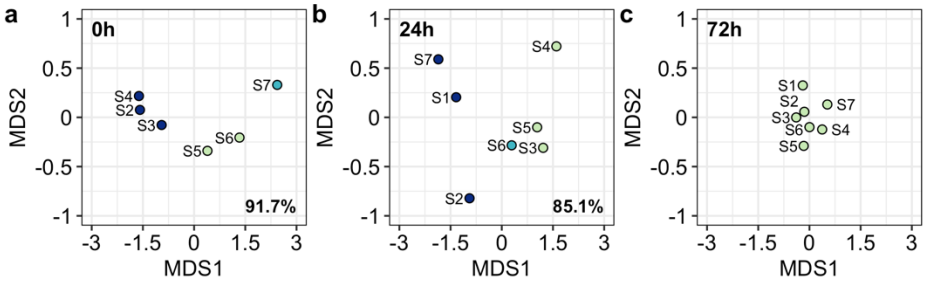

Figure 3.7. Metric Dimensional Scaling analysis (MDS) ordination plots at 0 h (a), 24 h (b) and 72 h (c). Colors refer to K-mean clustering results. Percentage refers to the BSS/TSS ratio. No BSS/TSS ratio is reported at 72 h since stations are grouped in only one cluster.

3.5. Discussion

3.5.1. Wind forcing frontogenesis

Oceanic fronts originated south of Gran Canaria in the area of eddy formation at the wind shear flanks were reported in earlier studies

describing the eddy field in the region (Arístegui et al., 1994, 1997; Barton et al., 1998). Later, Barton et al. (2000) and Basterretxea et al. (2002), in more front-focused studies, suggested a potential mechanism for their development. They observed that wind velocities dropped down up to one order of magnitude at the lee region of the island with respect to a station placed in the wind exposed region ~2 km apart. As a consequence, net westward Ekman transport in the lee region would be practically absent, favoring the convergence (divergence) of water in the eastern (western) side of the wake and its subsequent downwelling (upwelling).

Table 3.3. Percentage of total variance for each source of variability: distance among stations (Space); daily variability (Time) and the inner variability (Within) for Eukaryotes (Euk), *Prochlorococcus* sp. (Pro), *Synechococcus* sp. (Syn) and Chlorophyll *a* (Chl *a*). Statistical analysis was carried out for integrated biomass values in the whole water column (0-150 m), for the Deep Chlorophyll Maximum (DCM) and for the Mixed Layer (ML). Variances were extracted from Variance Component Analysis (VCA).

	Water column			**DCM**			**ML**		
	Space	**Time**	**Within**	**Space**	**Time**	**Within**	**Space**	**Time**	**Within**
Euk	26.54	64.08	9.38	18.36	72.23	9.41	43.25	48.22	8.53
Pro	68.56	25.32	6.12	17.04	73.62	9.34	51.54	40.58	7.88
Syn	56.63	35.96	7.41	38.69	52.47	8.84	47.78	44.02	8.20
Chl *a*	<0.01	99.99	<0.01	<0.01	99.99	<0.01	25.53	65.07	9.40

The data presented here fit the Barton et al. (2000) and Basterretxea et al. (2002)'s spatial wind field observations (Figs. 3.1.a and b) but they also indicate a positive temporal relationship between wind speed and front intensity. During the first 48 h, the increase in down-front blowing winds (Fig. 3.1.c) strengthened the front signal as seen in T_θ, σ_θ and S

plots (Figs. 3.2.a, b, d, e, g and h). Conversely, the change in wind direction at 72 h (up-front winds) caused the vanishing of the front signal and the increase in water column stratification, as suggested by the shallowest MLD (Figs. 3.2.c, f and i). This agrees with the nonlinear Ekman effect theory for frontogenesis of Thomas and Lee (2005), that proposes that winds blowing in the direction of the geostrophic flow generate an Ekman flux that tends to advect colder water from one side of the front over warmer water from the other side, enhancing convective mixing and, thus, strengthening the front. ASC-related upwelling in the warm side of the front and downwelling in the cold side would be triggered as consequence of convective mixing (Nagai et al., 2006; Pallàs-Sanz et al., 2010). By contrast, winds blowing against geostrophic flow generate the advection of warmer water over colder water favoring vertical stratification and, hence, the weakening of the front (frontolisis). This theory has been later sustained by several modelling and numerical studies (Thomas, 2005; Thomas and Lee, 2005; Thomas and Ferrari, 2008; Mahadevan et al., 2010).

The bipolar structure (upwelling/downwelling; warm/cold) described by the nonlinear Ekman effect theory agrees with the physical structure clearly shown in Fig. 3.2.b. A steep deepening of the isotherm in S2-S4 sinks water in the cold side of the front while doming of the isotherm in S5 and S6 entrained deep waters in the warm side suggesting downwelling and upwelling motions respectively. This is supported by downward and upward w_{GL} coinciding with S2-S4 and S5 and S6. At 0h, only the upwelling side of the front is observed (Figs. 3.2.a and 3.3.a), being characterized by a less intense doming of the isotherm in the warm side (S2-S4) compared to the one observed at 24 h. Notwithstanding,

positive w_{GL} were also observed at these stations, coinciding with 24 h observations.

3.5.2. Effects of frontal dynamics over nutrient distribution

Subtropical oligotrophic areas such as the Canary region are characterized by a well sun light illuminated mixed layer throughout the year, with very low inorganic nutrient concentrations (Levitus et al., 1993) due to the presence of a strong almost permanent thermocline that prevents the outcrop of deeper nutrient-rich waters into the euphotic zone (León and Braun, 1973). It has been suggested that ASC associated with submesoscale fronts may locally alleviate nutrient shortage in oligotrophic surface waters by driving vertical nutrient fluxes into the ML (Mahadevan and Tandon, 2006; Lévy et al., 2012a; Estrada-Allis et al., 2019).

In the present case, the canonical oligotrophic nutrient distribution was broken by high nutrient concentrations that outcropped trough the thermocline into the ML in S4 and S3 at 0h; S6 at 24 h and S5 at 72 h (Figs. 3.4.a, b and c). In all cases, nutrient intrusions were associated with isopleths doming driven by front-associated upwelling, where positive (upward) w_{GL} and F_{NOx} near the MLD occurred. Though small, the upward fluxes are consistent with other observations in areas of intense mesoscale and submesoscale activity (Arcos-Pulido et al., 2014; Corredor-Acosta et al., 2020). The overlapping of positive w_{GL} with F_{NOx} suggests that diapycnal mixing is acting as an important contributor to the vertical velocity (Ponte et al., 2013) and may be associated with submesoscale process (Estrada-Allis et al., 2019). In summary, upward

movements at each side of the front favors the injection of NO_x into the euphotic layer as well as downward motions deepens the nutricline impoverishing the ML, supporting earlier theoretical studies (Lévy et al., 2018 and reference therein).

3.5.3. Does frontal dynamics modulate picoplankton distribution and community structure?

The picoplankton distribution presented here (see Fig. 3.5) largely corroborates the commonly reported distribution described for each group in the region (e.g., Baltar et al., 2009). Syn was abundant in the well-mixed surface layers (Mackey et al., 2013; Grébert et al., 2018), whereas higher amounts of Pro were present in deeper layers (Bouman et al., 2006; Johnson et al., 2010; Biller et al., 2015). Euk were the main contributors to DCM laying close to the nitracline, suggesting that they require higher inorganic nutrients concentrations than prokaryotic phytoplankton for their growth (Painter et al., 2014). Nonetheless, these general distributions were eventually modified by frontal dynamics.

For instance, we observed high Syn concentrations at ~150 m depth at 24 h coinciding with the downwelling branch of the front. This distribution agrees with the subduction of phytoplankton by submesoscale front-associated downwelling as proposed by several authors (Lévy et al., 2001, 2012a, 2018). Whether the front-driven enlargement of the mixed layer at this station was responsible for the Syn distribution observed or, by contrast, Syn cells found at these depths were dragged from surface waters due to front intensification, is difficult to discern, although front dynamics seem to be behind the distribution

patterns in both cases. High Euk biomass at 72 h found below the DCM and the MLD of S1, S2 and S3, is another example of how frontal dynamics subducts phytoplankton biomass. In this case, the high Euk biomass patch appears to be a leftover from the intense DCM observed at 24 h, which has been left out the ML due to frontolisis restratification.

One of the most striking exceptions to the usually reported picoplankton distribution is observed in Pro. The fact that high Pro biomass patches consistently coincided with high nutrient concentrations (Figs. 3.3.a, b and c and Figs. 3.4.a, b and c) differs from the distribution patterns previously reported in the literature. Due to their high nutrient diffusion per unit of cell volume (Raven, 1998; Marañón, 2015) and their capacity of uptake dissolved organic matter (DOC) for growth (Berman and Bronk, 2003; Mulholland and Lee, 2009; Znachor and Nedoma, 2010; Duhamel et al., 2018; osmotrophy), Pro inorganic nutrient requirements are low and thus, they usually present higher abundances in nutrient-poor zones (Bouman et al., 2006; Johnson et al., 2006; Biller et al., 2015). Indeed, several studies have reported low Pro abundances related to eddy-driven nutrient upwelling in the region along with high Pro biomass associated with high dissolved organic matter concentrations (Baltar et al., 2009; Hernández-Hernández et al., 2020). Maximum DOC concentrations along the cruise (not shown here) also coincided with Pro biomass peaks. For these reasons, we considered that Pro and NO_x-maximums resemblance seems to be a coincidence rather than a causality, and that front-driven accumulation of DOC would be the reason of high abundances of Pro at nutrient upwelling stations.

Besides the general distribution, the data presented in Fig. 3.5 reveal high biomass patches for every picoplankton group. Several authors have reported local increases of different phytoplankton size groups across frontal zones due to the input of nutrients in a constrained zone, which usually favors the growth of large cells such as diatoms (Abraham, 1998; Rivière and Pondaven, 2006; Mahadevan et al., 2012). D'Ovidio et al. (2010) observed that phytoplankton is organized in submesoscale patches of dominant types separated by physical barriers. Our data reflect two main differences with respect to the studies mentioned above: (1) previous works observed that patches were dominated by different phytoplankton size-groups (i.e., pico, nano or microplankton; Abraham, 1998; Rivière and Pondaven, 2006; D'Ovidio et al., 2010; Mahadevan et al., 2012), while we observed that patchiness also occurs within the same size-group. This finding raises the question of at what level of organization patchiness actually works. (2) They observed high biomass patches related with local nutrient injection (Abraham, 1998; Rivière and Pondaven, 2006; D'Ovidio et al., 2010; Mahadevan et al., 2012). In our study, by contrast, only Pro high abundance spots are related to high nutrient concentrations albeit this is probably not due to a causality, as we explained above. While it is true that we only report picoplankton data, the occurrence of these non-nutrient related "hotspots" of high picoplankton biomass suggests that submesoscale dynamics modulates both the hydrographic and biogeochemical fields, favoring the local growth of some groups against others. It is known that although picoplankton groups generally co-occur in subtropical oceans, they present different nutrient requirements, light harvesting, different temperature, or physical forcing acclimation (Moore et al., 2002; Scanlan

et al., 2009; Mella-Flores et al., 2012; Flombaum et al., 2013; Luis Otero-Ferrer et al., 2018). Therefore, picoplankton groups' distribution across a submesoscale front would be expected to be affected by the front-generated physical and biogeochemical variability (Lévy et al., 2018 and references therein).

A relevant result of our study is the modulation of the picoplankton community structure by the front. Phytoplankton community assemblages were strongly structured in the MDS ordination space in accordance with the frontal structure (Fig. 3.7.). Few studies have reported the variability in phytoplankton community structures across a frontal system at submesoscale level (e.g., Taylor et al., 2012; Clayton et al., 2014; Mousing et al., 2016). In all these studies, different assemblages were observed; at each side of the front and within the front, as the result of the separation of two well-defined water masses and hence two different biomes, with two different communities. Conversely, we observed that picoplankton communities were not separated by the front but showed a mirror-like distribution with respect to the middle of the front. While observations from previously cited authors suggest that fronts work like a physical barrier for different niches, our results suggest that frontal dynamics modulates the phytoplankton community structure. However, it should be noted that while fronts reported by the authors mentioned above were permanent features that separate different water masses, we sampled an ephemeral front that is originated inside the same water mass (Lévy et al., 2018).

Due to section proximity to the coast, tidal forcing was initially considered as another potential driver for the observed

picophytoplankton variability. Sangrá et al. (2001) studied the effect of internal waves on Chl *a* in the shelf break of the lee region of Gran Canaria during a spring and a neap tide. They reported an increase in Chl *a* of up to 47 % during some pulses of the spring tide from a station situated over the shelf (100 m depth). Notwithstanding, depth integrated Chl *a* values presented little differences between samplings. Since our section was situated on the 2000 m isobath (i.e., the island slope), the cruise took place during a full neap tide, and phytoplankton biomass increases were significantly larger than those reported by Sangrá et al. (2001), we considered that the tidal forcing effects if any, they would be negligible compared to front-related effects.

3.5.4. Spatiotemporal variability

In an earlier study, Martin et al. (2005) observed higher variability in picoplankton community biomass at mesoscale ranges than in the normally-used large-scale ranges, arguing that sampling should be done at smaller scales to avoid inaccurate plankton distributions. The integrated biomass data presented here (Table 3.2) reveal that picoplankton biomass varies between 2 to 3-fold on spatial scales of ~ 2.5 km, and temporal scales of ~ 24h. This variability is comparable to the picoplankton biomass seasonality reported for the region (Zubkov et al., 2000b; Baltar et al., 2009).

In order to assess which source of variability was dominant, we compared the temporal and spatial variances observed during our study (Table 3.2). We found that picoplankton biomass variance is almost equally shared between time and space in the mixed layer, while it mostly

depends on time in the DCM, i.e., in the front reported here, picoplankton biomass temporal variability is just as important as, or even more important than spatial variability. Although the front is constrained to a marginal part of the Canary Current region, mesoscale processes and associated submesoscale motions, are ubiquitous around the global ocean (Chelton et al., 2007, 2011). Therefore, our results beg to question whether oceanographic samplings in regions of high mesoscale activity should be designed considering submesoscale spatiotemporal resolutions, in order to gain a more accurate approximation of the biogeochemical fields variability in the region of study.

3.6. Conclusions

The spatiotemporal development and decay of the convergent wind-driven submesoscale front south of Gran Canaria, as well as their effects on picoplankton community structure and distribution, is reported for the first time through in situ measurements. Like in earlier studies in the region (Barton et al., 2000; Basterretxea et al., 2002), our data shows a positive relationship between wind and front development and intensity. Upward diapycnal nutrient flux occurs near the mixed layer of the stations located on the front. This diapycnal mixing was implicated in the observed enhancement of nutrients and chlorophyll in the upper layer advected by positive vertical velocities based on the scaling of Garret and Loder (1981). Conversely, picophytoplankton biomass subduction is also reported. The present study is consistent with model outputs and past predictions, supporting that submesoscale fronts may drive nutrient fluxes into the euphotic layer and subduct picoplankton biomass below it (Mahadevan and Archer, 2000; Lévy et al., 2001, 2012a).

On the other hand, our results also provide new insights in front formation and erosion, pointing out to nonlinear Ekman effects as a potential driver of front dynamics, and their effects on picoplankton community structure. The front favours the patch formation of different picoplankton groups' dominance and modulates the picoplankton community structure. Temporal variability was found to be a significant source of error in phytoplankton variability providing evidence that, at least in regions of high hydrographic variability, plankton, as well as other biogeochemical features, must be sampled at shorter spatial and temporal resolutions than regularly done in order to obtain more accurate datasets. Although daily repeated cruises are in many cases economically unviable and time-consuming, submesoscale measurements would help to get more accurate regional and long-term interpretation of biogeochemical fluxes.

It is worth mentioning that the physical results presented in this study are constrained by the spatio-temporal scales of the survey and the lack of horizontal velocities. However, validated parameterizations and solid scaling of the vertical velocity formulations, allow us to provide a first approximation of submesoscale and diapycnal mixing impact on the biological system in the leeward side of Gran Canaria Island.

3.6.1. Author contributions

JA conceived and designed the cruise. NH-H, YS-F, and JA carried out the sampling and data analyses. SE-A contributed to the analysis of the physical data. NH-H wrote the manuscript with inputs from all authors. All authors contributed to the article and approved the submitted version.

3.6.2. Funding

This work is a contribution to the projects PUMP (CTM2012-33355), FLUXES (CTM2015-69392-C3-1-R), and e-IMPACT (PID2019-109084RB-C2) from the Spanish "Plan Nacional de ICD," co-funded with FEDER funds, and project TRIATLAS (AMD-817578-5) from the European Union's Horizon 2020 Research and Innovation Program. NH-H was supported by a grant (TESIS2015010036) of the Agencia Canaria de Investigación, Innovación y Sociedad de la Información (ACIISI).

3.6.3. Acknowledgments

We thank to the members of the Biological Oceanography group (GOB-IOCAG) for their help with the analysis of the samples, and Laura Marín for reviewing the English grammar.

Chapter Four

High CO_2 Under Nutrient Fertilization Increases Primary Production and Biomass in Subtropical Phytoplankton Communities: a Mesocosm Approach

Frontiers in Marine Science, 19 June 2018
doi: 10.3389/fmars.2018.00213

"Tampering can be dangerous. Natura can be vengeful. We should have a great deal of respect for the planet on which we live"

Carl-Gustaff Rossby, Times, 1956.

Nauzet Hernández-Hernández[1]*, Lennart T. Bach*[2]*, María F. Montero*[1]*, Jan Taucher*[2]*, Isabel Baños*[1]*, Wanchun Guan*[2,3]*, Mario Espósito*[2]*, Andrea Ludwig*[2]*, Eric P. Achterberg*[2]*, Ulf Riebesell*[2]*, Javier Arístegui*[1*]

[1] Instituto de Oceanografía y Cambio Global, IOCAG, Universidad de Las Palmas de Gran Canaria ULPGC, Las Palmas, Spain

[2] GEOMAR Helmholtz Center for Ocean Research, Kiel, Germany

[3] Department of Marine Biotechnology, School of Laboratory Medicine and Life Science, Wenzhou Medical University, Wenzhou, China

4.1. Abstract

The subtropical oceans are home to one of the largest ecosystems on Earth, contributing to nearly one third of global oceanic primary production. Ocean warming leads to enhanced stratification in the oligotrophic ocean but also intensification in cross-shore wind gradients and thus in eddy kinetic energy across eastern boundary regions of the subtropical gyres. Phytoplankton thriving in a future warmer oligotrophic subtropical ocean with enhanced CO_2 levels could therefore be patchily fertilized by increased mesoscale and submesoscale variability inducing nutrient pumping into the surface ocean. Under this premise, we have tested the response of three size classes (0.2-2, 2-20 and >20 μm) of subtropical phytoplankton communities in terms of primary production, chlorophyll and cell biomass, to increasing CO_2 concentrations and nutrient fertilization during an in situ mesocosm experiment in oligotrophic waters off of the island of Gran Canaria. We found no significant CO_2-related effect on primary production and biomass under oligotrophic conditions (phase I). In contrast, primary production, chlorophyll and biomass displayed a significant and pronounced increase under elevated CO_2 conditions in all groups after nutrient fertilization, both during the bloom (phase II) and post-bloom (phase III) conditions. Although the relative increase of primary production in picophytoplankton (250%) was 2.5 higher than in microphytoplankton (100%) after nutrient fertilization, comparing the high and low CO_2 treatments, microphytoplankton dominated in terms of biomass, contributing >57% to the total. These results contrast with similar studies conducted in temperate and cold waters, where

consistently small phytoplankton benefitted after nutrient additions at high CO_2, pointing to different CO_2–sensitivities across plankton communities and ecosystem types in the ocean.

4.2. Introduction

With a surface area of more than two hundred million square kilometers, subtropical oligotrophic waters form the largest ecosystem of the worlds' surface oceans, covering more than 60% of total ocean surface (Longhurst et al., 1995). These extensive areas are typically characterized by a deep and nutrient-poor mixed layer, which is prevented from mixing with deeper nutrient-rich waters by a strong, almost permanent thermocline. Consequently, both phytoplankton biomass and primary production are low during most of the year. Despite its low productivity per surface area (Longhurst et al., 1995), more than 30 million tons of carbon dioxide (CO_2) are photosynthetically fixed into organic compounds every day, contributing nearly one third of total oceanic primary production (Field et al., 1998; Behrenfeld et al., 2001, 2006), and thus playing a key role in the global carbon cycle (Falkowski, 1994; Falkowski et al., 2000).

Climate change is inducing physical and chemical changes in the marine environment, with profound consequences for ocean productivity (Bopp et al., 2001; Gruber et al., 2011; Doney et al., 2012; IPCC, 2014). The anthropogenic release of CO_2 through human activity since the beginning of the industrial revolution is leading to an increase of the partial pressure of this greenhouse gas in the ocean, and consequently both pH and calcium carbonate saturation states (Ω) are declining

rapidly, a process coined "ocean acidification" (Caldeira and Wickett, 2003; Sarmiento et al., 2004). Furthermore, as a consequence of increasing atmospheric greenhouse gas concentrations, the surface ocean is warming at a higher rate than the deep ocean, which may lead to a strengthening of the water column stratification (IPCC, 2014 and references therein).

Whereas increasing oceanic CO_2 levels are hypothesized to boost ocean productivity by relieving CO_2 limitation of the Ribulose-1,5-biphosphate carboxylase/oxygenase (RubisCO) enzyme (Beardall and Raven, 2004a; Reinfelder, 2011; Mackey, 2015), a more stratified ocean would lead to a decrease in nutrient supply to the euphotic layer and therefore a potential reduction of autotrophic productivity (Bopp et al., 2001; Steinacher et al., 2010). Nevertheless, it has been predicted that the heterogeneous warming of oceans and continents, may enhance upwelling-favorable winds in Eastern Boundary Current Systems (Bakun, 1990; Sydeman et al., 2014); Reyes et al. 2015). Stronger cross-shore wind gradients would lead to an intensification of the eddy kinetic energy fields across eastern boundary regions of the subtropical Gyres, favoring the upward pumping of nutrients driven by upwelling processes. Phytoplankton thriving in a future warmer and acidified oligotrophic subtropical ocean could therefore be patchily fertilized by increased mesoscale and submesoscale processes inducing nutrient pumping into the ocean surface.

Investigations of CO_2-related effects on marine productivity have experienced a remarkable surge over the last years (Riebesell and Gattuso, 2015). Theoretical studies based on chlorophyll-dependent

models predict a decrease in phytoplankton chlorophyll concentration, and consequently in primary production, in a warmer, acidified and more stratified ocean (Behrenfeld et al., 2006; Marinov et al., 2010; Steinacher et al., 2010). On the other hand, experimental studies have reported contrasting results about the potential effects of increasing CO_2 on marine productivity in natural assemblages (Table 4.1). Whereas some authors reported increased photosynthetic rates with increasing CO_2 (Hein and Sand-Jensen, 1997; Riebesell et al., 2007; Bellerby et al., 2008; Tortell et al., 2008; Egge et al., 2009; Engel et al., 2013; Eberlein et al., 2017), others have not observed significant relationships between marine productivity and ocean acidification (Tortell et al., 2002; Delille et al., 2005; Hare et al., 2007; Feng et al., 2009; Tanaka et al., 2013; Maugendre et al., 2017). Most of the experiments, however, have been carried out in nutrient-rich systems, with only a few performed in low-nutrient regions (Maugendre et al., 2017). Thus, there is a severe lack of information on how ocean acidification could affect primary production in subtropical oligotrophic regions.

This study investigates how an acidified and patchily fertilized subtropical ocean impacts marine autotrophic productivity. Therefore, we carried out a mesocosm experiment off the coast of Gran Canaria (Canary Islands) during the autumn of 2014. We studied the response of size-fractionated primary production, chlorophyll a and biomass of the phytoplankton community to enhanced CO_2 levels and nutrient fertilization to investigate which size-fraction, if any, responds more readily to these short-term perturbations.

Table 4.1. Published studies on the effect of ocean acidification on primary production in plankton communities. "Total" refers to the whole community, excluding the dissolved fraction (PP_{DOC}) in ^{14}C-based experiments. SF: size fractionated in the particulate organic fraction. NS = Not significant; + = Enhanced; * = Positive effect only in the size-fraction <1 µm.

Location	Experiment	method	PP_{POC}	PP_{DOC}	SF	Reference
Atlantic Ocean	Culture	^{14}C	+			Hein & Sand-Jensen (1997)
Peruvian upwelling	Microcosm	^{14}C	N.S.			Tortell et al. (2002)
Raune Fjord (Norway)	Mesocosm	^{14}C	N.S.			Delille et al. (2005)
Bering Sea	Microcosm	^{14}C	N.S.			Hare et al. (2007)
Raune Fjord (Norway)	Mesocosm	DIC	+			Riebesell et al. (2007)
Raune Fjord (Norway)	Mesocosm	C_T	+			Bellerby et al. (2008)
Ross Sea	Microcosm	^{14}C	+			Tortell et al. (2008)
Raune Fjord (Norway)	Mesocosm	^{14}C	+		+ *	Egge et al. (2009)
Raune Fjord (Norway)	Mesocosm	O_2	N.S.			Egge et al. (2009)
North Atlantic Ocean	Microcosm	^{14}C	N. S.			Feng et al. (2009)
BATS (North Atlantic)	Microcosm	^{14}C	N. S.			Lomas et al. (2012)
Kongs Fjord (Norway)	Mesocosm	^{14}C	+	+		Engel et al. (2013)
Kongs Fjord (Norway)	Mesocosm	O_2	N.S.			Tanaka et al. (2013)
Mediterranean Sea	Mesocosm	^{14}C	N.S.			Maugendre et al. (2015)
Mediterranean Sea	Mesocosm	O_2	N.S.			Maugendre et al. (2015)
Gullmar Fjord (Sweden)	Mesocosm	^{14}C	+			Eberlein et al. (2017)

4.3. Methods

4.3.1. Set-up and sampling

The experiment was carried out in Gando Bay (27º 55′ 41″ N, 15º 21′ 55″ W), Gran Canaria (Canary Island), as part of the BIOACID (Biological Impacts of Ocean ACIDification) project. Nine KOSMOS (Kiel Off-Shore Mesocosms for future Ocean Simulations; Riebesell et al. (2013) were deployed and enclosed ~35 m^3 of low-nutrient low-chlorophyll water off the east coast of Gran Canaria. In order to achieve a pCO_2 gradient from ~400 µatm to partial pressures corresponding to the year 2150 (~1000 µatm) according to the RCP8.5 scenario (IPCC, 2014), seven mesocosms were gradually enriched at the start of the experiment over a period of seven days (from t0 to t6), via the addition of different amounts of filtered CO_2-saturated seawater, although one of them (M6) was removed due to a leak in the plastic bag. Two more CO_2 addition were carried out on t24 and t38 to counteract the loss of CO_2 due to outgassing and biological uptake. The average pCO_2 concentrations along the whole experiment for each of the remaining six mesocosms were: M5 (448 µatm), M3 (563 µatm), M7 (668 µatm), M4 (716 µatm), M2 (887 µatm) and M8 (1025 µatm). Two other mesocosms -M1 (369 µatm) and M9 (352 µatm)- remained untreated, serving as controls (ambient pCO_2) (Fig. 4.1). After 24 days, between 31 and 38 m^3 of nutrient-rich deep water was added to each mesocosm with the purpose of simulating a natural fertilization event (Fig. 4.2). During the 56 day experimental period, integrated water samples (0-13 m) were collected by means of depth-integrated water samplers (IWS, HYDRO-

BIOS, Kiel), on days -1, 1, 5, 9, 13, 17, 21, 25, 27, 29, 31, 33, 35, 37, 41, 45, 50 and 55, from each of the nine mesocosms, plus an extra sample from ambient waters outside the mesocosms (referred to as Atlantic; A). Once on land, subsamples were taken for primary production, chlorophyll a, phytoplankton abundances, as well as for dissolved inorganic carbon and inorganic nutrients. Unfortunately, one of the high-CO_2 mesocosms (M6) was damaged on t26, and hence was not considered in the data analyses. More detailed information concerning the experimental set-up (CO_2 manipulation, deep water addition, sampling, etc.) is provided by Taucher et al. (2017).

4.3.2. *p*CO_2 and inorganic nutrients

Partial pressure of CO_2 (*p*CO_2) was derived from total alkalinity (TA) and dissolved inorganic carbon (DIC) data, following Pierrot et al. (2006) and Lueker et al. (2000). TA was measured by means of a Metrohm 862 Compact Titrosampler and a 907 Titrando unit. DIC was determined by infrared absorption using a LI-COR LI-700 on an ARICA system (MIRANDA, Kiel). Inorganic nutrients (NO_3^- , NO_2^-, PO_4^{3-} and $Si(OH)_4$) were determined by colorimetric methods following Murphy and Riley (1962) and Hansen and Grasshoff (1983). Ammonium (NH_4^+) was fluorometrically analyzed following Holmes et al. (1999). A SEAL Analytical QuAAtro AutoAnalyzer connected to a JASCO Model FP-2020 Intelligent Fluorescence Detector and a SEAL Analytical XY2 autosampler was used to measure NO_3^- , NO_2^-, PO_4^{3-}, $Si(OH)_4$, and NH_4^+ For details on the methodology of these measurements see Taucher et al. (2017).

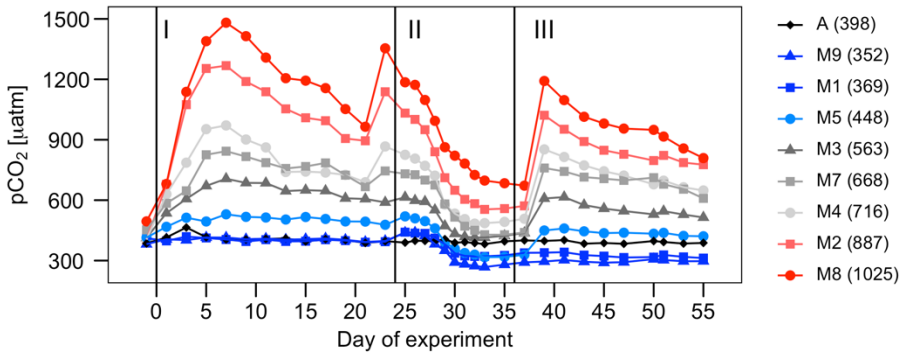

Figure 4.1. Temporal development of pCO_2 (µatm) over the course of the experiment in the mesocosms (MX) and the surrounding Atlantic waters (A). Vertical lines separate the three phases of the experiment. Values in parentheses indicate average pCO_2 concentrations for each mesocosm along the whole experiment.

4.3.3. Chlorophyll *a*

For chlorophyll *a* analysis, 500 mL of sea water were sampled and filtered sequentially through 20, 2 and 0.2 µm pore-size Whatman polycarbonate filters under low vacuum pressure. Filters were kept frozen at -20 ºC until analysis. Before chlorophyll determination, pigments were extracted using 10 mL of 90% acetone at 4 ºC in the dark for 24 h. Extracts were measured fluorometrically, before and after acidification, by means of a Turner Designs bench fluorometer 10-AU, previously calibrated with pure chlorophyll *a* (Sigma Chemical), following Holm-Hansen et al. (1965). The collected material on the 20, 2 and 0.2 µm filters was used to measure the corresponding microplankton (Chl_{Micro}), nanoplankton (Chl_{Nano}) and picoplankton (Chl_{Pico}) chlorophyll concentrations, respectively. Total chlorophyll (Chl_{Tot}) was derived from the sum of the three size fractions.

1.1.1. Phytoplankton abundance and biomass

Prochlorococcus and *Synechococcus* type cyanobacteria and small photosynthetic eukaryotic cells (picoeukaryotes) were enumerated with a FACScalibur (Becton and Dickinson) flow cytometer. Picoeukaryotes, Prochlorococcus and Synechococcus samples (about 1 mL) were analyzed in fresh material 30-60 min after subsampling from the carboys. Prochlorococcus were recurrently observed in Atlantic waters, but vanished inside all the mesocosms after two days. Thus, we did not use their abundances to compute biomass. Phytoplankton groups were identified by their signatures in a plot of side scatter (SSC) versus red (FL3) and orange (FL2) fluorescence. Samples were run at 60 $\mu L \cdot min^{-1}$. A suspension of yellow–green 1 μm latex beads ($x10^5$ $beads \cdot mL^{-1}$) was added as an internal standard (Polysciences, Inc.). Pigmented nanoeukaryotes (2-20 μm) were counted on fresh samples with a Cytobuoy cytometer (Dubelaar and Gerritzen, 2000), provided with flow-image. Samples (about 3 mL) were analyzed in vivo for 7 min at a flow rate of 300 $\mu L \cdot min^{-1}$. Microphytoplankton (mostly diatoms and dinoflagellates) were fixed with alkaline Lugol's iodine (1% final concentration), sedimented in Utermöhl chambers and counted by means of an inverted microscope (Utermöhl, 1931).

Biomass of *Synechococcus* and *picoeukaryotes* were estimated by multiplying their abundances by the average cell carbon content obtained for each group, using the conversion factors obtained by MF Montero (unpublished) from samples collected in coastal waters of Gran Canaria: 120 fg $C \cdot cell^{-1}$ (*Synechococcus*), 420 fg $C \cdot cell^{-1}$ (picoeukaryotes). Nanoeukaryotes' abundances were converted into biomass using an

estimated average biovolume of 20 μm^{-3} for organisms between 2-6 µm and a biovolume of 125 μm^{-3} for organisms between 6-11 µm, applying the conversion factor of 220 fg $C \cdot \mu m^{-3}$ proposed by Borsheim and Bratbak, (1987). Biovolumes and conversion factors used for diatoms and dinoflagellates were calculated following Menden-Deuer and Lessard (2000). Picoplankton biomass (B_{Pico}) was calculated as the sum of the biomasses of Synechococcus and picoeukaryotes, nanoplankton biomass (B_{Nano}) as the sum of all nanoeukaryotes' biomass, and microplankton biomass (B_{Micro}) as the sum of the diatoms and dinoflagellates biomass. Total biomass (B_{Tot}) refers to the sum of all size fractions.

4.3.4. ^{14}C-based primary production

Primary production was measured using the ^{14}C method. Four culture flasks per mesocosm, and per ambient Atlantic seawater sample, were filled with 70 mL of water, and inoculated with 15 µCi of ^{14}C-labelled sodium bicarbonate solution ($NaH^{14}CO_3$; Perkin Elmer). Three of them were in vitro incubated for 12 h in a temperature-controlled chamber reproducing in situ daily average light and temperature, while the remaining flask was incubated at the same temperature under complete darkness to measure the dark carbon uptake. Sixty mL of the samples were filtered with a vacuum pump sequentially through 20, 2 and 0.2 µm pore-size Whatman polycarbonate filters, to allow calculation of the particulate organic carbon fixed by microplankton (PP_{Micro}), nanoplankton (PP_{Nano}) and picoplankton (PP_{Pico}), respectively. The total particulate organic carbon production (PP_{POC}) was derived from the sum of the three size fractions. Filters were then placed in 4 mL scintillation

vials and exposed to concentrated HCl fumes overnight to remove ^{14}C-labeled inorganic carbon. To estimate the amount of carbon fixation into the dissolved organic carbon fraction (PP_{DOC}), 5 mL of water sample was gently filtered onto 0.2 µm Whatman polycarbonate filter under low vacuum pressure. The filtrate was transferred to a 20 mL scintillation vial. Liquid samples were acidified with 100 µl of 50% HCl and placed in an orbital oscillator for 24 h. Finally, scintillation cocktail (Ultima Gold XR) was added to every sample, thoroughly mixed, and stored in darkness for another 24 h, prior to measuring radioactivity in a scintillation counter Beckman LS-6500. Primary production (µg $C \cdot L^{-1} \cdot h^{-1}$) was calculated according to:

$$PP = \left[\frac{V_S}{V_F}\right] \cdot \frac{DIC \cdot (DPM_S - DPM_D)}{DPM_A \cdot t_i}$$

where V_S is the volume of the sample (mL); V_F the filtered volume (mL); DIC the dissolved inorganic carbon of the sample (µg $C \cdot L^{-1}$); DPM_S the disintegration per minute of the samples; DPM_D the disintegration per minute of the dark-incubated samples; DPM_A total initial addition of ^{14}C and ti the incubation time (h).

The percentage of extracellular carbon release (PER) was calculated as:

$$PER\ (\%) = \frac{PP_{DOC}}{PP_{TOT}}\ x\ 100$$

being PP_{TOT} the sum of PP_{DOC} and PP_{POC}.

4.3.5. Statistical analysis

To investigate the potential effects of ocean acidification on autotrophic productivity throughout the three phases of the experiment, model II (Reduced Major Axis) linear regressions (Sokal and Rohlf, 2013) between primary production, chlorophyll and biomass and pCO_2 concentrations were performed for each phase using Matlab (The MathWorks, Inc, Natick, Massachusetts, United States). For that purpose, all datasets were averaged per mesocosm and phase. The confidence level for all analysis was set at 95% ($p < 0.05$).

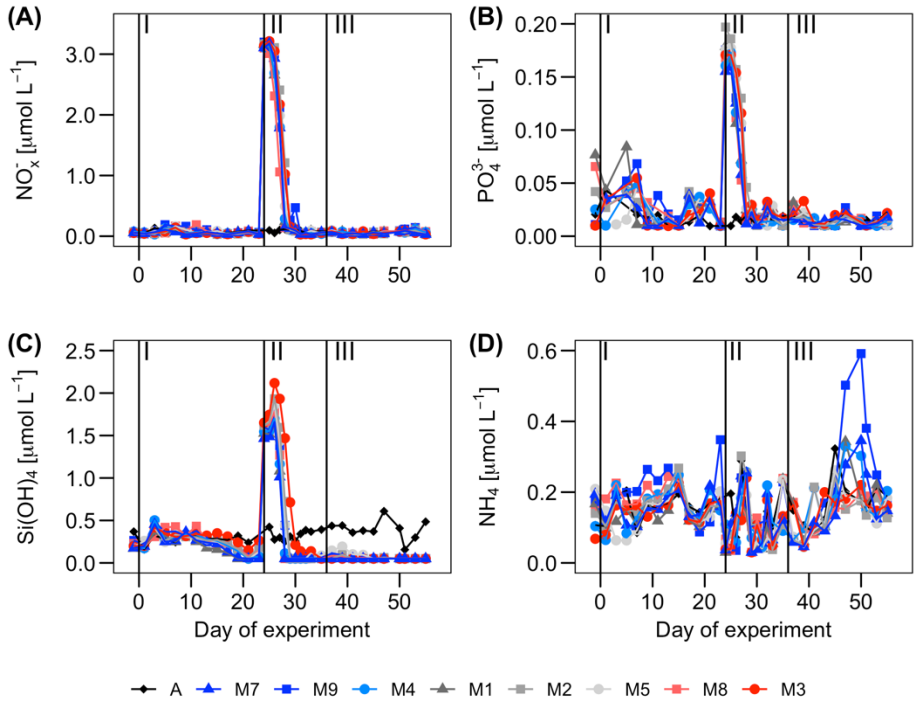

Figure 4.2. Temporal development of (A) nitrate + nitrite (NO_x^-) (µmol·L^{-1}), (B) phosphate (µmol·L^{-1}), (C) silicate (µmol·L^{-1}) and (D) ammonium (µmol·L^{-1}) over the course of the experiment. Vertical lines separate the three phases of the experiment.

4.4. Results

4.4.1. Temporal development of size-fractionated chlorophyll *a* and autotrophic biomass

Nutrient concentrations (Fig. 4.2), together with the development of chlorophyll and biomass (Figs. 4.3 and 4.4), allowed the differentiation of three well-defined phases over the experimental period: The pre-bloom phase (I), from t1 to t23; the bloom phase (II), from t25 to t35; and the post-bloom phase (III), from t37 until the end of the experiment (t55).

During phase I, the waters inside the mesocosms were characterized by relatively low nutrient concentrations (similar to ambient Atlantic waters), low Chl_{Tot}, and low B_{Tot} (Figs. 4.2, 4.3 and 4.4). Two to three days after enclosing the water inside the mesocosm bags (t1-t2), the concentration of all inorganic nutrients slightly increased both inside the mesocosms and in Atlantic waters. This suggests the influence of external inputs; perhaps caused by dust deposition on the surface waters (since during those days there was aerosols deposition with dust originating from NW Africa). Nitrate, phosphate and silicate displayed relative maxima around t5, dropping after t10 and reaching minimum values at t23. Ammonia peaked around t10-15 and dropped to minimum values around t20. The largest decrease in the meosocosm nutrient concentrations compared to the Atlantic waters was in the silicates, as a result of its consumption by diatoms (Taucher et al., 2017). Total chlorophyll and biomass increased from t0 to t23, following a general inverse trend with nutrient concentrations (Fig. 4.3). However, there were contrasting patterns between chlorophyll and biomass in the

different size-fractions. There were no significant differences in chlorophyll concentrations between the mesocosms and Atlantic waters in any of the size fractions (Fig. 4.3). In contrast, there were significant differences in biomass in the largest size fractions between mesocosms and Atlantic waters, suggesting a dominance of large mixotrophic organisms inside the mesocosms (Fig. 4.4). Figure 4.5 illustrates the relative contributions of the different size fractions (averaged from all the mesocosms) to chlorophyll, biomass and primary production over the course of the experiment. During phase I, picophytoplankton (Pico) contributed >40% to Chl_{Tot}, but <40% to B_{Tot}, with no significant differences with ambient waters. Nanophytoplankton (Nano) contributed 30-35% to Chl_{Tot}, but dominated in biomass (about 50%), although differences between mesocosms and Atlantic waters were not significant. Diatoms and dinoflagellates (Micro) contributed about 25% to Chl_{Tot} but only 10-20% to B_{Tot}, with clear differences with respect to Atlantic waters, particularly after t10.

Following the nutrient fertilization at t24, Chl_{Tot} and B_{Tot} increased exponentially reaching maximum average values (3.4 ± 0.5 $\mu g \cdot L^{-1}$ and 244 ± 122 $\mu g\ C \cdot L^{-1}$, respectively) at t29 (Fig. 4.3 and 4.4). Consequently, nutrient concentrations were rapidly utilized inside the mesocosms, dropping to levels similar to the Atlantic waters when the phytoplankton bloom was at its peak (Fig. 4.2). There was an exception with silicates, whose values dropped even below the Atlantic values after the bloom, as result of the large consumption by diatoms during phases II and III (Taucher et al., 2017). M8 and M2, the two mesocosms with highest CO_2 concentrations, were markedly elevated in biomass, both in the Micro

and Nano fractions, compared to the other mesocosms (Fig. 4.3). With the depletion of inorganic nutrients, the levels of chlorophyll as well as biomass decreased in the Pico and Nano fractions, with a change in the slopes at t36, when nutrients were almost exhausted. Biomass of Micro decreased more smoothly, maintaining high values in the high CO_2 treatments during the start of phase III. chlorophyll and biomass in phase II were dominated by Micro, contributing 40-60%, with a slightly higher dominance in biomass than in chlorophyll. In contrast, Pico contributed on average only 10-35% to chlorophyll and biomass inside the mesocosms, with values significantly lower than in the Atlantic waters.

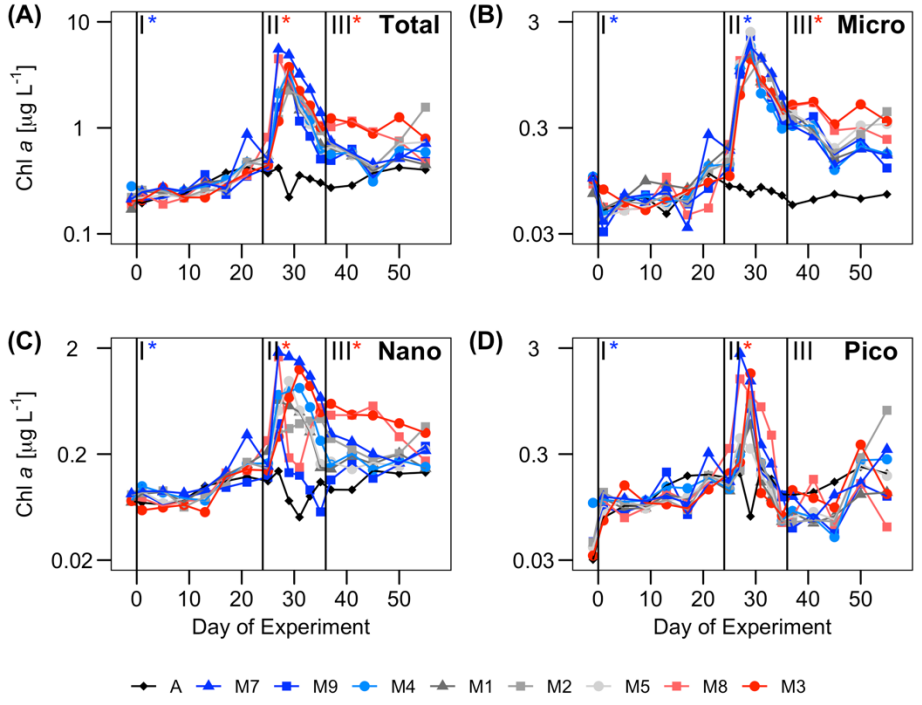

Figure 4.3. Temporal development of chlorophyll *a* (µg C·L^{-1}) in different size fractions: (A) total (Chl_{Tot}), (B) microplankton (Chl_{Micro}), (C) nanoplankton (Chl_{Nano}) and (D) picoplankton (Chl_{Pico}) over the course of the experiment. Vertical lines defined the three phases of the experiment.

During phase III, nutrient concentrations remained low (Fig. 4.2), with nitrate and phosphate occurring at similar levels compared to Atlantic waters, but silicate was almost depleted (due to the consumption by diatoms) to levels <0.08 µM, significantly below those of Atlantic waters. Only ammonium showed higher concentrations in some of the mesocosms, compared to Atlantic waters and phases I and II, probably due to higher excretion rates of grazers during this phase. Although Chl_{Tot} and B_{Tot} decreased with respect to phase II, they were still markedly higher than in Atlantic waters. The contribution of the larger size fractions to chlorophyll and biomass were always higher in the mesocosms than in Atlantic waters, but with apparent differences between chlorophyll and biomass (Fig. 4.5). Pico contributed in general to near 45% of Chl_{Tot} and 35% to B_{Tot} in Atlantic waters compared to <25% of Chl_{Tot} and <10% of B_{Tot} in the mesocosms. Nano and Micro contributed almost evenly to Chl_{Tot} in the mesocosms, but not to biomass.

4.4.2. Dynamics of size-fractionated ^{14}C-based primary production

Total primary production in the particulate fraction (PP_{POC}) displayed average rates in the mesocosms (0.93 ± 0.48 µg $C \cdot L^{-1} \cdot h^{-1}$) that were almost double than in Atlantic waters (0.56 ± 0.24 µg $C \cdot L^{-1} \cdot h^{-1}$) at the start of the experiment. Like chlorophyll and biomass, the rates increased 4 to 5-fold peaking at t10-12 in all size fractions (although more for the Pico), to decrease again to initial rates, just before nutrient fertilization (Fig. 4.6). The greatest differences between Atlantic waters and mesocosms were observed in Pico. This fraction contributed >50% to PP_{POC} in phase I, compared to ~30% in Atlantic waters.

After nutrient fertilization (phase II), PP_{POC} increased more than 15-fold in all mesocosms, peaking at t29 with the highest rates in M2, reaching 35 µg $C \cdot L^{-1} \cdot h^{-1}$, compared to values <2 µg $C \cdot L^{-1} \cdot h^{-1}$ in Atlantic waters (Fig. 4.6). Due to nutrient depletion, total PP_{POC} rates declined to <4 µg $C \cdot L^{-1} \cdot h^{-1}$ at t35 (end of phase II). Micro contributed almost a 75% to total PP_{POC}, even more than to chlorophyll and biomass (Fig. 4.5), while the contribution of Pico was about 10%.

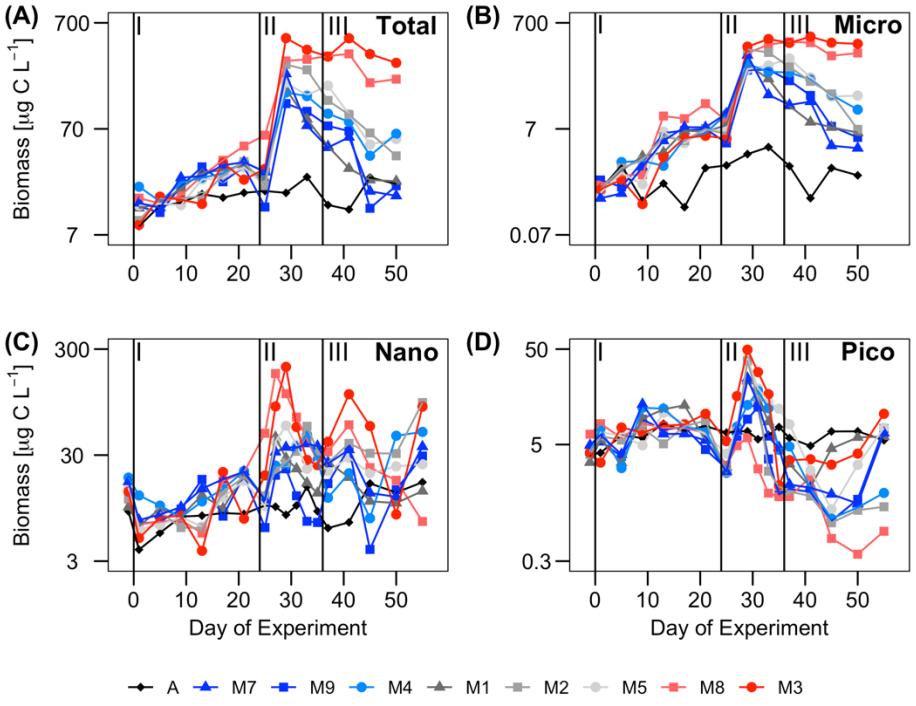

Figure 4.4. Temporal development of biomass (µg $C \cdot L^{-1}$) in different size fractions: (A) total (B_{Tot}), (B) microplankton (B_{Micro}), (C) nanoplankton (B_{Nano}) and (D) picoplankton (B_{Pico}) over the course of the experiment. Vertical lines defined the three phases of the experiment.

During phase III, PP_{POC} rates declined more smoothly than in phase II, following nutrient depletion, with higher rates in the mesocosms with higher CO_2 treatments (see following section). Like in phase II, the major

contribution to total PP_{POC} was due to Micro (60-70%), while Pico and Nano contributed about 15-20 % each.

The average rate of primary production contributing to the dissolved organic carbon fraction (PP_{DOC}; Fig. 4.7.a) inside the mesocosms varied strongly during the course of the experiment, between 34.7 µg $C \cdot L^{-1} \cdot h^{-1}$ in mesocosm M2 during the bloom phase and 0.23 µg $C \cdot L^{-1} \cdot h^{-1}$ in mesocosm M7 during phase I. Its temporal development matched PP_{POC} dynamics, increasing with nutrient addition in t24. However, the percentage of extracellular organic carbon release (PER; Fig. 4.7.b) decreased from the first week of the experiment (average 26.7 ± 8.6 %), to t29, when primary production reached their maximum values and PER its average minimum value (7.1 ±

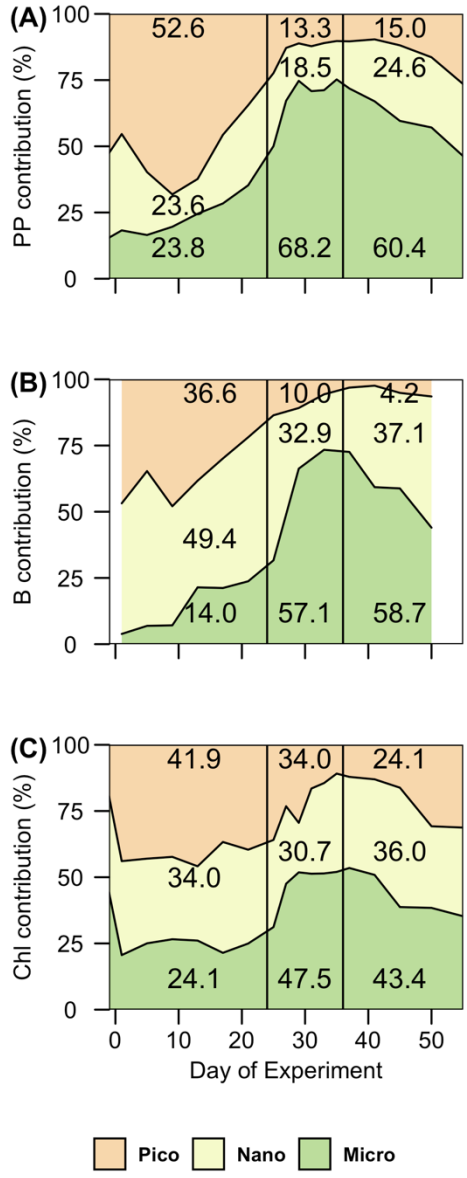

Figure 4.5. Contribution (%) of each size fraction to (**A**) total particulate primary production (PP), (**B**) total biomass (B) and (**C**) total chlorophyll (Chl) in phase I (t_1-t_{24}), phase II (t_{25}-t_{35}) and phase III (t_{36}-t_{55}). Micro: microplankton; Nano: nanoplankton; Pico: picoplankton.

3.7 %). In Atlantic waters, PP_{DOC} was similar (phase I) or lower (phases II and III) than in the experiments, but with higher and less stable PER, ranging from <10% to 35% (Fig. 4.7.b).

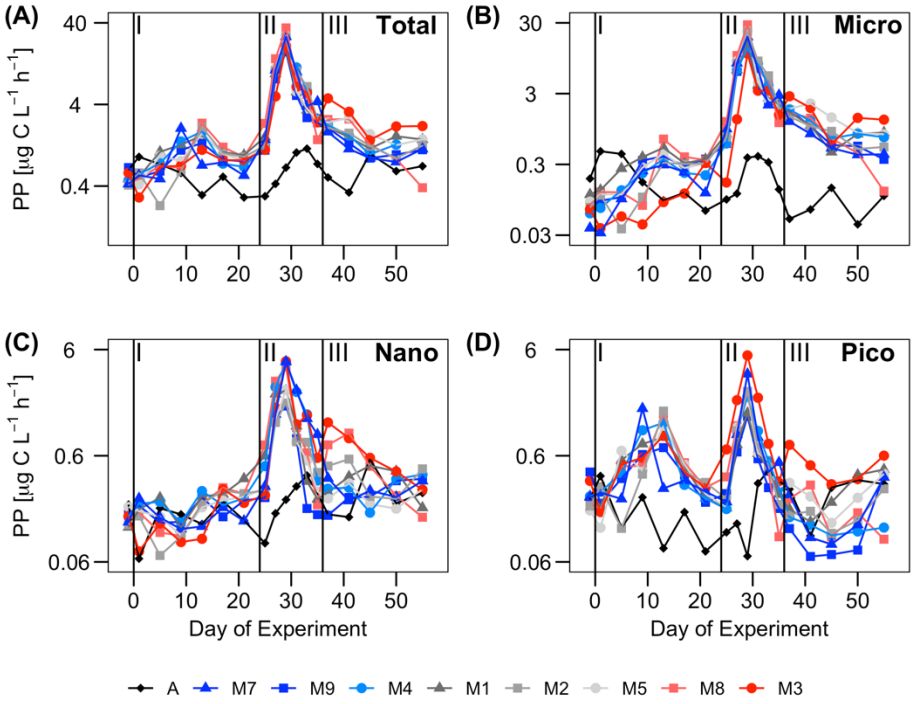

Figure 4.6. Temporal development of primary production (µg C·L^{-1}·h^{-1}) in (A) the total particulate faction (Total), and in the (B) microplankton (Micro), (C) nanoplankton (Nano) and (D) picoplankton (Pico) size fractions, over the course of the experiment. Vertical lines defined the three phases of the experiment. PP is represented in log scale to better illustrate the differences among mesocosms.

4.4.3. CO_2 effects on size-fractionated chlorophyll *a*, biomass and primary production

A total of 39 linear regressions were conducted to test potential CO_2 effects on total community and size-fractionated primary production, biomass and chlorophyll, and almost two thirds (28) showed statistically significant ($p<0.05$) relationships (Tables 4.2, 4.3 and 4.4, respectively). Total particulate primary production (PP_{POC}) remained unaffected during

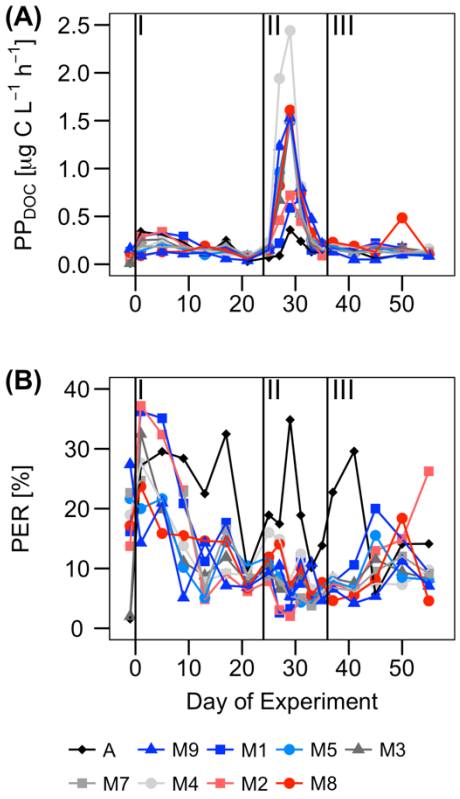

Figure 4.7. Temporal development of (A) rates of dissolved primary production (PP_{DOC}) (µg $C \cdot L^{-1} \cdot h^{-1}$) and (B) the percentage of extracellular release (PER: % $PP_{DOC}/(PP_{POC}+PP_{DOC})$) over the course of the experiment. Vertical lines separate the three phases of the experiment.

phase I, in contrast to B_{Tot}, B_{Nano}, Chl_{Nano} and Chl_{Tot}, which exhibited negative responses to increasing pCO_2. Negative responses (6) were only observed in the oligotrophic phase (phase I). Dissolved carbon production rate (PP_{DOC}) also presented a strong relationship with pCO_2, but a positive one. No statistically significant correlations with pCO_2 concentrations were found with the remaining parameters in phase I.

After nutrient fertilization in t24, the majority of the CO_2 correlations (23 out of 26) were statistically significant and mostly positive (Tables 4.2, 4.3 and 4.4). Fractionated primary production, biomass and chlorophyll, as well as PP_{POC}, B_{Tot} and Chl_{Tot} were positively related to increasing pCO_2 (except PP_{Nano}) in phase II. PP_{DOC} was statistically correlated with pCO_2 in phase III but not in phase II. We also observed strong significant and positive correlations between pCO_2 and both total and size-fractionated primary production, biomass and chlorophyll during phase III (except in the Pico fraction).

Table 4.2. Linear regressions statistics of the relationship between average primary production in the total particulate (PP_{POC}) and different size fractions (PP_{Micro}, PP_{Nano}, PP_{Pico}), as well as in the total dissolved fraction (PP_{DOC}), versus pCO_2 levels for the three experimental phases.

	Parameter	Slope (x10^4)	R^2	F statistic	p-value
Phase I		-3.92 ± 2.11	0.02	3.45	0.11
Phase II	PP_{POC}	**127.00 ± 36.00**	**0.70**	**12.27**	**0.03**
Phase III		**21.00 ± 5.57**	**0.64**	**14.74**	**< 0.01**
Phase I		-2.39 ± 1.22	0.05	3.83	0.10
Phase II	PP_{Micro}	**95.00 ± 29.00**	**0.59**	**10.68**	**0.02**
Phase III		**13.00 ± 4.41**	**0.43**	**8.71**	**0.03**
Phase I		-0.94 ± 0.45	0.10	4.36	0.08
Phase II	PP_{Nano}	24.00 ± 13.00	0.01	3.17	0.13
Phase III		**6.27 ± 1.64**	**0.63**	**14.63**	**< 0.01**
Phase I		1.75 ± 0.92	0.03	3.61	0.11
Phase II	PP_{Pico}	**23.00 ± 6.29**	**0.66**	**13.28**	**0.02**
Phase III		**5.17 ± 1.70**	**0.46**	**9.30**	**0.02**
Phase I		**1.50 ± 0.47**	**0.65**	**10.25**	**0.03**
Phase II	PP_{DOC}	11.00 ± 5.92	0.01	3.21	0.12
Phase III		**1.74 ± 0.53**	**0.51**	**10.60**	**0.02**

4.5. Discussion

4.5.1. CO_2 and nutrient impacts on phytoplankton biomass and productivity

The eight mesocosms during phase I displayed similar behaviors to the Atlantic ambient waters, showing a phytoplankton community dominated in terms of biomass by small picophytoplankton and nanophytoplankton (Fig. 4.5), characteristic of the oligotrophic subtropical northeast Atlantic (Zubkov et al., 2000a, 2000b; Arístegui

and Montero, 2005; Figueiras et al., 2016), although with somewhat higher primary production and biomass.

Table 4.3. Linear regressions statistics of the relationship between average total community biomass (B_{Tot}) and the biomass of the different size fractions (B_{Micro}, B_{Nano}, B_{Pico}) versus pCO_2 levels for the three experimental phases.

	Parameter	Slope (x10^4)	R^2	F statistic	p-value
Phase I	B_{Tot}	-0.86 ± 0.43	0.07	4.07	0.09
Phase II		**40.96 ± 7.15**	**0.83**	**32.86**	**< 0.01**
Phase III		**53.75 ± 12.12**	**0.72**	**19.68**	**< 0.01**
Phase I	B_{Micro}	0.59 ± 0.29	0.07	4.07	0.09
Phase II		**27.49 ± 5.69**	**0.76**	**23.37**	**< 0.01**
Phase III		**48.89 ± 11.27**	**0.71**	**18.83**	**< 0.01**
Phase I	B_{Nano}	**-0.55 ± 0.16**	**0.57**	**12.27**	**0.01**
Phase II		**11.96 ± 2.75**	**0.71**	**18.87**	**< 0.01**
Phase III		**6.28 ± 2.10**	**0.44**	**8.94**	**0.02**
Phase I	B_{Pico}	0.21 ± 0.11	0.02	3.51	0.11
Phase II		**2.37 ± 0.41**	**0.85**	**32.87**	**< 0.01**
Phase III		0.64 ± 0.32	0.06	3.91	0.10

Due to the low nutrient concentrations, PP_{POC} was low and relatively stable during phase I, showing no significant relationship with pCO_2. Although, theoretically, carbon fixation should be enhanced by high pCO_2 levels (Giordano et al., 2005; Reinfelder, 2011), the absence of a response of primary production to increasing CO_2 in oligotrophic waters dominated by small phytoplankton has been reported by other authors (Maugendre et al., 2017). Surprisingly, both chlorophyll and biomass decreased with increasing pCO_2 during phase I (Tables 4.3 and 4.4), even though primary production remained rather stable. Engel et al. (2013) observed the same behavior in a similar mesocosms study in Arctic

waters. They hypothesized that either the enhancement of particle aggregation and settling as a consequence of increasing Transparent Exopolymer Particles (TEP), the increase in remineralization of phytoplankton cells, the nutrient competition between auto- and heterotrophic organisms, or a combination of the preceding processes, could explain the mismatch between PP_{POC} and its accumulation as biomass. Due to the lack of response of TEPs to increasing pCO_2 in our experiment (data not shown), the first hypothesis would not apply in our case. A more likely explanation would be that a fraction of primary production is channeled through the dissolved fraction increasing the DOC pool inside the mesocosms. This hypothesis agrees with both the observed higher values of PP_{DOC} in the high-CO_2 mesocosms, and the increase in DOC from t3 to t23 reported by Zark et al. (2017) in this same study.

Table 4.4. Linear regressions statistics of the relationship between average total community chlorophyll *a* (Chl_{Tot}) and the chlorophyll of the different size fractions (Chl_{Micro}, Chl_{Nano}, Chl_{Pico}) versus pCO_2 levels for the three experimental phases.

	Parameter	Slope (x10^4)	R^2	F statistic	p-value
Phase I	Chl_{Tot}	**-1.27 ± 0.30**	**0.74**	**18.22**	**< 0.01**
Phase II		**14.00 ± 4.98**	**0.46**	**7.74**	**0.04**
Phase III		**8.51 ± 1.92**	**0.72**	**19.72**	**< 0.01**
Phase I	Chl_{Micro}	**-0.38 ± 0.14**	**0.47**	**7.87**	**0.04**
Phase II		**-5.39 ± 2.24**	**0.24**	**5.83**	**0.05**
Phase III		**3.33 ± 0.47**	**0.88**	**49.70**	**< 0.01**
Phase I	Chl_{Nano}	**-0.53 ± 0.14**	**0.71**	**15.64**	**0.01**
Phase II		**8.34 ± 3.08**	**0.43**	**7.33**	**0.04**
Phase III		**4.77 ± 1.33**	**0.59**	**12.90**	**0.01**
Phase I	Chl_{Pico}	**-0.39 ± 0.11**	**0.58**	**12.46**	**0.01**
Phase II		**9.20 ± 3.83**	**0.32**	**5.79**	**0.06**
Phase III		2.21 ± 1.15	0.04	3.71	0.10

Nutrient fertilization triggered autotrophic phytoplankton community growth, with higher maximum biomass build-up in the high-CO_2 mesocosms. The bloom that occurred during phase II, coincided with an increase in primary production and biomass inside all mesocosms. As a consequence, major nutrients were depleted to values similar (such as $NO_3^- + NO_2^-$ and PO_4^{3-}) or lower ($Si(OH)_4$) to phase I. Linear regressions between PP_{POC}, B_{Tot} and Chl_{Tot} vs pCO_2 revealed significantly positive relationships in phase II, although the strongest relationships of PP_{POC}, B_{Tot} and Chl_{Tot} vs pCO_2 occurred in phase III. A positive effect of increasing pCO_2 in seawater on primary production has been reported by other authors, from single species' experiments (Beardall and Raven, 2004a; Fu et al., 2007; Sobrino et al., 2008) to whole community level experiments (Egge et al., 2009; Engel et al., 2013). The positive effect of enhanced pCO_2 on primary production has been attributed to the relieve of CO_2 limitation of RubisCO (Giordano et al., 2005; Riebesell et al., 2007; Reinfelder, 2011; Mackey, 2015). The increase in the availability of CO_2 should thus produce an increase in photosynthetic rates, by relieving carbon limitation, or indirectly by lowering the energy required to concentrate CO_2 against a smaller concentration gradient.

In summary, our results show that all the positive significant correlations between plankton productivity and biomass and pCO_2 occur after nutrients addition, suggesting a synergistic effect of nutrients and CO_2. Indeed, as far as we know, the only ocean acidification mesocosm study carried out to test primary production responses in oligotrophic regions, report non-statistically significant effects of increasing pCO_2 on primary production under nutrient deplete conditions (Maugendre et al., 2017).

4.5.2. Community structure response to elevated CO_2 and nutrient fertilization

During phase I, Pico contributed > 40% to Chl and > 50% to primary production, although Nano was the dominant size fraction in terms of biomass. A marked change in the phytoplankton community occurred after the fertilisation through deep-water addition at the beginning of phase II and during phase III, where the community shifted to larger microphytoplankton (mostly diatoms; Taucher et al., 2017) with >57% dominance in biomass and > 60% in primary production (Fig. 4.5). Changes from small to large size fractions of phytoplankton have been described in the Canary Islands region, associated with transitional changes from oligotrophic to eutrophic conditions across upwelling filaments, eddies and fronts (Basterretxea and Aristegui, 2000; Arístegui et al., 2004).

Our results show that phytoplankton size-groups generally remained unresponsive during phase I to the increases in pCO_2, whereas all of them benefitted from the nutrient addition. This disagrees with a study by Egge et al. (2009), who reported non-significant changes in primary production among size fractions in a mesocosm experiment in Bergen (Norway), although differences in chlorophyll and biomass at group level have been observed during other mesocosm experiments (Brussaard et al., 2013; Schulz et al., 2017). For this present study, Taucher et al. (2017), using a non-metric multidimensional scaling (NMDS) analysis, described a significant effect of CO_2 on the whole planktonic community (including protozoa and mesozooplankton). The effect is apparent even in phase I, but became more pronounced after

nutrient fertilization. They reported that the response of the community structure to CO_2 treatments emerges not from one or two dominant species but from overall shifts across the entire plankton community. At the phytoplankton level, we find in most cases a significant effect of CO_2 on primary production, biomass and chlorophyll a in all the size fractions during phases II and III, pointing to a size independent stimulation of nutrients and CO_2 over all the phytoplankton groups, which particularly benefited the increase of diatoms in absolute terms (Taucher et al., 2017). However, a closer look to the linear correlations reveals significant differences among regression slopes, indicating differences in size fractions responses. Indeed, the relative increase of primary production after nutrient additions display a clear size-related pattern, where small PP_{Pico} was enhanced about 250 %, PP_{Nano} up to 150 % and PP_{Micro} about 100 % in the two high-CO_2 mesocosms compared to the two low-CO_2 mesocosms. Surprisingly, the highest relative change in biomass was observed in B_{Micro} followed by B_{Nano} and B_{Pico}. This could be partly explained by a more intense grazing pressure on the smallest size fractions compared to the largest ones.

A number of experimental and modeling studies have suggested the existence of potential winners and losers in a future acidified ocean (Dutkiewicz et al., 2013; Kroeker et al., 2013; Bach et al., 2017). In our mesocosm experiment, the shift from a cyanobacteria-dominated community to a large diatom-dominated community in the high CO_2 scenarios after nutrient fertilization, as well as the distinct size-related relative change observed among size-fractions, seems to support this hypothesis. Nevertheless, the fact that all phytoplankton size classes increased after nutrient addition in high CO_2 treatments, suggests that the

entire phytoplankton community in subtropical regions would benefit in an acidified and patchily fertilized ocean, although larger cells could outcompete the smaller ones under high nutrient inputs.

4.5.3. Biogeochemical implications

Oligotrophic regions are expanding at an annual rate of 0.8 to 4.3%, with the North Atlantic subtropical Gyre showing the fastest annual expansion (Sarmiento et al., 2004; Polovina et al., 2008). Approximately 0.8 million km^2 of productive waters are being replaced annually by warmer stratified oligotrophic waters. Most models predict a decline in primary production as well as in the downward carbon fluxes in these regions by the end of the century (Riebesell et al., 2009; Gruber et al., 2011; Bopp et al., 2013), due to a reduction of vertical nutrient supply related with the shoaling of the mixed layer depth (Bopp et al., 2001; Marinov et al., 2010; Steinacher et al., 2010). Nevertheless, these models do not take into account the effect of mesoscale and submesoscale processes, such as eddies or fronts, which are known to play a key role in enhancing primary production (e.g. McGillicuddy et al., 2007; Sangrà et al., 2009) and export fluxes (Omand et al., 2015) in the ocean. Under an scenario of an acidified and warmer ocean, leading to an intensification of cross-shore wind gradients and eddy kinetic energy across eastern boundary regions (Bakun, 1990; Sydeman et al., 2014; Reyes et al., 2015), mesoscale variability would increase mixing and upwelling of deeper nutrient-rich water into the euphotic zone (Renault et al., 2016; Xiu et al., 2018). Our data suggest that a patchy nutrient pumping in a more acidified ocean would increase primary productivity in subtropical warm regions. Furthermore, community structure would shift from small to

large cells, like diatoms, potentially leading to a more efficient carbon export to the deep ocean. The concomitant increase in dissolved organic carbon production (PP_{DOC}) may also contribute to the biological carbon pump, through particle aggregation and the subsequent increase of sinking rates (Engel et al., 2004; Schartau et al., 2007).

It has been estimated that mesoscale and submesoscale features account for 20-30% of the new primary production in the world's ocean (McGillicuddy et al., 2007). If global warming reinforces wind regimes in eastern boundary regions as predicted (Bakun, 1990; Sydeman et al., 2014), increasing the eddy kinetic energy field, new production could increase as well, counteracting the effect of enhanced stratification in subtropical regions. Nevertheless, further research is needed to constrain the synergistic or antagonistic effects of climate drivers on primary production and plankton community structure in subtropical oligotrophic waters, the most extensive ecosystems of the world's ocean.

4.6. Conclusions

This is the first mesocosm study addressing the response, in terms of primary production and community structure, of size-fractionated (0.2-2, 2-20 and >20 μm) natural plankton communities in subtropical oligotrophic regions to increasing CO_2 concentrations and nutrient fertilization. Our results reveal a non-significant CO_2-related effect on PP and B under nutrient depleted conditions, with a phytoplankton dominance of small cyanobacteria. After nutrient fertilization, however, the community shifts towards larger phytoplankton, with a diatom-dominated community, showing a significant marked increase in PP, B

and chlorophyll under higher CO_2 conditions in all groups. Our data suggest that in a future acidified subtropical ocean, mesoscale and submesoscale features –which are predicted to enhance under global warming in eastern boundary regions- would drive nutrient pumping to the surface ocean favoring the development of diatoms and increasing new production in the global ocean.

4.6.1. Author contributions

UR and JA: conceived and designed the experiment. All authors performed the experiment and analyzed the data. Wrote the paper: NH-H and JA with inputs from all co-authors.

4.6.2. Funding

The KOSMOS project was funded by the German Federal Ministry of Education and Research (BMBF) in the framework of the coordinated project BIOACID—Biological Impacts of Ocean Acidification, phase 2 (FKZ 03F06550). UR received additional funding from the Leibniz Award 2012 by the German Research Foundation (DFG). The Natural Environment Research Council provided funding for EA and ME as part of the UK Ocean Acidification Programme (NE/H017348/1). JA was supported by a Helmholtz International Fellow Award, 2015 (Helmholtz Association, Germany). NH-H was partially supported by KOSMOS funding during the experimental work, and by a grant of the Agencia Canaria de Investigación, Innovación y Sociedad de la Información (ACIISI) during the writing stage (TESIS2015010036). IB was supported by a FPI fellowship (BES-2016-078407) from the Spanish Ministry of Economy, Industry and Competitiveness (MINECO). NH-

H, MM, IB, and JA benefited also from the FLUXES project (CTM2015-69392-C3-1-R) funded by the Spanish government (Plan Nacional I+D).

4.6.3. Acknowledgments

We would like to thank the KOSMOS and the Plataforma Oceánica de Canarias (PLOCAN) teams assisting with all aspects of the organization and logistical support before, during and after this mesocosms campaign, as well as to Minerva Espino and Acorayda González (IOCAG, ULPGC) for their technical support in the sampling and analyses of phytoplankton and productivity data.

Chapter Five

Synthesis and future research

5.1. General discussion

The challenge of meso-submesoscale variability studies is consequence of the difficulty in collecting high-resolution, synoptic data (Gomis et al., 2005; Pascual et al., 2017), particularly when water samples are needed such as phytoplankton community structure and biogeochemical processes studies. In that framework, modelling studies have been the most common tool used to account for the impact of these mechanisms, even though models grid resolution is often too coarse to assess the impact of submesoscale processes on biogeochemical cycles. While significant progress has been made on grid resolution (Mason et al., 2010), models' accuracy is still questionable mostly due to the scarce *in situ* data sets available for validation. Although submesoscale-resolution cruises are in many cases economically unviable and time-consuming, *in situ* studies are required to test theoretical results and to improve models' reliability. This thesis dissertation presents novel results about the impact of submesoscale dynamics on the phytoplankton and the biogeochemistry of the CanC region and stands for a valuable *in situ* dataset. The high-resolution spatiotemporal sampling carried out during the cruises used here, allowed us to assess vertical motions occurred at submesoscale and the associated nutrient fluxes, as well as their impact

on the phytoplankton community. We studied the effect of the meso-submesoscale processes interaction and present, as far as we know, the first *in situ* description of the short-term temporal development of a submesoscale front. Additionally, we tested the potential effects of climate change in phytoplankton communities under nutrient fertilization such as it has been observed to be associated with meso-submesoscale processes.

The main results of this thesis are following discussed with the aim of to answer the question raised in **Chapter 1**.

5.1.1. *How phytoplankton organisms distribute across mesoscale eddies at submesoscale range and what drivers govern their distribution?*

In a classical view, vertical velocities in mesoscale eddies are generated at the core by eddy pumping (McGillicuddy, 2016). Upwelling eddy pumping in cyclonic eddies brings new nutrients to the euphotic zone favoring the growth for large phytoplankton such as diatoms (Mcgillicuddy Jr et al., 1998; McGillicuddy et al., 2007; McGillicuddy, 2016). Downwelling in anticyclonic eddies sinks surface nutrient-poor waters as well as surface phytoplankton communities within. Under nutrient starvation and light limitation cyanobacteria-like Syn and Pro proliferate (Sweeney et al., 2003; Arístegui et al., 2004; Baltar et al., 2009). However, the number of studies indicating that submesoscale vertical motions plays a key role in phytoplankton modulation by mesoscale eddies have increased in the last two decades (Klein and Lapeyre, 2009; Mahadevan, 2016; McWilliams, 2016; Lévy et al., 2018).

Intense vertical velocities associated with ASC may be generated at the frontal zone between the eddy edge and the surrounding waters (Barceló-Llull et al., 2017a; Lévy et al., 2018) or as a result of "eddy-eddy interaction" (Klein and Lapeyre, 2009). Despite mesoscale eddies have been subject of large biogeochemical research, the biological-biogeochemical implications of the eddy-associated submesoscale motions remains unknown mostly due to the inherent complexity of high-resolution samplings. During the cruise carried out in the frame of the project RODA (**Chapter two**), we studied the phytoplankton community structure across a meso-submesoscale multi-structure system south of Canary Island at submesoscale range. The system was formed by a cyclonic eddy (CE) interacting with two anticyclonic eddies at southwest (AE1) and northeast (AE2) of the position of the CE, and the offshore extension of an upwelling filament embedded between CE and AE2 (Fig. 2.1).

The distribution of the phytoplankton community was directly and/or indirectly driven by the complex hydrography of the studied meso-submesoscale system, i.e., phytoplankton cell advection and/or changes in biogeochemical properties due to vertical and horizontal motions, respectively. Increasing new nutrient availability driven by 'eddy pumping' in the CE and by ASC in the frontal zone fueled larger phytoplankton (NEuk and HNF) biomass as observed in previous modelling and field studies (Mcgillicuddy Jr et al., 1998; McGillicuddy et al., 2007; McGillicuddy, 2016). Decrease in nutrient concentrations as consequence of the downwelling motions observed in AE1 and AE2 favors the proliferation of cyanobacteria-like Pro and Syn mostly due to their advantages in nutrient acquisition compared with larger organisms

(Marañón, 2015). Horizontal velocities also modulated phytoplankton community. Indeed, the most noticeable trait of HB distribution was its accumulation in the convergent front between AE1-CE (station 66) down to 200 m (Fig. 2.6.a) where downwelling velocities associated with ASC sink the accumulated biomass (Niewiadomska et al., 2008; Lathuiliere et al., 2011).

In summary, the vertical and horizontal motions associated with meso-submesoscale processes lead to the generation of distinguished niches where the best adapted organisms outcompete to the others. Thus, the phytoplankton distribution across the meso-submesoscale processes was characterized by small patched dominated by different groups. Since vertical velocities play a key role in mesoscale eddies and submesoscale fronts, high variability was also observed in vertical distributions. We are aware that this study is limited to a single section and thus our observations are constrained to a particular time. Nevertheless, our data strongly suggest that phytoplankton community structure was modulated by physical forcing and therefore it would be expected that occurs in the same way during whole eddy and front life cycle, as the relative impact of physical processes vary. Further questions remain, however, about the dynamics of phytoplankton community structure along the life cycles of meso-submesoscale processes.

5.1.2. Does the interaction of mesoscale processes impact phytoplankton distribution?

The interaction of the CE and the AE1 during the RODA cruise resulted in both horizontal and vertical motions. Indeed, one prominent

characteristic of the AE1-CE frontal zone was the high horizontal V_g which reached up to ~1 $m \cdot s^{-1}$ (Fig. 2.3), i.e., five time higher than the average V_g reported for the CanC and of the same order than the highest ones registered in the ocean (Pelegrí et al., 2005; Mason et al., 2011; Nardelli, 2020). Modelling studies suggest that during "eddy-eddy interaction" the surface water parcel between both eddies may be stirred by eddy-associated currents. Eddy currents would laterally compress it in one direction, and stretched out in the other producing strong horizontal velocities capable of stir phytoplankton organisms (D'Ovidio et al., 2010; Lévy et al., 2018). The impact of these horizontal motions on phytoplankton community thus depends on the initial community. Since our observation are constrained to a single section we cannot discern the potential effects of such high horizontal velocities. However, clear accumulation of bacterioplankton was observed as consequence of converging eddies. While it is true that vertical motions were not measured, we obtained enough evidences to think that the observed advection of nitrate into the euphotic zone crossing the isopycnals were associated to ASC. As consequence, surface layers were fertilizated inducing to the enhancement of larger cells (NEuk and HNF).

The F, as observed in the satellite image, stems from the coastal upwelling system near Cape Bojador (~26.0º N) and recirculates around the cyclonic eddy (Fig. 2.1). Coastal filaments in the CanC are recurrently generated not only by Cape Bojador but also by Cape Blanc (~20.0º N), Cape Juby (~27.5º N) and Cape Ghir (30.5º N) all year around (Sangrà et al., 2015; Lovecchio et al., 2018; Santana-Falcón et al., 2020). The interaction of Cape Bojador filament with mesoscale eddies is also a common phenomenon (Arístegui et al., 1994, 1997;

Barton et al., 1998, 2004; Basterretxea et al., 2002; Sangrà et al., 2005). Filaments enhance the exchange between upwelling and open ocean waters being able of to export high Chl *a* water and large phytoplankton cells offshore (Basterretxea and Aristegui, 2000; Barton et al., 2004; Cravo et al., 2013; Santana-Falcón et al., 2016). We did not observe enhanced Chl *a* concentration in F which, on the other hand, was dominated by larger phytoplankton (Neuk and HNF) probably transported from the coastal upwelling.

5.1.3. How submesoscale frontal dynamics affect phytoplankton spatiotemporal variability?

Since picoplankton organisms present different nutrients requierements, light harvesting and different temperature or physical forcing acclimatations (Mella-Flores et al., 2012; Flombaum et al., 2013; Luis Otero-Ferrer et al., 2018), it is expected that under the intense physical motions and biogeochemical changes occurred in submesoscale fronts there would be "winners" and "losers" depending on the features of every new niche created (Lévy et al., 2012b, 2018). The potential impact of submesoscale front are mostly related to the vertical motions associated with ASC (Mahadevan and Archer, 2000; Mahadevan, 2016; Lévy et al., 2018). However, neither vertical velocities pattern nor intensity remains invariant throughout the life cycle of a front. Theoretical and modelling studies indicates that during front formation (Frontogenesis), a dipole structure may be observed centered in the front. The pole in the warm side of the front is characterized by upwelling motions that may alleviate surface nutrient starvation and light limitation by driving nutrient fluxes or dragging phytoplankton cells into the well

illuminated surface layer. By contrast, decreased phytoplankton biomass would be expected in the cold side of the front where downward transport of organisms occurs as consequence of downwelling motion (Mahadevan and Archer, 2000; Mahadevan and Tandon, 2006; Lévy et al., 2012a, 2018).The cessation of the front-generating forcing leads to the advection of warmer water over colder one restoring water column stratification (Frontolisis; Thomas, 2005; Thomas and Lee, 2005; Mahadevan et al., 2010). Consequently, horizontal phytoplankton variability induced by frontogenesis should decrease.

During the ESTELA cruise (**Chapter 3**) we recordered the life cycle of a submesoscale front at the lee region of Gran Canaria island from its formation (frontogenesis) as consequence of favorable wind stress, to its destruction (frontolisis) along with the decrease of wind intensity (Section 3.5.1). Both phases had a distinguishing impact over picoplankton community. (1) Patches of high picoplankton biomass were characteristic of the frontogenesis phase as a consequence of the associated vertical velocities. Both processes dragging of phytoplankton cells and stirring of the previous community were responsible for the observed picoplankton distribution. Frontogenesis associated dynamics also modulated the community structure. Picoplankton assemblages presented a mirror-like distribution with respect to the middle of the front as suggested by MDS analysis. (2) The destruction of the front lead to a homogeneous picoplankton distribution and community structure. Collectively, submesoscale front dynamics induced intense changes in the picoplankton distribution and community structure increasing phytoplankton variability during its development and intensification and reducing it during front decay.

5.1.4. Which role plays temporal changes in phytoplankton variability?

Meso- and submesoscale processes such as eddies, filaments, and fronts are evolving structures. They generally arise as consequence of the perturbation of both atmospheric and oceanic flow, they are then intensified, and finally they decay (Sweeney et al., 2003; Sangrà et al., 2005; Thomas, 2005; Thomas and Lee, 2005; McGillicuddy et al., 2007; Eden and Dietze, 2009). Distinguishing hydrography results from the temporal development of the structure and therefore it would be expected that the biological and biogeochemical features evolve alongside with the process. Sweeney et al. (2003) reported changes in phytoplankton distribution and community structure throughout the life cycle of mesoscale eddies at Bermudas Atlantic Time-Series (BATS) station. Basterretxea and Arístegui (2000) and Arístegui et al. (2004) observed an along-filament shift in phytoplankton community structure being the waters dominated by larger cells restricted to the African shelf. They proposed that the initial coastal community dominated by diatoms progressively decay as consequence of sinking, lack of nutrient, and/or grazing as the filament expand into the open ocean. What we know about the submesoscale frontal dynamics and its biogeochemical implications, however, is mostly constrained to theoretical and modelling works despite most results suggest that submesoscale motions dominate vertical velocities in the ocean (e.g., Lévy et al., 2001; Klein and Lapeyre, 2009); and they may emerge as individual structures or associated with eddy and filament frontal zones (McWilliams, 2016; Lévy et al., 2018).

The submesoscale front at lee of Gran Canaria induced changes in picoplankton distribution and community structure that vary alongside with frontal development as discussed in the previous section. Frontal dynamics lead to the patchiness of the picoplankton groups resulting in high vertical, horizontal and temporal variability. Picoplankton biomass varied between 2 and 3-fold on spatial scale on ~2.5 km, and temporal scales of ~24 h, which is comparable to picoplankton seasonal variability in the region (Zubkov et al., 2000a; Baltar et al., 2009). We found that temporal and spatial changes contribute equally to picoplankton variability in the mixed layer while it mostly depends on time in the DCM. Beside our novel results, the knowledge about the temporal dynamics of meso-submesoscale structures present important lacks yet, mostly due to the spatiotemporal coverage of most oceanographic cruise. Due to the role played by these processes in the global biogeochemical cycles (Levy and Martin, 2013; Mahadevan, 2016; Harrison et al., 2018), heat fluxes (Volkov et al., 2008; Siegelman et al., 2020) or ocean general circulation (D'Asaro et al., 2011; Zhang et al., 2014), the better understanding of the temporal dynamics of these structures would also lead to a considerable increase in our knowledge of the global ocean. High-resolution spatiotemporal samplings should thus be considered in regions of high hydrographic variability in order to obtain more accurate regional and long-term interpretation of the ocean biological and biogeochemical cycles.

5.1.5. Will ocean acidification impact phytoplankton productivity under nutrient fertilization?

A major effort has been made to understand the effects of OA in phytoplankton productivity, yet many uncertainties remain unresolved. Theoretically, enhanced pCO_2 in the future oceans should benefit phytoplankton productivity by alleviating current CO_2 limitation of the RubisCO enzyme (Beardall and Raven, 2004b; Reinfelder, 2011; Mackey, 2015). Nevertheless, contradictory results have been obtained so far. Most experiments reporting positive CO_2 effects in phytoplankton production have been carried out in arctic and temperate waters (e.g., Riebesell et al., 2007; Bellerby et al., 2008; Tortell et al., 2008). The only ocean acidification study testing primary production responses in oligotrophic regions, as far as we know, reported non-statistically significant effects of increasing pCO_2 on primary production under nutrient deplete conditions (Maugendre et al., 2017). Our data partially agree with this finding: On the one hand, under strict oligotrophic conditions (phase I), no significant CO_2-related effects were observed in phytoplankton PP, B, and Chl *a* (Tables 4.2, 4.3 and 4.4). Phytoplankton size-groups productivity also remained unresponsive to CO_2 perturbations during oligotrophic phase, while Taucher et al. (2017) reported significant CO_2 effects on the whole planktonic community (including protozoa and mesozooplankton) for the same experiment. On the other hand, after nutrient addition, phytoplankton productivity scaled with increasing pCO_2 concentrations, suggesting a synergetic effects of CO_2 levels and nutrient availability (Tables 4.2, 4.3 and 4.4). Alvarez-Fernandez et al. (2018) combining results from 4 mesocosms studies carried out in arctic and temperate waters, observed that phytoplankton

only benefit of high CO_2 concentration under nutrient replete conditions, and thus reached to our same hypothesis. Wei et al. (2021) also observed synergetic effects of increasing CO_2 and phosphorus availability on oligotrophic phytoplankton communities of Western Pacific. The whole phytoplankton community positively responded to high pCO_2 levels. Nevertheless, larger cells productivity displayed the largest CO_2-related enhancement as linear regressions slopes indicated. This agrees with experimental and modeling studies reporting the existence of winners and looser in a future acidified ocean (Dutkiewicz et al., 2013; Kroeker et al., 2013; Schulz et al., 2017; Alvarez-Fernandez et al., 2018). However, it is hard to discern whether those different increments rates were due to a distinguishing response of the phytoplankton size groups or a higher grazing pressure on smaller organisms.

5.1.6. What would be the potential biogeochemical implications?

We are starting to understand the potential impact that climate change induces to the global ocean environment (IPCC 2014, 2021), though how the different marine physical, biological, and biogeochemical systems will response to those stressors at regional scales is still matter of discussion. EBUS will be one of the regions projected to suffer the most intense effects (IPCC 2014, 2021). However, predicting how EBUS will respond to climate change remains very difficult: On the one hand, rising temperatures are expected to result in stronger thermal stratification, which would lead to a decrease in deep, new nutrient supply to the euphotic zone and thus in NPP (Pörtner et al., 2014; Bindoff et al., 2019). Decadal trends evidence a decrease or at least not an increase in primary production in all EBUS for the last ~40 years (Behrenfeld et al., 2006;

Martinez et al., 2009; Chavez et al., 2011; Gómez-Letona et al., 2017). Nevertheless, both trends and forecast, should be taken carefully as they depend on productivity models outputs that displays significant bias, in some cases providing contradictory results for the different models (Gómez-Letona et al., 2017); and their resolution does not allow to resolve mesoscale structure and therefore their contribution to global NPP besides in oligotrophic region eddy-driven new production may account up to 40 % of the total (McGillicuddy et al., 2007).

On the other hand, future changes in wind patterns as a result of global warming are predicted to increase upwelling-favourable winds in EBUS, which would also lead to an increase of the eddy kinetic energy and associated upward pumping of nutrients in these regions (Demarcq, 2009; Sydeman et al., 2014; Wang et al., 2015; Martínez-Moreno et al., 2021; Richards et al., 2021). Phytoplankton thriving in a future warmer oligotrophic subtropical ocean with enhanced CO_2 levels could therefore be patchily fertilized by increased mesoscale and submesoscale variability inducing nutrient pumping into the surface ocean. Under this scenario, primary productivity would increase by CO_2-nutrients synergetic effects according with our findings. Whether this PP increase may counteract the negative effects of enhanced stratification in subtropical oligotrophic regions remains unknown. To address this question, improvements of primary productivity models estimations and grid resolution, as well as further research in the combined effects of climate change are necessary.

5.2. General conclusions

Attending to the results reported throughout the thesis, the main conclusions are:

I. Submesoscale motions associated with mesoscale eddies not considered in regular mesoscale cruises, modulated phytoplankton distribution inducing to short-term patchiness, dominated by best adapted groups.

II. The interaction between meso-submesoscale processes results in frontal zones where Ageostrophic Secondary Circulation (ASC) develops, adding complexity to an already complicated hydrography, and thus favoring phytoplankton patchiness

III. Wind stress triggers ASC in the convergent front as observed at the lee of Gran Canaria island

IV. ASC modulates phytoplankton distribution and community structure, although the organisms were strongly subjected to frontogenesis and frontolisis phases.

V. The short-term temporal variability may contribute as much as short-term spatial variability to phytoplankton distribution across unstable mesoscale fronts.

VI. Synergetic effects of high CO_2 levels and nutrient fertilization enhanced primary production, biomass and Chl *a.* Although all the phytoplankton community positively respond to increasing CO_2 concentrations, larger cells presented the largest CO_2-related enhancement

VII. Thus, in a future ocean, where meso-submesoscale processes dominate, large phytoplankton would benefit from patchy fertilization of high nutrient and high CO_2 levels.

Caminante, son tus huellas
el camino y nada más,
Caminante, no hay comino,
se hace camino al andar.

Antonio Machado, Campos de Castilla
1912

5.3. Future research

The research that comprise this thesis contributes to enhance our knowledge about the linkages between meso- and submesoscale processes, and their impacts on phytoplankton variability and community structure. However, some loose threads have been left and new questions have been put forward. In the following section we pose, under our perspective, the main unresolved and raised question.

5.3.1. Unresolved questions

- The role of phytoplankton functional groups and diversity in driving changes in primary and export production is a fundamental question in oceanography and carbon cycle science. Enhancement of microplankton biomass, for example, is associated with largest primary production rates, intense carbon fluxes into the deep ocean, and higher transference into upper trophic levels. Even though the subtropical oligotrophic waters of the CanC are dominated by small cyanobacteria, vertical nutrient fluxes driven by meso-submesoscale processes may supply new nutrients to the surface layers stimulating microplankton growth. This may results in hotspot of high primary production and export rates. During this thesis, microplankton activity was only

reported for **Chapter 4** since traditional "particle counting" method used for microplankton analysis (Microscopy) is tedious and time consuming. We could not therefore address the impact of meso-submesoscale processes on microphytoplankton groups. The recent development of new imaging analysis merging flow cytometry technologies and imaging microscope such as FlowCam, is expected to reduce the time needed for microscopy analysis. Furthermore, these new technologies captures digital images of particles in a fluid stream using laser light detection, enabling the measurement of many cell parameters, such as length, width, equivalent spherical diameter and fluorescence. More accurate cell-size and biomass measurements should be therefore achieved with these technologies.

- Unlike microplankton, we measured the abundances of nanoplankton cells as reported in **Chapter 2**. However, the drivers modulating nanoplankton distribution remain unclear mostly due to the lack of information about mixotrophy in natural phytoplankton communities. Due to their metabolic plasticity, it is hard to discern the ecological role played by mixotrophs at certain time. Experimental and *in situ* studies are necessary to improve our knowledge about mixotrophic metabolisms and their role in the biogeochemical cycles. Nevertheless, the complexity of the available methodologies difficult their implementation in oceanographic cruises. First steps may consist in micro- and mesocosms experiments focused on studying natural communities under controlled conditions. Disentangling mixotrophy in natural communities could solve several

remaining questions about marine biogeochemical cycles as the available small literature suggest.

- Though we were able to indirectly assess vertical motions associated with submesoscale fronts, further questions remain about the intensity and the horizontal and vertical scope of these structures. As far as we know, there is only one reliable method to measure submesoscale vertical velocities, i.e., by applying the omega equation. This approach requires tridimensional hydrography fields that are only achieved by means of autonomous and towed underwater vehicles. During projects PUMP (Study of the Vertical Oceanic Pump in Mesoscale Eddies; CTM2012-33355) and FLUXES (Constraining Organic Carbon Fluxes in and Eastern Boundary Upwelling Ecosystems (NW Africa): The Role of non-Sinking carbon in the context of the "biological pump"; CMT2015-69392-C3), we studied the phytoplankton community structure across and ITE and a mesoscale front at submesoscale range by combining in situ measurements and autonomous vehicles. The information compiled during both projects will helpfully contribute to better understand the effect of vertical velocities in phytoplankton community structure, distribution, and metabolisms.

5.3.2. Raised questions

- The results obtained in **Chapter 2** indicate that submesoscale processes associated with eddies as well as the interaction of mesoscale structures have a profound impact in phytoplankton

distribution and variability. In **Chapter 3**, on the other hand, we observe that the effects of submesoscale frontal dynamics on phytoplankton distribution depended on the state of development of the front. Phytoplankton distribution across mesoscale eddies could thus vary along the life cycle of these structures as well. Nevertheless, the linkages between mesoscale and sub-mesoscale dynamics, and their biological-biogeochemical effects, are still largely unknown. The lack of information on processes-oriented field studies with high spatial resolution, necessary to understand submesoscale dynamics and validate coupled physical-biological models is dumbing our knowledge. In the short-term, time repeating studies are necessary in order to shed light into this subject and to enlarge *in situ* data bases, from which model can be validated.

We expect to test this hypothesis within the research project e-IMPACT (Biogeochemical Impact of mesoscale and sub-mesoscale processes along the life history of cyclonic and anticyclonic eddies), in wich I will participate. The project aims to study the linkages between the dynamics of mesoscale and sub-mesoscale processes occurring along the life history of cyclonic and anticyclonic eddies in the Canary Eddy Corridor (CEC), and their effects on the structure and metabolism of the planktonic community, as well as in their role in the vertical carbon flux to the deep ocean.

- In **Chapter 5** we found that OA effects on phytoplankton organisms, as most climate change-related impacts, scaled with

increasing CO_2. Climate change impacts will be then considerably worse with a high emissions scenario than with a scenario that limits the temperature increase to 2 °C relative to pre-industrial levels. Current emission reduction pledges under the 2015 Paris Agreement are insufficient to keep global temperature below +2 °C in 2100 relative to pre-industrial level and therefore additional actions are required to mitigate this and other undesired climate change effects. Negative emissions technologies (NET's) are means of withdrawing greenhouse gases from the environment such that atmospheric concentrations are reduced. To what extent, and under what conditions, the large-scale deployment of ocean-based NETs could contribute to realistic pathways for achieve climate neutrality is still largely unknown. During the EU projects Ocean ArtUp and OceaNETs, we have tested the feasibility of artificial upwelling, ocean fertilization, and ocean alkalinization as NETs by means of mesocosms experiments. In particular, we studied the response of phytoplankton community structure and metabolisms to the biogeochemical changes induced by NETs. Scientific papers are being prepared based on the compiled data.

Chapter Six

Resumen en español

6.1. Introducción

Las capas superficiales y bien iluminadas de los océanos están dominadas por una gran diversidad de organismos unicelulares que derivan con las corrientes y que se conocen conjuntamente como fitoplancton. El primer organismo fitoplanctónico aparece hace unos 2.600 millones de años, evolucionando a través de condiciones ambientales dispares en los cientos de miles de especies que actualmente pueblan los océanos (Fig. 1.1.; Hedges et al., 2001; Falkowski et al., 2004; Yoon et al., 2004; Simon et al., 2009; Cardona, 2019). A pesar de que esta miscelánea de historias evolutivas resultó en una gran variedad de rasgos morfológicos y fisiológicos (Chrétiennot-Dinet et al., 1993; Smetacek, 2001; Beardall et al., 2009; Litchman et al., 2015; Worden et al., 2015; Stoecker et al., 2017), para la mayoría de estos organismos su principal fuente de energía proviene de la luz solar, la cual captan y usan para transformar materia inorgánica en materia orgánica, i.e. la Fotosíntesis. A pesar de que suponen menos del 1% de la biomasa autotrófica de La Tierra (~1 Gt C; Field et al., 1998; Le Quéré et al., 2005; Bar-On et al., 2018), estos organismos son los responsables de alrededor del 50% de la producción primaria global (~50 Gt C·yr-1;

Falkowski, 1994; Field et al., 1998; Behrenfeld et al., 2005; McClain, 2009; Buitenhuis et al., 2013a).

Uno de los rasgos más importantes, ecológicamente hablando, de los organismos fitoplanctónicos es el tamaño celular. De hecho, desde la biología individual de cada organismo hasta la de la comunidad completa, está influenciada por el tamaño celular (Brown et al., 2004; Litchman and Klausmeier, 2008; Litchman et al., 2010; Marañón, 2015). Debido al papel clave que juega el tamaño en la ecología del fitoplancton, se ha usado históricamente para agrupar a los diferentes organismos que componen la comunidad (Fig. 1.2; Sieburth and Smetacek, 1978). Así el fitoplancton, el cual se expande por un rango de tamaño que va de las ~0.2 µm a más de 200 µm, quedaría dividido en tres grupos de tamaños (Figs. 1.1 y 1.2); picoplancton (0.2 - 2 µm), nanoplancton (2 - 20 µm) y microplancton (20 - 200 µm). La distribución de la biomasa de la comunidad entre los diferentes grupos de tamaño es lo que se conoce como estructura de la comunidad, y es clave en la ecología de los ecosistemas pelágicos (Falkowski and Oliver, 2007; Finkel et al., 2010; Marañón, 2015). Está dominada por complejas interacciones físicas, tales como temperatura o disponibilidad de luz (Fuhrman et al., 2008; Righetti et al., 2019); interacciones biológicas cómo competición por lo recursos o pastaje (Vallina et al., 2014; Ward et al., 2014); dispersión (Fuhrman, 2009; Ward et al., 2021); y la disponibilidad de nutrientes inorgánicos (Acevedo-Trejos et al., 2013; Maranón et al., 2014; Mousing et al., 2018). La producción primaria en el océano superficial, los flujos de carbono hacia el océano profundo o las pesquerías dependen íntimamente de la estructura de la comunidad (Arrigo, 2005; Fuhrman, 2009; Guidi et al., 2009, 2016; Marañón, 2015). Y en menor medida,

también la regulación del clima de La Tierra por parte del océano y la mayoría de los ciclos biogeoquímicos oceánicos (Boyd, 2015; Basu and Mackey, 2018; Buesseler et al., 2020).

A gran escala, las características físico-biogeoquímicas de cada región modulan la estructura de la comunidad fitoplanctónica. En las regiones dónde existe una alta disponibilidad de nutrientes inorgánicos en la capa fótica, como por ejemplo las aguas ecuatoriales y las zonas de afloramiento, la comunidad está dominada por organismos de mayor tamaño, principalmente diatomeas y dinoflagelados (Alvain et al., 2008; Buitenhuis et al., 2013b). Estos organismos presentan alta capacidad para asimilar nuevos nutrientes, lo que les da ventaja sobre organismos más pequeños en condiciones de abundancia (Uitz et al., 2010; Malviya et al., 2016; Tréguer et al., 2018). En las regiones dónde los nutrientes en superficie escasean, como los giros subtropicales, encontramos el escenario opuesto. La comunidad está dominada por pequeñas cianobacterias del género *Prochlorococcus* y *Synechococcus*, que gracias a la alta difusión de nutrientes por volumen celular (Raven, 1998; Marañón, 2015) y la elevada absorción de luz por unidad de clorofila (Finkel, 2001; Finkel et al., 2004) que le confiere su pequeño tamaño, son capaces de proliferar en condiciones de baja disponibilidad de nutrientes y luz.

A más corta escala, i.e., meso y submesoscala, la hidrodinámica asociada a remolinos, filamentos y frentes pueden inducir cambios en la distribución del fitoplancton y por lo tanto en la estructura de la comunidad (McGillicuddy et al., 2003; Benitez-Nelson and McGillicuddy, 2008; Sweeney et al., 2003; Baltar et al., 2009; Mouriño-

Carballido, 2009; Davis and McGillicuddy, 2006). Los cambios inducidos en la comunidad fitoplanctónica por estas estructuras depende de las características hidrodinámicas de cada proceso:

Los remolinos de mesoscala pueden ser divididos en dos grupos basándose en el sentido de su giro. En el hemisferio Norte (Sur), los remolinos ciclónicos (CE) presentan vorticidad vertical relativa negativa (positiva), es decir, giran en sentido antihorario (horario). Los remolinos anticiclónicos (AE) en cambio presentan vorticidad vertical positiva (negative), girando en sentido horario (antihorario). Durante su formación los remolinos capturan en su núcleo parcelas de agua las cuales pueden ser transportadas lejos de su lugar de origen, así como los organismos fitoplanctónicos que contenga y sus características biogeoquímicas ("Eddy Trapping"; Fig. 1.3.b; d'Ovidio et al., 2013; Gaube et al., 2014). Una vez formado, el bombeo de Ekman asociado al giro del remolino produce velocidades verticales en el núcleo, hacía la superficie en los CE y hacia el fondo del océano en los AE. El afloramiento producido en los CE trae aguas frías y profundas cargadas de nutrientes hacía las capas bien iluminadas estimulando el crecimiento del fitoplancton de mayor tamaño, como las diatomeas. El hundimiento que se produce en los AE, en cambio, lleva aguas superficiales agotadas de nutrientes hacía capas más profundas favoreciendo el crecimiento de pequeñas cianobacterias y picoeucariotas ("Eddy Pumping"; Fig. 1.3.c; Falkowski et al., 1991; Arístegui et al., 1997; Mcgillicuddy Jr et al., 1998). La periferia del remolino también puede producir cambios en la comunidad fitoplanctónica. En su flujo rotacional, los remolinos perturban las aguas colindantes siendo capaces de arrastrar las partículas

flotantes cómo el fitoplancton y redistribuirlas formando pequeños filamentos (“Eddy Stirring”; Fig. 1.3.a; Abraham, 1998; Martin, 2003).

A diferencia de los remolinos de mesoscala que pueden llegar a ocupar hasta un 25% de la superficie oceánica (Chelton et al., 2007, 2011), los filamentos están restringidos a la línea de costa dónde son generados como consecuencia de la interacción de las corrientes de gran escala con irregularidades de la costa como los cabos (Haynes et al., 1993; Arístegui et al., 2009; Sangrà et al., 2015; Lovecchio et al., 2018; Santana-Falcón et al., 2020). En sistemas de afloramiento costeros orientales (EBU’s) como la corriente de Canarias (CanC), los filamentos transportan aguas ricas en nutrientes, materia orgánica y clorofila del afloramiento hacia las aguas oligotróficas del giro subtropical del Atlántico Norte. Cómo consecuencia, producen zonas de alta productividad dominadas por organismos del microplancton en las aguas poco productivas del giro subtropical (Barton et al., 2004; Álvarez-Salgado et al., 2007; Cravo et al., 2013; Santana-Falcón et al., 2016, 2020).

A diferencia de los remolinos y la mayoría de los filamentos costeros, los procesos asociados a zonas frontales operan a escalas inferiores al radio de deformación de Rossby, lo cual se conoce como submesoescala. La hidrodinámica submesoescalar ha atraído la atención de la comunidad científica en las últimas dos décadas, principalmente debido a dos factores: (1) La mayoría de estudio teóricos y de modelización llevados a cabo hasta el momento, concluyen que la intensidad de las velocidades verticales y horizontales generadas en zonas frontales pueden ser de hasta 2 ordenes de magnitud superiores a las generadas por remolinos mesoescalares (Mahadevan and Tandon, 2006; Gaube et al., 2014), y por

lo tanto, sus efectos sobre la comunidad fitoplanctónica y la biogeoquímica son mayores (Lévy et al., 2001; Mahadevan and Campbell, 2002; Mahadevan and Tandon, 2006; Klein and Lapeyre, 2009). (2) Los frentes submesoescalares son estructuras generalizadas en las capas superficiales de los océanos que se pueden generar mediante varios procesos a partir de pequeños gradientes horizontales preexistentes (McWilliams, 2016); en los planos de encuentro entre remolinos de mesoescala y el agua circundante (Barceló-Llull et al., 2017a); y/o como resultado de la interacción entre procesos mesoescalares (Klein and Lapeyre, 2009; McWilliams, 2016; Lévy et al., 2018).

La dinámica frontal se caracteriza por la presencia de circulación ageostrófica secundaria (ASC). El aumento de las velocidades horizontales a lo largo del frente lleva a un desequilibrio del balance geostrófico. Para restaurar dicho equilibrio, se generan velocidades verticales positivas en el lado más cálido del frente (menos denso), y negativa en lado frío (más denso) (Fig. 1.4; Hoskins and Bretherton, 1972; Hoskins, 1982; Mahadevan and Tandon, 2006; Thomas et al., 2008; Klein and Lapeyre, 2009; McWilliams, 2016). Como el fitoplancton responde a las dinámicas frontales depende principalmente de que factor esté limitando el crecimiento de la comunidad; nutrientes o luz (Mahadevan, 2016; Lévy et al., 2018). En el lado cálido del frente, las velocidades verticales afloran aguas ricas en nutrientes desde capas más profundas hacia la zona fótica, favoreciendo un aumento de la producción primaria. De la misma manera, las comunidades fitoplanctónicas son arrastradas hacia capas mejor iluminadas aliviando la limitación del crecimiento por falta luz (Mahadevan and Archer, 2000;

Lévy et al., 2001; Pidcock et al., 2010; Taylor and Ferrari, 2011; Ramachandran et al., 2014). En el lado más denso, las aguas superficiales son hundidas, lo que puede conllevar una disminución en la productividad o el aumento de los flujos de carbono hacia el océano profundo (Niewiadomska et al., 2008; Lathuiliere et al., 2011).

Los efectos del cambio climático son otro factor a tener en cuenta en la variabilidad, distribución, metabolismo y estructura de la comunidad del fitoplancton. Le emisión antropogénica de gases de efecto invernadero (GHG) desde la Revolución Industrial (principalmente CO2; Fig. 1.5), está produciendo un cambio en la composición química de la atmósfera y el océano (IPCC 2014, 2016, 2021). El aumento de las concentraciones del CO_2 atmosférico desestabiliza el equilibrio atmósfera-océano, favoreciendo la disolución de este GHG a través de la superficie oceánica (Zebee, 2001). Así, los océanos globales han captado sobre el 30% de las emisiones de origen antrópico, lo que está produciendo un aumento en la acidez de las aguas (Sabine et al., 2004; Doney et al., 2009; Khatiwala et al., 2009; Gattuso, 2011; Khatiwala et al., 2013). El aumento del CO_2 disuelto en las aguas superficiales debería aliviar la actual limitación de la fotosíntesis por este GHG, favoreciendo el incremento de la producción primaria (Beardall and Raven, 2004a; Reinfelder, 2011; Mackey, 2015). Los efectos del calentamiento del medio marino por otro lado, se esperan que produzcan un aumento de la estratificación del océano, limitando el afloramiento de nutrientes a superficie y por lo tanto restringiendo la producción primaria (Pörtner et al., 2014; Bindoff et al., 2019). Debido a las diferencias fisiológicas de los distintos grupos que conforman el fitoplancton, varios autores han sugerido que los efectos del cambio climático podrían ser específicos de cada uno de estos grupos,

lo que conllevaría una situación de "ganadores" y "perdedores" (Dutkiewicz et al., 2013; Kroeker et al., 2013; Bach et al., 2017). O lo que es lo mismo, los efectos del cambio climático podrían producir grandes cambios en la estructura de la comunidad del fitoplancton a nivel global.

6.2. Estado actual del tema

Los remolinos ciclónicos y anticiclónicos de mesoescala -O(100 km)- son estructuras habituales en todos los océanos del mundo. La mayoría se concentra en corredores de remolinos que se propagan hacia el oeste y que se encuentran en ambos hemisferios de los principales océanos (Chelton et al., 2011). En particular, se observa una alta actividad mesosescalar asociada a los cuatro grandes sistemas de afloramiento, donde estos corredores de reomolinos se observan recurrentemente a lo largo de las zonas de transición entre la costa y el océano abierto y al sur de los principales archipiélagos (Chaigneau et al., 2009; Sangrà et al., 2009). Se cree que el impacto de los remolinos de mesoescala en la mejora de la productividad y la contribución a la bomba biológica de carbono es de suma importancia (McGillicuddy, 2016; Mahadevan, 2016), aunque todavía existe una gran incertidumbre sobre la magnitud de esta contribución a escala regional y global (Dufois et al., 2016; Resplandy et al., 2019). Los trabajos anteriores que combinan teoría, observaciones de campo y de teledetección, y la modelización han ayudado a comprender las relaciones entre los procesos físicos y las respuestas biológicas y biogeoquímicas en la mesoescala (McGillicuddy, 2016; Lehahn et al., 2017). Sin embargo, recientes estudios han sugerido que los procesos físicos que operan a submesoescala (0.1-10 km) son

más relevantes que la variabilidad mesoescalar para la productividad del fitoplancton (Mahadevan, 2016), así como para la subducción de carbono orgánico particulado hacia el interior del océano (Omand et al., 2015; Resplandy et al., 2019), con grandes implicaciones a escala global.

A pesar de la importancia atribuida a la variabilidad submesoescalar en la modulación de la estructura de la comunidad y la productividad del plancton (Lévy et al., 2012), los vínculos entre la dinámica de mesoescala y submesoescala, así como sus efectos biológicos y biogeoquímicos, siguen siendo en gran medida desconocidos. La causa es la escasa información disponible sobre estudios de campo orientados a los procesos con alta resolución espacial, necesarios para comprender estos procesos y validar los modelos físico-biológicos (Omad et al., 2015). Además, la evolución de estos procesos y sus efectos en el ecosistema planctónico a lo largo de la historia vital de los remolinos ciclónicos y anticiclónicos; y las zonas frontales se desconocen casi por completo.

6.3. Objetivos y estructura de la tesis

El objetivo principal de esta tesis es el de estudiar la variabilidad espaciotemporal a submesosecala de la estructura de la comunidad del fitoplancton y la producción primaria inducida por procesos meso y submesoescalares. El fitoplancton es la piedra angular de las redes tróficas marinas, de los ciclos biogeoquímicos oceánicos, de la bomba del carbono y de la regulación oceánica del clima terrestre. Por ello, el estudio de los factores que intervienen en la dinámica del fitoplancton ha atraído el interés de los científicos marinos desde los inicios de la

oceanografía. Junto con el desarrollo y la mejora de las imágenes por satélite, las escalas de los procesos que dominan la distribución del fitoplancton se han ido reduciendo desde las corrientes a gran escala, a los procesos de mesoescala como los remolinos y, en las últimas décadas, a los procesos de submesoescala como las dinámicas frontales. Sin embargo, a pesar de que los procesos submesoescalares se consideran en la actualidad el principal motor que gobierna la distribución del fitoplancton y los flujos de carbono, debido a la complejidad inherente a los muestreos de alta resolución, el conocimiento sobre la variabilidad espacial del fitoplancton inducida por la submesoescala se limita, en su mayor parte, a los resultados comunicados por estudios teóricos y de modelización. La información disponible sobre su variabilidad temporal es aún más escasa. Con el fin de ampliar el conocimiento sobre la variabilidad a corto plazo de las comunidades fitoplanctónicas, se abordaron varios objetivos específicos para responder a las siguientes preguntas:

I. ¿Cómo se distribuyen los organismos del fitoplancton a través de los remolinos de mesoescala a resolución submesoescalar?

II. ¿Qué factores rigen esta distribución?

III. ¿Influye la interacción de los procesos de mesoescala en la distribución del fitoplancton?

IV. ¿Cómo afecta la dinámica frontal submesoescalar a la variabilidad espaciotemporal del fitoplancton?

V. ¿Qué papel juega el tiempo en la variabilidad del fitoplancton?

VI. ¿Influirá la acidificación de los océanos sobre la productividad del fitoplancton en situaciones de fertilización con nutrientes?

VII. ¿Cuáles son las posibles implicaciones biogeoquímicas?

Las preguntas I-III se responden en el **Capítulo 2**, en el que se describen los resultados de una campaña oceanográfica que atravesó un remolino ciclónico que interactuaba con dos remolinos anticiclónicos y un filamento proveniente del afloramiento costero. La sección consistió en 20 estaciones separadas 4 millas náuticas entre sí. En cada estación se tomaron muestras físicas, biogeoquímicas y biológicas. Con el fin de conocer los factores que rigen la distribución del plancton a submesoescala, se realizaron análisis de redundancia basados en la distancia.

Este trabajo ha dado lugar a la siguiente publicación:

"Drivers of Plankton Distribution Across Mesoscale Eddies at Submesoscale Range", en Frontiers in Marine Science como parte de la colección *"Small Scale Spatial and Temporal Patterns in Particles, Plankton and Other Organisms"*.

Como sugieren los estudios teóricos y de modelización, el movimiento físico asociado a las zonas frontales de submesoescala puede afectar a la distribución y variabilidad del fitoplancton. En el **Capítulo 3** se presentan resultados novedosos sobre el desarrollo y decaimiento de un frente de submesoescala al sur de Gran Canaria. El frente fue muestreado a escalas espaciotemporales no consideradas en los cruceros oceanográficos regulares con el fin de abordar las preguntas IV y V.

Este trabajo ha dado lugar a la siguiente publicación:

“Shor-Term Spatiotemporal Variability in Picoplankton Induced by a Submesoscale Front South of Gran Canaria (Canary Islands)”, en Frontiers in Marine Science como parte de la colección *"Island Dynamical Systems: Ocean and Biogeochemical Processes"*.

Actualmente estamos experimentando el efecto del cambio climático y lo seguiremos haciendo al menos hasta mediados de siglo según todos los escenarios de emisiones considerados por el Panel Intergubernamental de Expertos sobre el Cambio Climático (IPCC, 2021). Con el objetivo de contribuir a aumentar en el conocimiento sobre los potenciales efectos que el cambio climático produce en las comunidades fitoplanctónicas, realizamos un experimento de mesocosmos en la costa este de Gran Canaria. Nuestra hipótesis es que la acidificación del océano bajo una situación de fertilización de nutrientes, como ocurre en los núcleos de remolinos ciclónicos, aumenta la productividad primaria en aguas oligotróficas. El resultado de este experimento se recoge en el **Capítulo 4** que trata de resolver las preguntas VI y VII.

Este trabajo ha dado lugar a la siguiente publicación:

High CO_2 Under Nutrient Fertilization Increases Primary Production and Biomass in Subtropical Phytoplankton Communities: A Mesocosm Approach, en Frontiers in Marine Science como parte de la colección *"Impacts of CO_2 perturbations on the Ecology and Biogeochemistry of Plankton Communities During a Simulated Upwelling Event: A mesocosms Experiment in Oligotrophic Subtropical Waters "*.

La discusión general de los trabajos de la tesis y las conclusiones generales extraídas se presentan en el **Capítulo 5**.

6.4. Principales resultados y conclusiones

Los principales resultados obtenidos durante los estudios que engloba esta tesis, así como las conclusiones que se extraen de ellos, se resumen a continuación:

- La dinámica submesoescalar asociada a los remolinos de mesoescala modulan la distribución del fitoplancton. Durante la campaña RODA, recogida en el **Capítulo 2**, observamos que las corrientes submesoscalares inducen cambios biogeoquímicos en pequeñas parcelas de aguas, favoreciendo el crecimiento de unos u otros organismos dependiendo de las características del nuevo nicho. Esto se traduce en una distribución caracterizada por pequeños "parches" dominados por el grupo mejor adaptado. Este resultado pone de manifiesto la necesidad de estudios de campo a resolución submesoescalar, la cual rara vez es considerada en campañas oceanográfica

- La interacción entre los procesos de meso-submesoescala estudiados durante el proyecto RODA, dieron lugar zonas frontales dominadas por ASC, añadiendo complejidad a la ya intrincada hidrografía y favoreciendo así la variabilidad del fitoplancton. La interacción del AE1 y el CE resultó en una zona frontal dominada por intensas corrientes verticales y horizontales. La acumulación de bacterias como consecuencia de la convergencia de los dos remolinos, así como su hundimiento

hasta más de 200 m como consecuencias de velocidades verticales de subducción, o el crecimiento de organismos más grandes como consecuencia del afloramiento de nutrientes resultaron de la hidrodinámica del frente.

- El estrés del viento es el desencadenante del frente convergente a sotavento de Gran Canaria. Barton et al. (2000) y Basterretxea et al. (2002) ya habían propuesto esta relación como causante de los frentes en la estela de Gran Canaria, sin embargo, debido a que ambos estudios estaban restringidos a una sola sección, no pudieron comprobar esta hipótesis. La intima relación observada en el **Capítulo 3** entre la intensidad y la evolución temporal del viento, y del frente apoyan la hipótesis de Barton y Basterrexea. La presencia de ASC además sugiere que la teoría de los efectos no lineales de Ekman propuesta por Thomas, (2005) y Thomas and Lee, (2005) podría ser el mecanismo detrás de la formación y destrucción de estos frentes.

- La ASC moduló la distribución del picoplancton y la estructura de la comunidad, aunque se observaron efectos diferenciados para las fases de frontogénesis y frontolisis. Durante su formación/intensificación, la distribución y la estructura del picoplancton presentaron simetría con respecto al frente, sugiriendo que la hidrodinámica del frente induce cambios en la comunidad. Con la destrucción del frente, tanto la hidrodinámica como la comunidad picoplanctónica presentaron indicios de restauración a condiciones iniciales. Esto supuso una

disminución drástica de la variabilidad en la distribución y la estructura de la comunidad.

- Los cambios temporales en la comunidad fitoplanctónica son una fuente de variabilidad tan o más importante que los cambios espaciales. Las contribuciones de cada una de estas fuentes de variabilidad a la varianza total de la comunidad (**Capítulo 3**) ponen de manifiesto que en la capa de mezcla la variabilidad del fitoplancton depende de tiempo y espacio de igual manera. Sin embargo, los cambios temporales dominan la varianza de las comunidades que habitan el máximo profundo de clorofila.

- La sinergia entre altos niveles de CO_2 y la fertilización con nutrientes producen un claro aumento de la productividad de las comunidades fitoplanctónicas de aguas oligotróficas. En los resultados obtenidos durante el experimento de mesocosmos recogido en el **Capítulo 4**, se observa que, bajo condiciones de alta disponibilidad de nutrientes, altas concentraciones de CO_2 en el océano favorecen la producción primaria, la biomasa y la clorofila del fitoplancton oligotrófico.

- De la anterior conclusión se desprende que, bajo las previsiones de incremento de la actividad de meso y submesoscala en los EBUS, las comunidades fitoplanctónicas fertilizadas por estos fenómenos se verían beneficiadas por un incremento en las concentraciones de CO_2 en el océano.

- Toda la comunidad del fitoplancton oligotrófico respondió positivamente al aumento de las concentraciones de CO_2. A pesar

de que varios trabajos anteriores sugieren que el cambio climático puede llevar a una situación de ganadores y perdedores en cuanto al fitoplancton se refiere, toda la comunidad, es decir, el pico, nano y microplancton estudiadas en el **Capítulo 4** se beneficiaron de las altas concentraciones de CO_2 y nutrientes, si bien es cierto que los organismos del microplancton presentaron el mayor incremento de productividad.

References

Abraham, E. R. (1998). The Generation of Plankton Patchiness by turbulent stirring. Science (80-.). 391, 577–581.

Abram, N., J.-P. Gattuso, A. Prakash, L. Cheng, M.P. Chidichimo, S. Crate, H. Enomoto, M. Garschagen, N. Gruber, S. Harper, E. Holland, R.M. Kudela, J. Rice, K. Steffen, and K. von Schuckmann, 2019: Framing and Context of the Report. In: IPCC Special Report on the Ocean and Cryosphere in a Changing Climate [H.-O. Pörtner, D.C. Roberts, V. Masson-Delmotte, P. Zhai, M. Tignor, E. Poloczanska, K. Mintenbeck, A. Alegría, M. Nicolai, A. Okem, J. Petzold, B. Rama, N.M. Weyer (eds.)]. In press.

Acevedo-Trejos, E., Brandt, G., Merico, A., and Smith, S. L. (2013). Biogeographical patterns of phytoplankton community size structure in the oceans. *Glob. Ecol. Biogeogr*. 22, 1060–1070. doi:10.1111/geb.12071.

Acevedo-Trejos, E., Marañón, E., and Merico, A. (2018). Phytoplankton size diversity and ecosystem function relationships across oceanic regions. *Proc. R. Soc. B Biol. Sci*. 285. doi:10.1098/rspb.2018.0621.

Agawin, N. S. R., Duarte, C. M., and Agustí, S. (2000). Nutrient and temperature control of the contribution of picoplankton to phytoplankton biomass and production. *Limnol. Oceanogr*. 45, 591–600. doi:10.4319/lo.2000.45.3.0591.

Allen, J. T., Brown, L., Sanders, R., Moore, C. M., Mustard, A., Fielding, S., et al. (2005). Diatom carbon export enhanced by silicate upwelling in the northeast Atlantic. *Nature* 437, 728–732. doi:10.1038/nature03948.

Alvain, S., Moulin, C., Dandonneau, Y., and Loisel, H. (2008). Seasonal distribution and succession of dominant phytoplankton groups in the global ocean: A satellite view. *Global Biogeochem. Cycles* 22. doi:10.1029/2007GB003154.

Alvarez-Fernandez, S., Bach, L. T., Taucher, J., Riebesell, U., Sommer, U., Aberle, N., et al. (2018). Plankton responses to ocean

acidification: The role of nutrient limitation. *Prog. Oceanogr*. 165, 11–18. doi:10.1016/j.pocean.2018.04.006.

Álvarez-Salgado, X. A., Arístegui, J., Barton, E. D., and Hansell, D. A. (2007). Contribution of upwelling filaments to offshore carbon export in the subtropical Northeast Atlantic Ocean. *Limnol. Oceanogr*. 52, 1287–1292. doi:10.4319/lo.2007.52.3.1287.

Anderson, T. R., and Turley, C. M. (2003). Low bacterial growth efficiency in the oligotrophic eastern Mediterranean Sea: A modelling analysis. *J. Plankton Res*. 25, 1011–1019. doi:10.1093/plankt/25.9.1011.

Arcos-Pulido, M., Rodríguez-Santana, A., Emelianov, M., Paka, V., Arístegui, J., Benavides, M., et al. (2014). Diapycnal nutrient fluxes on the northern boundary of Cape Ghir upwelling region. *Deep. Res. Part I Oceanogr. Res. Pap.* 84, 100–109. doi:10.1016/j.dsr.2013.10.010.

Arístegui, J., Barton, E. D., Álvarez-Salgado, X. A., Santos, A. M. P., Figueiras, F. G., Kifani, S., et al. (2009). Sub-regional ecosystem variability in the Canary Current upwelling. *Prog. Oceanogr.* 83, 33–48. doi:10.1016/j.pocean.2009.07.031.

Arístegui, J., Barton, E. D., Tett, P., Montero, M. F., García-Muñoz, M., Basterretxea, G., et al. (2004). Variability in plankton community structure, metabolism, and vertical carbon fluxes along an upwelling filament (Cape Juby, NW Africa). *Prog. Oceanogr.* 62, 95–113. doi:10.1016/j.pocean.2004.07.004.

Arístegui, J., Barton, E., Montero, M. F., García-Muñoz, M., and Escánez, J. (2003). Organic carbon distribution and water column respiration in the NW Africa-Canaries Coastal Transition Zone. *Aquat. Microb. Ecol*. 33, 289–301.

Arístegui, J., and Montero, M. F. (2005). Temporal and spatial changes in plankton respiration and biomass in the Canary Islands region: The effect of mesoscale variability. *J. Mar. Syst*. 54, 65–82. doi:10.1016/j.jmarsys.2004.07.004.

Arístegui, J., Sangrá, P., Hernández-León, S., Cantón, M., Hernández-Guerra, A., and Kerling, J. L. (1994). Island-induced eddies in the Canary islands. *Deep. Res. Part I* 41, 1509–1525. doi:10.1016/0967-0637(94)90058-2.

Arístegui, J., Tett, P., Hernández-Guerra, A., Basterretxea, G., Montero, M. F., Wild, K., et al. (1997). The influence of island-generated eddies on chlorophyll distribution: A study of mesoscale variation around Gran Canaria. *Deep. Res. Part I Oceanogr. Res. Pap.* 44, 71–96. doi:10.1016/S0967-0637(96)00093-3.

Armbrust, E. V. (2009). The life of diatoms in the world's oceans. *Nature* 459, 185–192. doi:10.1038/nature08057.

Arrigo, K. R. (2005). Marine Microorganisms and Global Nutrient Cycles. *Nature* 437, 349–355. doi:10.1038/nature04158.

Azam, F., Fenchel, T., Field, J. G., Gray, J., Meyer-Reil, L. A., and Thingstad, F. (1993). The Ecological Role of Water-Column Microbes in the Sea. *Mar. Ecol. Prog. Ser.* 10, 257–263.

Bach LT, Alvarez-Fernandez S, Hornick T, Stuhr A, Riebesell U (2017) Simulated ocean acidification reveals winners and losers in coastal phytoplankton. *PLoS ONE* 12(11): e0188198. doi.org/10.1371/journal.pone.0188198

Bakun, A. (1990). Global climate change and intensification of coastal ocean upwelling. *Science* (80-.). 247, 198–201. doi:10.1126/science.247.4939.198.

Baltar, F., Arístegui, J., Montero, M. F., Espino, M., Gasol, J. M., and Herndl, G. J. (2009). Mesoscale variability modulates seasonal changes in the trophic structure of nano- and picoplankton communities across the NW Africa-Canary Islands transition zone. *Prog. Oceanogr.* 83, 180–188. doi:10.1016/j.pocean.2009.07.016.

Baltar, F., Palovaara, J., Unrein, F., Catala, P., Horňák, K., Šimek, K., et al. (2016). Marine bacterial community structure resilience to changes in protist predation under phytoplankton bloom conditions. *ISME J.* 10, 568–581. doi:10.1038/ismej.2015.135.

Bar-On, Y. M., Phillips, R., and Milo, R. (2018). The biomass distribution on Earth. *Proc. Natl. Acad. Sci. U. S. A.* 115, 6506–6511. doi:10.1073/pnas.1711842115.

Barceló-Llull, B., Pallàs-Sanz, E., Sangrà, P., Martínez-Marrero, A., Estrada-Allis, S. N., and Arístegui, J. (2017a). Ageostrophic secondary circulation in a subtropical intrathermocline eddy. *J. Phys. Oceanogr*. 47, 1107–1123. doi:10.1175/JPO-D-16-0235.1.

Barceló-Llull, B., Sangrà, P., Pallàs-Sanz, E., Barton, E. D., Estrada-Allis, S. N., Martínez-Marrero, A., et al. (2017b). Anatomy of a subtropical intrathermocline eddy. *Deep. Res. Part I Oceanogr. Res. Pap.* 124, 126–139. doi:10.1016/j.dsr.2017.03.012.

Barton, E. D., Aristegui, J., Tett, P., Canton, M., García-Braun, J., Hernández-León, S., et al. (1998). The transition zone of the Canary Current upwelling region. *Prog. Oceanogr.* 41, 455–504. doi:10.1016/S0079-6611(98)00023-8.

Barton, E. D., Arístegui, J., Tett, P., and Navarro-Pérez, E. (2004). Variability in the Canary Islands area of filament-eddy exchanges. *Prog. Oceanogr*. 62, 71–94. doi:10.1016/j.pocean.2004.07.003.

Barton, E. D., Basterretxea, G., Flament, P., Mitchelson-jacob, E. G., Jones, B., Arístegui, J., et al. (2000). Lee region of Gran Canaria. *J. Geophys. Res*. 105, 173–193.

Basterretxea, G., and Aristegui, J. (2000). Mesoscale variability in phytoplankton biomass distribution and photosynthetic parameters in the Canary-NW African coastal transition zone. *Mar. Ecol. Prog. Ser. 197, 27-40*

Basterretxea, G., Barton, E. D., Tett, P., Sangrá, P., Navarro-Perez, E., and Arístegui, J. (2002). Eddy and deep chlorophyl maximum response to wind-shear in the lee of Gran Canaria. *Deep. Res. Part I Oceanogr. Res. Pap.* 49, 1087–1101. doi:10.1016/S0967-0637(02)00009-2.

Basu, S., and Mackey, K. R. M. (2018). Phytoplankton as key mediators of the biological carbon pump: Their responses to a changing climate. *Sustain*. 10. doi:10.3390/su10030869.

Beardall, J., Allen, D., Bragg, J., Finkel, Z. V., Flynn, K. J., Quigg, A., et al. (2009). Allometry and stoichiometry of unicellular, colonial and multicellular phytoplankton. *New Phytol*. 181, 295–309. doi:10.1111/j.1469-8137.2008.02660.x.

Beardall, J., and Raven, J. A. (2004a). The potential effects of global climate change on microalgal photosynthesis, growth and ecology. *Phycologia* 43, 26–40. doi:10.2216/i0031-8884-43-1-26.1.

Behrenfeld, M. J., Boss, E., Siegel, D. A., and Shea, D. M. (2005). Carbon-based ocean productivity and phytoplankton physiology from space. *Global Biogeochem. Cycles* 19, 1–14. doi:10.1029/2004GB002299.

Behrenfeld, M. J., Malley, R. T. O., Siegel, D. A., Mcclain, C. R., Sarmiento, J. L., Feldman, G. C., et al. (2006). Climate-driven trends in contemporary ocean productivity. *Nature* 444, 752–756. doi:10.1038/nature05317.

Behrenfeld, M. J., O'Malley, R. T., Boss, E. S., Westberry, T. K., Graff, J. R., Halsey, K. H., et al. (2016). Revaluating ocean warming impacts on global phytoplankton. *Nat. Clim. Chang*. 6, 323–330. doi:10.1038/nclimate2838.

Behrenfeld, M. J., Randerson, J. T., Mcclain, C. R., Feldman, G. C., Los, S. O., Tucker, C. J., et al. (2001). Biospheric Primary Production During an ENSO Transition. *Science* 291, 2594–2597.

Bellerby, R. G. J., Schulz, K. G., Riebesell, U., Neill, C., Nondal, G., Heegaard, E., et al. (2008). Marine ecosystem community carbon and nutrient uptake stoichiometry under varying ocean acidification during the PeECE III experiment. *Biogeosciences* 5, 1517–1527.

Benitez-Nelson, C. R., Bidigare, R. R., DIckey, T. M., Landry, M. ., Leonard, C. L., Brown, S. L., et al. (2007). Mesoscale Eddies Drive Increased Silica Export in the Subtropical Pacific *Ocean. Science* (80- .). 316, 1017–1022.

Benitez-Nelson, C. R., and McGillicuddy, D. J. (2008). Mesoscale physical-biological-biogeochemical linkages in the open ocean: An introduction to the results of the E-Flux and EDDIES programs. *Deep.*

Res. Part II Top. Stud. Oceanogr. 55, 1133–1138. doi:10.1016/j.dsr2.2008.03.001.

Berman, T., and Bronk, D. A. (2003). Dissolved organic nitrogen: A dynamic participant in aquatic ecosystems. doi:10.3354/ame031279.

Bibby, T. S., and Moore, C. M. (2011). Silicate:nitrate ratios of upwelled waters control the phytoplankton community sustained by mesoscale eddies in sub-tropical North Atlantic and Pacific. *Biogeosciences* 8, 657–666. doi:10.5194/bg-8-657-2011.

Biller, S. J., Berube, P. M., Lindell, D., and Chisholm, S. W. (2015). Prochlorococcus: The structure and function of collective diversity. *Nat. Rev. Microbiol*. 13, 13–27. doi:10.1038/nrmicro3378.

Bindoff, N.L., W.W.L. Cheung, J.G. Kairo, J. Arístegui, V.A. Guinder, R. Hallberg, N. Hilmi, N. Jiao, M.S. Karim, L. Levin, S. O'Donoghue, S.R. Purca Cuicapusa, B. Rinkevich, T. Suga, A. Tagliabue, and P. Williamson, 2019: Changing Ocean, Marine Ecosystems, and Dependent Communities. In: IPCC Special Report on the Ocean and Cryosphere in a Changing Climate [H.-O. Pörtner, D.C. Roberts, V. Masson-Delmotte, P. Zhai, M. Tignor, E. Poloczanska, K. Mintenbeck, A. Alegría, M. Nicolai, A. Okem, J. Petzold, B. Rama, N.M. Weyer (eds.)]. In press.

Bopp, L., Monfray, P., Aumont, O., Dufresne, J.-L., Treut, H. Le, Madec, G., et al. (2001). Potential impact of climate change on marine export production. *Global Biogeochem. Cycles* 15, 81–99.

Bopp, L., Resplandy, L., Orr, J. C., Doney, S. C., Dunne, J. P., Gehlen, M., et al. (2013). Multiple stressors of ocean ecosystems in the 21st century : projections with CMIP5 models. *Biogeosciences* 10, 6225–6245. doi:10.5194/bg-10-6225-2013.

Borsheim, K. Y., and Bratbak, G. (1987). bacterivorous Monas sp. enriched from seawater. *Mar. Ecol. Prog. Ser.* 36, 171–175. doi: 10.3354/meps03617

Bouman, H. A., Ulloa, O., Scanlan, D. J., Zwirglmaier, K., Li, W. K. W., Platt, T., et al. (2006). Oceanographic basis of the global surface

distribution of Prochlorococcus ecotypes. *Science* (80-.). 312, 918–921. doi:10.1126/science.1122692.

Boyd, P. W. (2015). Toward quantifying the response of the oceans' biological pump to climate change. *Front. Mar. Sci*. 2, 1–15. doi:10.3389/fmars.2015.00077.

Brown, J. H., Gillooly, J. F., Allen, A. P., Savage, V. M., and West, G. B. (2004). Toward a Metabolic Theory of Ecology. *Ecology* 85, 1771–1789. doi:10.1007/978-3-030-64130-6_8.

Brussaard, C. P. D., Noordeloos, A. A. M., White, H., Collenteur, M. C. J., Schulz, K. G., Ludwig, A., et al. (2013). Arctic microbial community dynamics influenced by elevated CO_2 levels. *Biogeosciences* 10, 719–731. doi:10.5194/bg-10-719-2013.

Buesseler, K. O., Boyd, P. W., Black, E. E., and Siegel, D. A. (2020). Metrics that matter for assessing the ocean biological carbon pump. *Proc. Natl. Acad. Sci. U. S. A.* 117, 9679–9687. doi:10.1073/pnas.1918114117.

Buitenhuis, E. T., Hashioka, T., and Quéré, C. Le (2013a). Combined constraints on global ocean primary production using observations and models. *Global Biogeochem. Cycles* 27, 847–858. doi:10.1002/gbc.20074.

Buitenhuis, E. T., Vogt, M., Moriarty, R., Bednaršek, N., Doney, S. C., Leblanc, K., et al. (2013b). MAREDAT: Towards a world atlas of MARine Ecosystem DATa. *Earth Syst. Sci. Data* 5, 227–239. doi:10.5194/essd-5-227-2013.

Caldeira, K., and Wickett, M. E. (2003). Anthropogenic carbon and ocean pH. *Nature* 425, 365. doi:10.1038/425365a.

Capet, X., McWilliams, J. C., Molemaker, M. J., and Shchepetkin, A. F. (2008a). Mesoscale to submesoscale transition in the California Current system. Part I: Flow structure, eddy flux, and observational tests. *J. Phys. Oceanogr.* 38, 29–43. doi:10.1175/2007JPO3671.1.

Capet, X., McWilliams, J. C., Molemaker, M. J., and Shchepetkin, A. F. (2008b). Mesoscale to submesoscale transition in the California

Current system. Part II: Frontal processes. *J. Phys. Oceanogr.* 38, 44–64. doi:10.1175/2007JPO3672.1.

Cardona, T. (2019). Thinking twice about the evolution of photosynthesis. *Open Biol.* 9. doi:10.1098/rsob.180246.

Caron, D. A. (2016). Mixotrophy stirs up our understanding of marine food webs. *Proc. Natl. Acad. Sci. U. S. A.* 113, 2806–2808. doi:10.1073/pnas.1600718113.

Caron, D. A., Countway, P. D., Jones, A. C., Kim, D. Y., and Schnetzer, A. (2012). Marine protistan diversity. *Ann. Rev. Mar. Sci.* 4, 467–493. doi:10.1146/annurev-marine-120709-142802.

Carpenter, J. R., and Timmermans, M. L. (2012). Deep mesoscale eddies in the Canada Basin, Arctic Ocean. *Geophys. Res. Lett.* 39, 1–6. doi:10.1029/2012GL053025.

Carr, M. E. (2001). Estimation of potential productivity in Eastern Boundary Currents using remote sensing. *Deep. Res. Part II Top. Stud. Oceanogr*. 49, 59–80. doi:10.1016/S0967-0645(01)00094-7.

Chaigneau, A., Eldin, G., and Dewitte, B. (2009). Eddy activity in the four major upwelling systems from satellite altimetry (1992-2007). *Prog. Oceanogr*. 83, 117–123. doi:10.1016/j.pocean.2009.07.012.

Chavez, F. P., and Messié, M. (2009). A comparison of Eastern Boundary Upwelling Ecosystems. *Prog. Oceanogr*. 83, 80–96. doi:10.1016/j.pocean.2009.07.032.

Chavez, F. P., Messié, M., and Pennington, J. T. (2011). Marine primary production in relation to climate variability and change. *Ann. Rev. Mar. Sci*. 3, 227–260. doi:10.1146/annurev.marine.010908.163917.

Chelton, D. B., Deszoeke, R. A., Schlax, M. G., El Naggar, K., and Siwertz, N. (1998). Geographical variability of the first baroclinic Rossby radius of deformation. *J. Phys. Oceanogr*. 28, 433–460. doi:10.1175/1520-0485(1998)028<0433:GVOTFB>2.0.CO;2.

Chelton, D. B., Schlax, M. G., and Samelson, R. M. (2011). Global observations of nonlinear mesoscale eddies. *Prog. Oceanogr*. 91, 167–216. doi:10.1016/j.pocean.2011.01.002.

Chelton, D. B., Schlax, M. G., Samelson, R. M., and de Szoeke, R. A. (2007). Global observations of large oceanic eddies. *Geophys. Res. Lett*. 34, 1–5. doi:10.1029/2007GL030812.

Chenillat, F., Franks, P. J. S., Rivière, P., Capet, X., Grima, N., and Blanke, B. (2015). Plankton dynamics in a cyclonic eddu in the Southern California Current System. *J. Geophys. Res*. Ocean. 120, 5566–5588. doi:10.1038/175238c0.

Chevin, L. M., Lande, R., and Mace, G. M. (2010). Adaptation, plasticity, and extinction in a changing environment: Towards a predictive theory. *PLoS Biol*. 8. doi:10.1371/journal.pbio.1000357.

Chrétiennot-Dinet, M.-J., Sournia, A., Ricard, M., and Billard, C. (1993). A classification of the marine phytoplankton of the world from class to genus. *Phycologia* 32, 159–179. doi:10.2216/i0031-8884-32-3-159.1.

Christaki, U., Vázquez-Domínguez, E., Courties, C., and Lebaron, P. (2005). Grazing impact of different heterotrophic nanoflagellates on eukaryotic (Ostreococcus tauri) and prokaryotic picoautotrophs (Prochlorococcus and Synechococcus). *Environ. Microbiol*. 7, 1200–1210. doi:10.1111/j.1462-2920.2005.00800.x.

Ciais, P., Sabine, C., Govindasamy, B., Bopp, L., Brovkin, V., Canadell, J., Chhabra, A., DeFries, R., Galloway, J., Heimann, M., Jones, C., Le Quéré, C., Myneni, R., Piao, S., and Thornton, P.: Chapter 6: Carbon and Other Biogeochemical Cycles, in: Climate Change 2013 The Physical Science Basis, edited by: Stocker, T., Qin, D., and Platner, G.-K., Cambridge University Press, Cambridge, 2013.

Clayton, S., Nagai, T., and Follows, M. J. (2014). Fine scale phytoplankton community structure across the Kuroshio Front. *J. Plankton Res*. 36, 1017–1030. doi:10.1093/plankt/fbu020.

Corredor-Acosta, A., Morales, C. E., Rodríguez-Santana, A., Anabalón, V., Valencia, L. P., and Hormazabal, S. (2020). The Influence of Diapycnal Nutrient Fluxes on Phytoplankton Size Distribution in an Area of Intense Mesoscale and Submesoscale Activity off Concepción, Chile. *J. Geophys. Res. Ocean*. 125. doi:10.1029/2019JC015539.

Cotti-Rausch, B. E., Lomas, M. W., Lachenmyer, E. M., Goldman, E. A., Bell, D. W., Goldberg, S. R., et al. (2016). Mesoscale and sub-mesoscale variability in phytoplankton community composition in the Sargasso Sea. *Deep. Res. Part I Oceanogr. Res. Pap*. 110, 106–122. doi:10.1016/j.dsr.2015.11.008.

Cravo, A., Relvas, P., Cardeira, S., and Rita, F. (2013). Nutrient and chlorophyll a transports during an upwelling event in the NW margin of the Gulf of Cadiz. *J. Mar. Syst*. 128, 208–221. doi:10.1016/j.jmarsys.2013.05.001.

Crease, J. (1962). Velocity measurements in the deep water of the western North Atlantic: Summary. *J. Geophys. Res*. 67, 3173–3176. doi:https://doi.org/10.1029/JZ067i008p03173.

D'Asaro, E., Lee, C., Rainville, L., Harcourt, R., and Thomas, L. (2011). Enhanced turbulence and energy dissipation at ocean fronts. *Science* (80-.). 332, 318–322. doi:10.1126/science.1201515.

D'Ovidio, F., De Monte, S., Alvain, S., Dandonneau, Y., and Lévy, M. (2010). Fluid dynamical niches of phytoplankton types. *Proc. Natl. Acad. Sci. U. S. A*. 107, 18366–18370. doi:10.1073/pnas.1004620107.

d'Ovidio, F., De Monte, S., Penna, A. Della, Cotté, C., and Guinet, C. (2013). Ecological implications of eddy retention in the open ocean: A Lagrangian approach. *J. Phys. A Math*. Theor. 46. doi:10.1088/1751-8113/46/25/254023.

Davis, C. S., and McGillicuddy, D. J. (2006). Transatlantic abundance of the N_2-fixing colonial cyanobacterium Trichodesmium. *Science* (80-.). 312, 1517–1520. doi:10.1126/science.1123570.

de Boyer Montégut, C., Madec, G., Fischer, A. S., Lazar, A., and Iudicone, D. (2004). Mixed layer depth over the global ocean: An examination of profile data and a profile-based climatology. *J. Geophys. Res. C Ocean*. 109, 1–20. doi:10.1029/2004JC002378.

De Vargas, C., Audic, S., Henry, N., Decelle, J., Mahé, F., Logares, R., et al. (2015). Eukaryotic plankton diversity in the sunlit ocean. *Science* (80-.). 348. doi:10.1126/science.1261605.

Delille, B., Zondervan, I., Jacquet, S., Chou, L., Wollast, R., Bellerby, R. G. J., et al. (2005). Response of primary production and calcification to changes of p CO_2 during experimental blooms of the coccolithophorid Emiliania huxleyi. *Global Biogeochem. Cycles* 19, 1–14. doi:10.1029/2004GB002318.

Demarcq, H. (2009). Trends in primary production, sea surface temperature and wind in upwelling systems (1998-2007). *Prog. Oceanogr*. 83, 376–385. doi:10.1016/j.pocean.2009.07.022.

Doney, S. C., Busch, D. S., Cooley, S. R., and Kroeker, K. J. (2020). The impacts of ocean acidification on marine ecosystems and reliant human communities. *Annu. Rev. Environ. Resour*. 45, 83–112. doi:10.1146/annurev-environ-012320-083019.

Doney, S. C., Fabry, V. J., Feely, R. A., and Kleypas, J. A. (2009). Ocean acidification: The other CO_2 problem. *Ann. Rev. Mar. Sci*. 1, 169–192. doi:10.1146/annurev.marine.010908.163834.

Doney, S. C., Ruckelshaus, M., Duffy, J. E., Barry, J. P., Chan, F., English, C. A., et al. (2012). Climate Change Impacts on Marine Ecosystems. *Ann. Rev. Mar. Sci*. 4, 12-37, doi:10.1146/annurev-marine-041911-111611.

Doney, S. C., and Schimel, D. S. (2007). Carbon and climate system coupling on timescales from the precambrian to the anthropocene. *Annu. Rev. Environ. Resour*. 32, 31–66. doi:10.1146/annurev.energy.32.041706.124700.

Dubelaar, G. B. J., and Gerritzen, P. L. (2000). Cytobuoy: a step forward towards using flow cytometry in operational oceanography. *Sci. Mar*. 64, 255–265. doi: 10.3989/scimar.2000.64n2255

Dufois, F., Hardman-Mountford, N. J., Greenwood, J., Richardson, A. J., Feng, M., & Matear, R. J. (2016). Anticyclonic eddies are more productive than cyclonic eddies in subtropical gyres because of winter mixing. *Science Advances*, 2(5), e1600282–e1600282.doi:10.1126/sciadv.1600282

Duhamel, S., Van Wambeke, F., Lefevre, D., Benavides, M., and Bonnet, S. (2018). Mixotrophic metabolism by natural communities

of unicellular cyanobacteria in the western tropical South Pacific Ocean. *Environ. Microbiol*. 20, 2743–2756. doi:https://doi.org/10.1111/1462-2920.14111.

Dutkiewicz, S., Cermeno, P., Jahn, O., Follows, M. J., Hickman, A. A., Taniguchi, D. A. A., et al. (2020). Dimensions of marine phytoplankton diversity. *Biogeosciences* 17, 609–634. doi:10.5194/bg-17-609-2020.

Dutkiewicz, S., Scott, J. R., and Follows, M. J. (2013). Winners and losers : Ecological and biogeochemical changes in a warming ocean. *Global Biogeochem. Cycles* 27, 463–477. doi:10.1002/gbc.20042.

Eberlein, T., Wohlrab, S., Rost, B., John, U., Bach, L. T., Riebesell, U., et al. (2017). Effects of ocean acidification on primary production in a coastal North Sea phytoplankton community. *PLoS One* 12, 1–15. doi:10.1371/journal.pone.0172594.

Eden, C., and Dietze, H. (2009). Effects of mesoscale eddy/wind interactions on biological new production and eddy kinetic energy. *J. Geophys. Res. Ocean*. 114, 1–13. doi:10.1029/2008JC005129.

Edwards, K. F. (2019). Mixotrophy in nanoflagellates across environmental gradients in the ocean. *Proc. Natl. Acad. Sci. U. S. A*. 116, 6211–6220. doi:10.1073/pnas.1814860116.

Egge, J. K., Thingstad, T. F., Larsen, A., Engel, A., Wohlers, J., Bellerby, R. G. J., et al. (2009). Primary production during nutrient-induced blooms at elevated CO_2 concentrations. *Biogeosciences* 6, 877–885.

Engel, A., Borchard, C., Piontek, J., Schulz, K. G., Riebesell, U., and Bellerby, R. (2013). CO_2 increases ^{14}C primary production in an Arctic plankton community. *Biogeosciences* 10, 1291–1308. doi:10.5194/bg-10-1291-2013.

Engel, A., Delille, B., Jacquet, S., Riebesell, U., Rochelle-newall, E., Terbrüggen, A., et al. (2004). Transparent exopolymer particles and dissolved organic carbon production by Emiliania huxleyi exposed to different CO_2 concentrations : a mesocosm experiment C : N C : P. *Aquat. Microb. Ecol* 34, 93–104.

Estrada-Allis, S. N., Barceló-Llull, B., Pallàs-Sanz, E., Rodríguez-Santana, A., Souza, J. M. A. C., Mason, E., et al. (2019). Vertical velocity dynamics and mixing in an anticyclone near the Canary Islands. *J. Phys. Oceanogr*. 49, 431–451. doi:10.1175/JPO-D-17-0156.1.

Falkowski, P. G. (1994). The role of phytoplankton photosynthesis in global biogeochemical cycles. *Photosynth. Res*. 39, 235–258. doi:10.1007/BF00014586.

Falkowski, P. G., Katz, M. E., Knoll, A. H., Quigg, A., Raven, J. A., Schofield, O., et al. (2004). The evolution of modern eukaryotic phytoplankton. *Science* (80-.). 305, 354–360. doi:10.1126/science.1095964.

Falkowski, P. G., and Oliver, M. J. (2007). Mix and match: How climate selects phytoplankton. *Nat. Rev. Microbiol*. 5, 813–819. doi:10.1038/nrmicro1751.

Falkowski, P. G., Ziemann, D., Kolber, Z., and Bienfang, P. K. (1991). Role of eddy pumping in enhancing primary production in the ocean. *Nature* 352, 55–58. doi:10.1038/352055a0.

Falkowski, P., Scholes, R. J., Boyle, E., Canadell, J., Canfield, D., Elser, J., et al. (2000). The Global Carbon Cycle : A Test of Our Knowledge of Earth as a System. *Science* (80-.). 290, 291–296.

Feely, R. A., Sabine, C. L., Lee, K., Berelson, W., Kleypas, J., Fabry, V. J., et al. (2004). Impact of anthropogenic CO_2 on the $CaCO_3$ system in the oceans. *Science* (80-.). 305, 362–366. doi:10.1126/science.1097329.

Feng, Y., Hare, C. E., Leblanc, K., Rose, J. M., Zhang, Y., Ditullio, G. R., et al. (2009). Effects of increased pCO_2 and temperature on the North Atlantic spring bloom . I . The phytoplankton community and biogeochemical response. *Mar. Ecol. Prog. Ser* 388, 13–25. doi:10.3354/meps08133.

Ferrari, R. (2011). A frontal challenge for climate models. *Science* (80-.). 332, 316–317. doi:10.1126/science.1203632.

Field, C. B., Behrenfeld, M. J., Randerson, J. T., and Falkowski, P. (1998). Primary production of the biosphere: Integrating terrestrial and oceanic components. *Science* (80-.). 281, 237–240. doi:10.1126/science.281.5374.237.

Fielding, S., Crisp, N., Allen, J. T., Hartman, M. C., Rabe, B., and Roe, H. S. J. (2001). Mesoscale subduction at the Almeria-Oran front Part 2. Biophysical interactions. *J. Mar. Syst*. 30, 287–304. doi:10.1016/S0924-7963(01)00063-X.

Figueiras, F. G., Arbones, B., Montero, M. F., Barton, E. D., and Arístegui, J. (2016). Photophysiological variability and its in fl uence on primary production in the NW Africa – Canary Islands coastal transition zone. *J. Mar. Syst*. 157, 92–100. doi:10.1016/j.jmarsys.2016.01.003.

Finkel, Z. V. (2001). Light absorption and size scaling of light-limited metabolism in marine diatoms. *Limnol. Oceanogr*. 46, 86–94. doi:10.4319/lo.2001.46.1.0086.

Finkel, Z. V., Beardall, J., Flynn, K. J., Quigg, A., Rees, T. A. V., and Raven, J. A. (2010). Phytoplankton in a changing world: Cell size and elemental stoichiometry. *J. Plankton Res*. 32, 119–137. doi:10.1093/plankt/fbp098.

Finkel, Z. V., Irwin, A. J., and Schofield, O. (2004). Resource limitation alters the 3/4 size scaling of metabolic rates in phytoplankton. *Mar. Ecol. Prog. Ser*. 273, 269–279. doi:10.3354/meps273269.

Flombaum, P., Gallegos, J. L., Gordillo, R. A., Rincón, J., Zabala, L. L., Jiao, N., et al. (2013). Present and future global distributions of the marine Cyanobacteria Prochlorococcus and Synechococcus. *Proc. Natl. Acad. Sci. U. S. A*. 110, 9824–9829. doi:10.1073/pnas.1307701110.

Flynn, K. J., Stoecker, D. K., Mitra, A., Raven, J. A., Glibert, P. M., Hansen, P. J., et al. (2013). Misuse of the phytoplankton-zooplankton dichotomy: The need to assign organisms as mixotrophs within plankton functional types. *J. Plankton Res*. 35, 3–11. doi:10.1093/plankt/fbs062.

Fox-Kemper, B., Ferrari, R., and Hallberg, R. (2008). Parameterization of mixed layer eddies. Part I: Theory and diagnosis. *J. Phys. Oceanogr*. 38, 1145–1165. doi:10.1175/2007JPO3792.1.

Fu, F., Warner, M. E., Zhang, Y., Feng, Y., and Hutchins, D. A. (2007). Effects of Increased Temperature and CO_2 on Photosynthesis, Growth, and Elemental Ratios in Marine Synechococcus and Prochlorococcus (Cyanobacteria). *J. Phycol*. 43, 485–496. doi:10.1111/j.1529-8817.2007.00355.x.

Fuglister, F. C. (1972) Cyclonic rings formed by the Gulf Stream 1965-66. *Studies in Physical Oceanography*. A. L. Gordon, Ed., Gordon and Breach, 137-168

Fuhrman, J. A. (2009). Microbial community structure and its functional implications. *Nature* 459, 193–199. doi:10.1038/nature08058.

Fuhrman, J. A., Steele, J. A., Hewson, I., Schwalbach, M. S., Brown, M. V., Green, J. L., et al. (2008). A latitudinal diversity gradient in planktonic marine bacteria. *Proc. Natl. Acad. Sci. U. S. A.* 105, 7774–7778. doi:10.1073/pnas.0803070105.

García-Muñoz, M., Arístegui, J., Montero, M. F., and Barton, E. D. (2004). Distribution and transport of organic matter along a filament-eddy system in the Canaries - NW Africa coastal transition zone region. *Prog. Oceanogr*. 62, 115–129. doi:10.1016/j.pocean.2004.07.005.

García-Muñoz, M., Arístegui, J., Pelegrí, J. L., Antoranz, A., Ojeda, A., and Torres, M. (2005). Exchange of carbon by an upwelling filament off Cape Ghir (NW Africa). *J. Mar. Syst*. 54, 83–95. doi:10.1016/j.jmarsys.2004.07.005.

García-Reyes, M., Sydeman, W. J., Schoeman, D. S., Rykaczewski, R. R., Black, B. A., Smit, A. J., et al. (2015). Under pressure: climate change, upwelling, and eastern boundary upwelling ecosystems. *Front. Mar. Sci*. 2:109. doi: 10.3389/fmars.2015.00109

Garrett, C. . J. . R., and Loder, J. W. (1981). Dynamical Aspects of Shallow Sea Fronts. Philos. Trans. R. Soc. A Math. *Phys. Eng. Sci*. 302, 563–581.

Gasol, J. M., Li Zweifel, U., Peters, F., Fuhrman, J. A., and Hagström, Å. (1999). Significance of size and nucleic acid content heterogeneity as measured by flow cytometry in natural planktonic bacteria. *Appl. Environ. Microbiol*. 65, 4475–4483. doi:10.1128/aem.65.10.4475-4483.1999.

Gattuso J-P, 8. First authoritative Hansson L, eds. 2011. Ocean Acidification. Oxford, UK: Oxford Univ. Press

Gaube, P., McGuillicuddy Jr, D. J., Chelton, D. B., Behrenfeld, M. J., and Strutton, P. G. (2014). Regional variations in the influence of mesoscale eddies on near-surface chlorophyll. *J. Geophys. Res. Ocean*. 119, 8195–8229. doi:10.1038/175238c0.

Gingerich, P. D. (2019). Temporal Scaling of Carbon Emission and Accumulation Rates: Modern Anthropogenic Emissions Compared to Estimates of PETM Onset Accumulation. Paleoceanogr. *Paleoclimatology* 34, 329–335. doi:10.1029/2018PA003379.

Giordano, M., Beardall, J., and Raven, J. A. (2005). CO_2 Concentrating Mechanisms in Algae : Mechanisms , Environmental Modulation , and Evolution. *Ann. Rev. Plant Biol.* 56, 99-131. doi:10.1146/annurev.arplant.56.032604.144052.

Gómez-Letona, M., Ramos, A. G., Coca, J., and Arístegui, J. (2017). Trends in primary production in the canary current upwelling system-A regional perspective comparing remote sensing models. *Front. Mar. Sci*. 4, 1–18. doi:10.3389/fmars.2017.00370.

Gomis, D., Pascual, A., and Pedder, M. A. (2005). Errors in dynamical fields inferred from oceanographic cruise data: Part II. The impact of the lack of synopticity. *J. Mar. Syst*. 56, 334–351. doi:10.1016/j.jmarsys.2005.02.003.

Grébert, T., Doré, H., Partensky, F., Farrant, G. K., Boss, E. S., Picheral, M., et al. (2018). Light color acclimation is a key process in the global ocean distribution of Synechococcus cyanobacteria. *Proc. Natl. Acad. Sci. U. S. A*. 115, E2010–E2019. doi:10.1073/pnas.1717069115.

Gruber, N., Lachkar, Z., Frenzel, H., Marchesiello, P., Münnich, M., McWilliams, J. C., et al. (2011). Eddy-induced reduction of biological

production in eastern boundary upwelling systems. *Nat. Geosci*. 4, 787–792. doi:10.1038/ngeo1273.

Guidi, L., Calil, P. H. R., Duhamel, S., Björkman, K. M., Doney, S. C., Jackson, G. A., et al. (2012). Does eddy-eddy interaction control surface phytoplankton distribution and carbon export in the North Pacific Subtropical Gyre? *J. Geophys. Res. Biogeosciences* 117, 1–12. doi:10.1029/2012JG001984.

Guidi, L., Chaffron, S., Bittner, L., Eveillard, D., Larhlimi, A., Roux, S., et al. (2016). Plankton networks driving carbon export in the oligotrophic ocean. *Nature* 532, 465–470. doi:10.1038/nature16942.

Guidi, L., Stemmann, L., Jackson, G. A., Ibanez, F., Claustre, H., Legendre, L., et al. (2009). Effects of phytoplankton community on production, size and export of large aggregates: A world-ocean analysis. *Limnol. Oceanogr*. 54, 1951–1963. doi:10.4319/lo.2009.54.6.1951.

Gula, J., Molemaker, J. J., and Mcwilliams, J. C. (2014). Submesoscale cold filaments in the Gulf Stream. *J. Phys. Oceanogr*. 44, 2617–2643. doi:10.1175/JPO-D-14-0029.1.

Hagström, Å., Azam, F., Andersson, A., Wikner, J., and Rassoulzadegan, F. (1988). Microbial loop in an oligotrophic pelagic marine ecosystem: possible roles of cyanobacteria and nanoflagellates in the organic fluxes. *Mar. Ecol. Prog. Ser*. 49, 171–178. doi:10.3354/meps049171.

Hamm, C. E., Merkel, R., Springer, O., Jurkojc, P., Maiert, C., Prechtelt, K., et al. (2003). Architecture and material properties of diatom shells provide effective mechanical protection. *Nature* 421, 841–843. doi:10.1038/nature01416.

Hansen, H. P., and Koroleff, F. (1999). Determination of nutrients. Methods Seawater Anal., 159–228. doi:https://doi.org/10.1002/9783527613984.ch10.

Hare, C. E., Leblanc, K., DiTullio, G. R., Kudela, R. M., Zhang, Y., Lee, P. A., et al. (2007). Consequences of increased temperature and CO_2

for phytoplankton community structure in the Bering Sea. *Mar. Ecol. Prog. Ser*. 352, 9–16. doi:10.3354/meps07182.

Harrison, C. S., Long, M. C., Lovenduski, N. S., and Moore, J. K. (2018). Mesoscale Effects on Carbon Export: A Global Perspective. *Global Biogeochem. Cycles* 32, 680–703. doi:10.1002/2017GB005751.

Hartmann, M., Grob, C., Tarran, G. A., Martin, A. P., Burkill, P. H., Scanlan, D. J., et al. (2012). Mixotrophic basis of Atlantic oligotrophic ecosystems. *Proc. Natl. Acad. Sci. U. S. A.* 109, 5756–5760. doi:10.1073/pnas.1118179109.

Haynes, R., Barton, E. D., and Pilling, I. (1993). Development, persistence, and variability of upwelling filaments off the Atlantic coast of the Iberian Peninsula. *J. Geophys. Res*. 98. doi:10.1029/93jc02016.

Hedges, S. B., Chen, H., Kumar, S., Wang, D. Y. C., Thompson, A. S., and Watanabe, H. (2001). A genomic timescale for the origin of eukaryotes. *BMC Evol. Biol*. 1. doi:10.1186/1471-2148-1-4.

Hein, M., and Sand-Jensen, K. (1997). CO_2 increases oceanic primary production. *Nature* 388.

Hernández-Hernández, N., Arístegui, J., Montero, M. F., Velasco-Senovilla, E., Baltar, F., Marrero-Díaz, Á., et al. (2020). Drivers of Plankton Distribution Across Mesoscale Eddies at Submesoscale Range. *Front. Mar. Sci*. 7, 1–13. doi:10.3389/fmars.2020.00667.

Holm-Hansen, O., Lorenzen, C. J., Holmes, R. W., and Strickland, J. D. (1965). Fluorometric determination of chlorophyll. Chloropyhll 30, 3–15.

Hosegood, P. J., Nightingale, P. D., Rees, A. P., Widdicombe, C. E., Woodward, E. M. S., Clark, D. R., et al. (2017). Nutrient pumping by submesoscale circulations in the mauritanian upwelling system. *Prog. Oceanogr*. 159, 223–236. doi:10.1016/j.pocean.2017.10.004.

Hoskins, B. J., and Bretherton, F. P. (1972). Atmospheric Frontogenesis Models: Mathematical Formulation and Solution. *J. Atmos. Sci*. 29, 11–37. doi:10.1175/1520-0469(1972)029<0011:afmmfa>2.0.co;2.

Hoskins, J. B. (1982). The mathematical theory of frontogenesis. *Annu. Rev. Fluid Mech*. 14, M. Va, 131–151. doi:10.1146/annurev.fl.14.010182.001023.

Hutchins, D. A., and Fu, F. (2017). Microorganisms and ocean global change. *Nat. Microbiol*. 2, 1–11. doi:10.1038/nmicrobiol.2017.58.

Inoue, R., Yamazaki, H., Wolk, F., Kono, T., and Yoshida, J. (2007). An estimation of buoyancy flux for a mixture of turbulence and double diffusion. *J. Phys. Oceanogr*. 37, 611–624. doi:10.1175/JPO2996.1.

IPCC, 2014: Climate Change 2014: Synthesis Report. Contribution of Working Groups I, II and III to the Fifth Assessment Report of the Intergovernmental Panel on Climate Change [Core Writing Team, R.K. Pachauri and L.A. Meyer (eds.)]. IPCC, Geneva, Switzerland, 151 pp.

IPCC, 2021: Climate Change 2021: The Physical Science Basis. Contribution of Working Group I to the Sixth Assessment Report of the Intergovernmental Panel on Climate Change [Masson-Delmotte, V., P. Zhai, A. Pirani, S.L. Connors, C. Péan, S. Berger, N. Caud, Y. Chen, L. Goldfarb, M.I. Gomis, M. Huang, K. Leitzell, E. Lonnoy, J.B.R. Matthews, T.K. Maycock, T. Waterfield, O. Yelekçi, R. Yu, and B. Zhou (eds.)]. Cambridge University Press. In Press.

Janouskovec, J., Gavelis, G. S., Burki, F., Dinh, D., Bachvaroff, T. R., Gornik, S. G., et al. (2017). Major transitions in dinoflagellate evolution unveiled by phylotranscriptomics. *Proc. Natl. Acad. Sci. U. S. A*. 114, E171–E180. doi:10.1073/pnas.1614842114.

Jenkins, W. J. (1988). Nitrate flux into the euphotic zone near Bermuda. *Nature* 331, 521–523.

Johnson, K. S., Riser, S. C., and Karl, D. M. (2010). Nitrate supply from deep to near-surface waters of the North Pacific subtropical gyre. *Nature* 465, 1062–1065. doi:10.1038/nature09170.

Johnson, Z. I., Zinser, E. R., Coe, A., Mcnulty, N., Malcolm, E., Woodward, S., et al. (2006). Niche partitioning among Prochlorococcus ecotypes along ocean-scale enviromental gradients. *Science* (80-.). 311, 1737–1740.

Joos, F., and Spahni, R. (2008). Rates of change in natural and anthropogenic radiative forcing over the past 20,000 years. *Proc. Natl. Acad. Sci. U. S. A.* 105, 1425–1430. doi:10.1073/pnas.0707386105.

Katz, M. E., Finkel, Z. V., Grzebyk, D., Knoll, A. H., and Falkowski, P. G. (2004). Evolutionary trajectories and biogeochemical impacts of marine eukaryotic phytoplankton. *Annu. Rev. Ecol. Evol. Syst*. 35, 523–556. doi:10.1146/annurev.ecolsys.35.112202.130137.

Khatiwala, S., Primeau, F., and Hall, T. (2009). Reconstruction of the history of anthropogenic CO_2 concentrations in the ocean. *Nature* 462, 346–349. doi:10.1038/nature08526.

Khatiwala, S., Tanhua, T., Mikaloff Fletcher, S., Gerber, M., Doney, S. C., Graven, H. D., et al. (2013). Global ocean storage of anthropogenic carbon. *Biogeosciences* 10, 2169–2191. doi:10.5194/bg-10-2169-2013.

Klaas, C., and Archer, D. E. (2002). Association of sinking organic matter with various types of mineral ballast in the deep sea: Implications for the rain ratio. *Global Biogeochem. Cycles* 16, 63-1-63–14. doi:10.1029/2001gb001765.

Klein, P., and Lapeyre, G. (2009). The oceanic vertical pump induced by mesoscale and submesoscale turbulence. *Ann. Rev. Mar. Sci.* 1, 351–375. doi:10.1146/annurev.marine.010908.163704.

Kroeker, K. J., Kordas, R. L., Crim, R., and Hendriks, I. E. (2013). Impacts of ocean acidification on marine organisms : quantifying sensitivities and interaction with warming. *Glob. Chang. Biol.* 19, 1884–1896. doi:10.1111/gcb.12179.

Laffoley, D. & Baxter, J. M. (editors). 2016. Explaining ocean warming: Causes, scale, effects and consequences. Full report. Gland, Switzerland: IUCN. 456 pp.

Lathuiliere, C., Levy, M., and Echevin, V. (2011). Impact of eddy-driven vertical fluxes on phytoplankton abundance in the euphotic layer. *J. Plankton Res*. 33, 827–831. doi:10.1093/plankt/fbq131.

Lauvset, S. K., Gruber, N., Landschützer, P., Olsen, A., and Tjiputra, J. (2015). Trends and drivers in global surface ocean pH over the past 3 decades. *Biogeosciences* 12, 1285–1298. doi:10.5194/bg-12-1285-2015.

Legendre, P., and Legendre, L. (eds) (2012). Numerical Ecology, 3rd Edn, Amsterdam: Elsevier, doi: 10.1016/B978-0-444-53868-0.50016-2

Le Quéré, C., Andrew, R. M., Friedlingstein, P., Sitch, S., Pongratz, J., Manning, A. C., et al. (2018). Global Carbon Budget 2018. *Earth Syst. Sci. Data* 10, 2141–2194.

Le Quéré, C., Harrison, S. P., Prentice, I. C., Buitenhuis, E. T., Aumonts, O., Bopp, L., et al. (2005). Ecosystem dynamics based on plankton functional types for global ocean biogeochemistry models. *Glob. Chang. Biol.* 11, 2016–2040. doi:10.1111/j.1365-2486.2005.01004.x.

Leblanc, K., Arístegui, J., Armand, L., Assmy, P., Beker, B., Bode, A., et al. (2012). A global diatom database- A bundance, biovolume and biomass in the world ocean. *Earth Syst. Sci. Data* 4, 149–165. doi:10.5194/essd-4-149-2012.

Legendre, L., and Le Fevre, J. (1995). Microbial food webs and the export of biogenic carbon in oceans. *Aquat. Microb. Ecol.* 9, 69–77. doi:10.3354/ame009069.

Lehahn, Y., Koren, I., Sharoni, S., D'Ovidio, F., Vardi, A., and Boss, E. (2017). Dispersion/dilution enhances phytoplankton blooms in low-nutrient waters. *Nat. Commun.* 8, 1–8. doi:10.1038/ncomms14868.

León, A. R., and Braun, J. G. (1973). Ciclo anual de la producción primaria y su relación con los nutrientes en aguas Canarias. *Bol. Inst. Esp. Ocean*. 167, 1–24.

Levitus, S., Conkright, M. E., Reid, J. L., Najjar, R. G., and Mantyla, A. (1993). Distribution of nitrate, phosphate and silicate in the world oceans. *Prog. Oceanogr*. 31, 245–273. doi:https://doi.org/10.1016/0079-6611(93)90003-V.

Lévy, M., Ferrari, R., Franks, P. J. S., Martin, A. P., and Rivière, P. (2012a). Bringing physics to life at the submesoscale. *Geophys. Res. Lett*. 39, 1–14. doi:10.1029/2012GL052756.

Lévy, M., Franks, P. J. S., and Smith, K. S. (2018). The role of submesoscale currents in structuring marine ecosystems. *Nat. Commun*. 9, 4758. doi:10.1038/s41467-018-07059-3.

Lévy, M., Iovino, D., Resplandy, L., Klein, P., Madec, G., Tréguier, A. M., et al. (2012b). Large-scale impacts of submesoscale dynamics on phytoplankton: Local and remote effects. *Ocean Model*. 43–44, 77–93. doi:10.1016/j.ocemod.2011.12.003.

Lévy, M., and Klein, P. (2004). Does the low frequency variability of mesoscale dynamics explain a part of the phytoplankton and zooplankton spectral variability? *Proc. R. Soc. A Math. Phys. Eng. Sci*. 460, 1673–1687. doi:10.1098/rspa.2003.1219.

Lévy, M., Klein, P., and Jelloul, M. Ben (2009). New production stimulated by high-frequency winds in a turbulent mesoscale eddy field. *Geophys. Res. Lett*. 36, 1–6. doi:10.1029/2009GL039490.

Lévy, M., Klein, P., and Treguier, A. M. (2001). Impact of sub-mesoscale physics on production and subduction of phytoplankton in an oligotrophic regime. *J. Mar. Res*. 59, 535–565. doi:10.1357/002224001762842181.

Levy, M., and Martin, A. P. (2013). The influence of mesoscale and submesoscale heterogeneity on ocean biogeochemical reactions. *Global Biogeochem. Cycles* 27, 1139–1150. doi:10.1002/2012GB004518.

Li, Q. P., Franks, P. J. S., Ohman, M. D., and Landry, M. R. (2012). Enhanced nitrate fluxes and biological processes at a frontal zone in the southern California current system. *J. Plankton Res*. 34, 790–801. doi:10.1093/plankt/fbs006.

Litchman, E., de Tezanos Pinto, P., Edwards, K. F., Klausmeier, C. A., Kremer, C. T., and Thomas, M. K. (2015). Global biogeochemical impacts of phytoplankton: A trait-based perspective. *J. Ecol.* 103, 1384–1396. doi:10.1111/1365-2745.12438.

Litchman, E., de Tezanos Pinto, P., Klausmeier, C. A., Thomas, M. K., and Yoshiyama, K. (2010). Linking traits to species diversity and community structure in phytoplankton. *Hydrobiologia* 653, 15–28. doi:10.1007/s10750-010-0341-5.

Litchman, E., and Klausmeier, C. A. (2008). Trait-based community ecology of phytoplankton. *Annu. Rev. Ecol. Evol. Syst*. 39, 615–639. doi:10.1146/annurev.ecolsys.39.110707.173549.

Liu, X., and Levine, N. M. (2016). Enhancement of phytoplankton chlorophyll by submesoscale frontal dynamics in the North Pacific Subtropical Gyre. *Geophys. Res. Lett*. 43, 1651–1659. doi:10.1002/2015GL066996.

Livanou, E., Lagaria, A., Santi, I., Mandalakis, M., Pavlidou, A., Lika, K., et al. (2019). Pigmented and heterotrophic nanoflagellates: Abundance and grazing on prokaryotic picoplankton in the ultra-oligotrophic Eastern Mediterranean Sea. *Deep. Res. Part II Top. Stud. Oceanogr.* 164, 100–111. doi:10.1016/j.dsr2.2019.04.007.

Longhurst, A., Sathyendranath, S., Platt, T., and Caverhill, C. (1995). An estimate of global primary production in the ocean from satellite radiometer data. *J. Plankton Res*. 17, 1245–1271.

Lovecchio, E., Gruber, N., and Münnich, M. (2018). Mesoscale contribution to the long-range offshore transport of organic carbon from the Canary Upwelling System to the open North Atlantic. *Biogeosciences 15, 5061-5091.* doi:10.5194/bg-15-5061-2018.

Lueker, T. J., Dickson, A. G., and Keeling, C. D. (2000). Ocean pCO_2 calculated from dissolved inorganic carbon , alkalinity , and equations for K 1 and K 2 : validation based on laboratory measurements of CO_2 in gas and seawater at equilibrium. *Mar. Chemi*. 70, 105-119.

Luis Otero-Ferrer, J., Cermeño, P., Bode, A., Fernández-Castro, B., Gasol, J. M., Morán, X. A. G., et al. (2018). Factors controlling the community structure of picoplankton in contrasting marine environments. *Biogeosciences* 15, 6199–6220. doi:10.5194/bg-15-6199-2018.

Lüthi, D., Le Floch, M., Bereiter, B., Blunier, T., Barnola, J. M., Siegenthaler, U., et al. (2008). High-resolution carbon dioxide concentration record 650,000-800,000 years before present. *Nature* 453, 379–382. doi:10.1038/nature06949.

Mackey, K. R. M. (2015). Response of Photosynthesis to Ocean Acidification Emerging Themes in Ocean Acidifcations Science. *Oceanography* 2828, 74–91.

Mackey, K. R. M., Paytan, A., Caldeira, K., Grossman, A. R., Moran, D., Mcilvin, M., et al. (2013). Effect of temperature on photosynthesis and growth in marine Synechococcus spp. *Plant Physiol*. 163, 815–829. doi:10.1104/pp.113.221937.

Mahadevan, A. (2016). The Impact of Submesoscale Physics on Primary Productivity of Plankton. *Ann. Rev. Mar. Sci*. 8, 161–184. doi:10.1146/annurev-marine-010814-015912.

Mahadevan, A., and Archer, D. (2000). Modeling the impact of fronts and mesoscale circulation on the nutrient supply and biogeochemistry of the upper ocean. *J. Geophys. Res. Ocean*. 105, 1209–1225. doi:10.1029/1999jc900216.

Mahadevan, A., and Campbell, J. W. (2002). Biogeochemical patchiness at the sea surface. *Geophys. Res. Lett*. 29, 1–4. doi:10.1029/2001GL014116.

Mahadevan, A., D'Asaro, E., Lee, C., and Perry, M. J. (2012). Eddy-driven stratification initiates North Atlantic spring phytoplankton blooms. *Science* (80-.). 336, 54–58. doi:10.1126/science.1218740.

Mahadevan, A., and Tandon, A. (2006). An analysis of mechanisms for submesoscale vertical motion at ocean fronts. *Ocean Model.* 14, 241–256. doi:10.1016/j.ocemod.2006.05.006.

Mahadevan, A., Tandon, A., and Ferrari, R. (2010). Rapid changes in mixed layer stratification driven by submesoscale instabilities and winds. *J. Geophys. Res. Ocean*. 115, 1–12. doi:10.1029/2008JC005203.

Malviya, S., Scalco, E., Audic, S., Vincent, F., Veluchamy, A., Poulain, J., et al. (2016). Insights into global diatom distribution and diversity

in the world's ocean. *Proc. Natl. Acad. Sci. U. S. A*. 113, E1516–E1525. doi:10.1073/pnas.1509523113.

Marañón, E. (2015). Cell Size as a key determinant of phytoplankton metabolism and community structure. *Ann. Rev. Mar. Sci*. 7, 241–264. doi:10.1146/annurev-marine-010814-015955.

Maranón, E., Cermeño, P., Huete-Ortega, M., López-Sandoval, D. C., Mouriño-Carballido, B., and Rodríguez-Ramos, T. (2014). Resource supply overrides temperature as a controlling factor of marine phytoplankton growth. *PLoS One* 9, 20–23. doi:10.1371/journal.pone.0099312.

Marañón, E., Cermeño, P., López-Sandoval, D. C., Rodríguez-Ramos, T., Sobrino, C., Huete-Ortega, M., et al. (2013). Unimodal size scaling of phytoplankton growth and the size dependence of nutrient uptake and use. *Ecol. Lett*. 16, 371–379. doi:10.1111/ele.12052.

Marañón, E., Holligan, P. M., Barciela, R., González, N., Mouriño, B., Pazó, M. J., et al. (2001). Patterns of phytoplankton size structure and productivity in contrasting open-ocean environments. *Mar. Ecol. Prog. Ser*. 216, 43–56. doi:10.3354/meps216043.

Marinov, I., Doney, S. C., and Lima, I. D. (2010). Response of ocean phytoplankton community structure to climate change over the 21st century : partitioning the effects of nutrients , temperature and light. *Biogeosciences 7,* 3941–3959. doi:10.5194/bg-7-3941-2010.

Martin, A. P. (2003). Phytoplankton patchiness : the role of lateral stirring and mixing. *Prog. Oceanogr* 57, 125–174. doi:10.1016/S0079-6611(03)00085-5.

Martin, A. P., Zubkov, M. V., Burkill, P. H., and Holland, R. J. (2005). Extreme spatial variability in marine picoplankton and its consequences for interpreting Eulerian time-series. *Biol. Lett*. 1, 366–369. doi:10.1098/rsbl.2005.0316.

Martínez-Moreno, J., Hogg, A. M., England, M. H., Constantinou, N. C., Kiss, A. E., and Morrison, A. K. (2021). Global changes in oceanic mesoscale currents over the satellite altimetry record. *Nat. Clim. Chang*. 11, 397–403. doi:10.1038/s41558-021-01006-9.

Martinez, E., Antoine, D., Ortenzio, F. D., and Gentili, B. (2009). Climate-Driven Basin Scale Decadal Oscillations of Oceanic Phytoplankton. *Science* (80-.). 326, 1253–1256. doi:10.1126/science.os-2.57.341-a.

Mason, E., Colas, F., Molemaker, J., Shchepetkin, A. F., Troupin, C., McWilliams, J. C., et al. (2011). Seasonal variability of the Canary Current: A numerical study. *J. Geophys. Res. Ocean*. 116, 1–20. doi:10.1029/2010JC006665.

Mason, E., Molemaker, J., Shchepetkin, A. F., Colas, F., McWilliams, J. C., and Sangrà, P. (2010). Procedures for offline grid nesting in regional ocean models. *Ocean Model*. 35, 1–15. doi:10.1016/j.ocemod.2010.05.007.

Massana, R., Unrein, F., Rodríguez-Martínez, R., Forn, I., Lefort, T., Pinhassi, J., et al. (2009). Grazing rates and functional diversity of uncultured heterotrophic flagellates. *ISME J.* 3, 588–595. doi:10.1038/ismej.2008.130.

Maugendre, L., Gattuso, J. P., Poulton, A. J., Dellisanti, W., Gaubert, M., Guieu, C., et al. (2017). No detectable effect of ocean acidification on plankton metabolism in the NW oligotrophic Mediterranean Sea: Results from two mesocosm studies. *Estuar. Coast. Shelf Sci.* 186, 89–99. doi:10.1016/j.ecss.2015.03.009.

Mayot, N., D'Ortenzio, F., Uitz, J., Gentili, B., Ras, J., Vellucci, V., et al. (2017). Influence of the Phytoplankton Community Structure on the Spring and Annual Primary Production in the Northwestern Mediterranean Sea. *J. Geophys. Res. Ocean*. 122, 9918–9936. doi:10.1002/2016JC012668.

McClain, C. R. (2009). A decade of satellite ocean color observations. *Ann. Rev. Mar. Sci*. 1, 19–42. doi:10.1146/annurev.marine.010908.163650.

McGillicuddy, D. J. (2016). Mechanisms of Physical-Biological-Biogeochemical Interaction at the Oceanic Mesoscale. *Ann. Rev. Mar. Sci. 8,13.1-13.36.* doi:10.1146/annurev-marine-010814-015606.

McGillicuddy, D. J., Anderson, L. A., Bates, N. R., Bibby, T., Buesseler, K. O., Carlson, C. A., et al. (2007). Eddy / Wind Interactions Stimulate Extraordinary Mid-Ocean Plankton Blooms. *Science* (80-.). 0, 1021–1026.

McGillicuddy, J. J., Anderson, L. A., Doney, S. C., and Maltrud, M. E. (2003a). Eddy-driven sources and sinks of nutrients in the upper ocean: Results from a 0.1° resolution model of the North Atlantic. *Global Biogeochem. Cycles* 17. doi:10.1029/2002gb001987.

McGillicuddy, J. J., Anderson, L. A., Doney, S. C., and Maltrud, M. E. (2003b). Eddy-driven sources and sinks of nutrients in the upper ocean: Results from a 0.1° resolution model of the North Atlantic. *Global Biogeochem. Cycles* 17. doi:10.1029/2002gb001987.

Mcgillicuddy Jr, D. J., Robinson, A. R., Siegel, D. A., Jannasch, H. W., Johnson, R., Dickey, T. D., et al. (1998). Influence of mesoscale eddies on new peoduction in the Sargasso Sea. *Nature* 394, 263–266.

McWilliams, J. C. (2016). Submesoscale currents in the ocean. *Proc. R. Soc. A Math. Phys. Eng. Sci*. 472. doi:10.1098/rspa.2016.0117.

Mella-Flores, D., Six, C., Ratin, M., Partensky, F., Boutte, C., Le Corguillé, G., et al. (2012). Prochlorococcus and synechococcus have evolved different adaptive mechanisms to cope with light and uv stress. *Front. Microbiol*. 3, 1–20. doi:10.3389/fmicb.2012.00285.

Menden-Deuer, S., and Lessard, E. J. (2000). Carbon to volume relationships for dinoflagellates, diatoms, and other protist plankton. *Limnol. Oceanogr*. 45, 569–579. doi: 10.4319/lo.2000.45.3.0569

Messié, M., and Chavez, F. P. (2015). Seasonal regulation of primary production in eastern boundary upwelling systems. *Prog. Oceanogr*. 134, 1–18. doi:10.1016/j.pocean.2014.10.011.

Mitra, A., Flynn, K. J., Burkholder, J. M., Berge, T., Calbet, A., Raven, J. A., et al. (2014). The role of mixotrophic protists in the biological carbon pump. *Biogeosciences* 11, 995–1005. doi:10.5194/bg-11-995-2014.

Moestrup, Ø.; Akselmann-Cardella, R.; Churro, C.; Fraga, S.; Hoppenrath, M.; Iwataki, M.; Larsen, J.; Lundholm, N.; Zingone, A.

(Eds) (2009 onwards). IOC-UNESCO Taxonomic *Reference List of Harmful Micro Algae*. Accessed at http://www.marinespecies.org/hab on 2020-11-19. doi:10.14284/362

Moore, L. R., Post, A. F., Rocap, G., and Chisholm, S. W. (2002). Utilization of different nitrogen sources by the marine cyanobacteria Prochlorococcus and Synechococcus, 989-996. 47, 1–8. *Limnol. Oceanogr.* 47, 989-996.

Mouriño-Carballido, B. (2009). Eddy-driven pulses of respiration in the Sargasso Sea. *Deep. Res. Part I Oceanogr. Res. Pap*. 56, 1242–1250. doi:10.1016/j.dsr.2009.03.001.

Mousing, E. A., Richardson, K., Bendtsen, J., Cetinić, I., and Perry, M. J. (2016). Evidence of small-scale spatial structuring of phytoplankton alpha- and beta-diversity in the open ocean. *J. Ecol*. 104, 1682–1695. doi:10.1111/1365-2745.12634.

Mousing, E. A., Richardson, K., and Ellegaard, M. (2018). Global patterns in phytoplankton biomass and community size structure in relation to macronutrients in the open ocean. *Limnol. Oceanogr*. 63, 1298–1312. doi:10.1002/lno.10772.

Mouw, C. B., A. Barnett, G. A. McKinley, L. Gloege, and D. Pilcher (2016), Phytoplankton size impact on export flux in the global ocean. *Global Biogeochem. Cycles,* 30, 1542–1562, doi:10.1002/2015GB005355.

Mulholland, M. R., and Lee, C. (2009). Peptide hydrolysis and the uptake of dipeptides by phytoplankton. *Limnol. Oceanogr*. 54, 856–868. doi:10.4319/lo.2009.54.3.0856.

Müller, O. F. (1773). Vermivm terrestrium et fluviatilium, seu, Animalium infusoriorum, helminthicorum et testaceorum, non marinorum, succincta historia . et Lipsiae : apud Heineck et Faber.

Müller, O. F. (1774). Vermivm terrestrium et fluviatilium, seu, Animalium infusoriorum, helminthicorum et testaceorum, non marinorum, succincta historia . et Lipsiae : apud Heineck et Faber.

Nagai, T., Tandon, A., Gruber, N., and McWilliams, J. C. (2008). Biological and physical impacts of ageostrophic frontal circulations

driven by confluent flow and vertical mixing. *Dyn. Atmos. Ocean*. 45, 229–251. doi:10.1016/j.dynatmoce.2007.12.001.

Nagai, T., Tandon, A., and Rudnick, D. L. (2006). Two-dimensional ageostrophic secondary circulation at ocean fronts due to vertical mixing and large-scale deformation. *J. Geophys. Res. Ocean*. 111. doi:10.1029/2005JC002964.

Nardelli, B. B. (2020). A multi-year time series of observation-based 3D horizontal and vertical quasi-geostrophic global ocean currents. *Earth Syst. Sci. Data* 12, 1711–1723. doi:10.5194/essd-12-1711-2020.

Nencioli, F., Kuwahara, V. S., Dickey, T. D., Rii, Y. M., and Bidigare, R. R. (2008). Physical dynamics and biological implications of a mesoscale eddy in the lee of Hawaii: Cyclone Opal observations during E-Flux III. *Deep. Res. Part II Top. Stud. Oceanogr*. 55, 1252–1274. doi:10.1016/j.dsr2.2008.02.003.

Niewiadomska, K., Claustre, H., Prieur, L., and D'Ortenzio, F. (2008). Submesoscale physical-biogeochemical coupling across the Ligurian Current (northwestern Mediterranean) using a bio-optical glider. *Limnol. Oceanogr*. 53, 2210–2225. doi:10.4319/lo.2008.53.5_part_2.2210.

Omand, M. M., and Mahadevan, A. (2015). The shape of the oceanic nitracline. *Biogeosciences* 12, 3273–3287. doi:10.5194/bg-12-3273-2015.

Omta, A. W., Kooijman, S. A. L. M., and Dijkstra, H. A. (2008). Critical turbulence revisited: The impact of submesoscale vertical mixing on plankton patchiness. *J. Mar. Res*. 66, 61–85. doi:10.1357/002224008784815766.

Oschlies, A., and Garçon, V. (1998). Eddy-influenced enhancement of primary production in a model of the North Atlantic Ocean. *Nature* 394, 266–269. doi:10.1038/28373.

Painter, S. C., Patey, M. D., Tarran, G. A., and Torres-Valdés, S. (2014). Picoeukaryote distribution in relation to nitrate uptake in the oceanic nitracline. *Aquat. Microb. Ecol*. 72, 195–213. doi:10.3354/ame01695.

Pallàs-Sanz, E., Johnston, T. M. S., and Rudnick, D. L. (2010). Frontal dynamics in a California Current System shallow front: 1. Frontal processes and tracer structure. *J. Geophys. Res*. *Ocean*. 115. doi:10.1029/2009JC006032.

Pascual, A., Ruiz, S., Olita, A., Troupin, C., Claret, M., Casas, B., et al. (2017). A Multiplatform Experiment to Unravel Meso- and Submesoscale Processes in an Intense Front (AlborEx). *Front. Mar. Sci*. 4, 1–16. doi:10.3389/fmars.2017.00039.

Pelegrí, J. L., Arístegui, J., Cana, L., González-Dávila, M., Hernández-Guerra, A., Hernández-León, S., et al. (2005). Coupling between the open ocean and the coastal upwelling region off northwest Africa: Water recirculation and offshore pumping of organic matter. *J. Mar. Syst*. 54, 3–37. doi:10.1016/j.jmarsys.2004.07.003.

Pidcock, R., Srokosz, M., Allen, J., Hartman, M., Painter, S., Mowlem, M., et al. (2010). A novel integration of an ultraviolet nitrate sensor on board a towed vehicle for mapping open-ocean submesoscale nitrate variability. *J. Atmos. Ocean. Technol*. 27, 1410–1416. doi:10.1175/2010JTECHO780.1.

Piedeleu, M., Sangra, P., Sánchez-Vidal, A., Fabrés, J., Gordo, C., and Calafat, A. (2009). An observational study of oceanic eddy generation mechanisms by tall deep-water islands (Gran Canaria). *Geophys. Res. Lett*. 36. doi:10.1029/2008GL037010.

Pierella Karlusich, J. J., Ibarbalz, F. M., and Bowler, C. (2020). Phytoplankton in the Tara Ocean. *Ann. Rev. Mar. Sci*. 12, 233–265.

Pierrot, D. E., Lewis, E., andWallace, D.W. R. (2006).MS Excel Program Developed for CO_2 System Calculations. Oak Ridge, TN: Carbon Dioxide Information Analysis Center (CDIAC).

Polovina, J. J., Howell, E. A., and Abecassis, M. (2008). Ocean's least productive waters are expanding. *Geophys. Res. Lett* 35, 2–6. doi:10.1029/2007GL031745.

Ponte, A. L., Klein, P., Capet, X., Le Traon, P. Y., Chapron, B., and Lherminier, P. (2013). Diagnosing surface mixed layer dynamics

from high-resolution satellite observations: Numerical insights. *J. Phys. Oceanogr*. 43, 1345–1355. doi:10.1175/JPO-D-12-0136.1.

Porter, K. G., and Feig, Y. S. (1980). The use of DAPI for identifiying and counting aquatic microflora. *Limnol. Oceanogr*. 25, 943–948.

Pörtner, H.-O., D.M. Karl, P.W. Boyd, W.W.L. Cheung, S.E. Lluch-Cota, Y. Nojiri, D.N. Schmidt, and P.O. Zavialov, 2014: Ocean systems. In: Climate Change 2014: Impacts, Adaptation, and Vulnerability. Part A: Global and Sectoral Aspects. Contribution of Working Group II to the Fifth Assessment Report of the Intergovernmental Panel on Climate Change [Field, C.B., V.R. Barros, D.J. Dokken, K.J. Mach, M.D. Mastrandrea, T.E. Bilir, M. Chatterjee, K.L. Ebi, Y.O. Estrada, R.C. Genova, B. Girma, E.S. Kissel, A.N. Levy, S. MacCracken, P.R. Mastrandrea, and L.L. White (eds.)]. Cambridge University Press, Cambridge, United Kingdom and New York, NY, USA, pp. 411-484.

Ramachandran, S., Tandom, A., and Mahadevan, A. (2014). Enhancement in vertical fluxes at a front by mesoscale-submesoscale coupling. *J. Geophys. Res. Ocean*. 119, 6121–6139. doi:10.1002/2014JC010211.Received.

Raven, J. A. (1998). The twelfth Tansley Lecture. Small is beautiful: The picophytoplankton. *Funct. Ecol*. 12, 503–513. doi:10.1046/j.1365-2435.1998.00233.x.

Reinfelder, J. R. (2011). Carbon concentrating mechanisms in eukaryotic marine phytoplankton. *Ann. Rev. Mar. Sci*. 3, 291–315. doi:10.1146/annurev-marine-120709-142720.

Renault, L., Deutsch, C., McWilliams, J. C., Frenzel, H., Liang, J.-H., and Colas, F. (2016). Partial decoupling of primary productivity from upwelling in the California current system. *Nat. Geosci*. 9, 505–508. doi: 10.1038/ngeo2722

Resplandy L., Lévy M., McGillicuddy, D. J. Jr. (2019). Effects of eddy-driven subduction on ocean biological carbon pump. *Global Biogeochem. Cycles*, 33. doi: 10.1029/2018GB006125

Rhein, M., S.R. Rintoul, S. Aoki, E. Campos, D. Chambers, R.A. Feely, S. Gulev, G.C. Johnson, S.A. Josey, A. Kostianoy, C. Mauritzen, D. Roemmich, L.D. Talley and F. Wang, 2013: Observations: Ocean. In: Climate Change 2013: The Physical Science Basis. Contribution of Working Group I to the Fifth Assessment Report of the Intergovernmental Panel on Climate Change [Stocker, T.F., D. Qin, G.-K. Plattner, M. Tignor, S.K. Allen, J. Boschung, A. Nauels, Y. Xia, V. Bex and P.M. Midgley (eds.)]. Cambridge University Press, Cambridge, United Kingdom and New York, NY, USA.

Richards, K. J., Whitt, D. B., Brett, G., Bryan, F. O., Feloy, K., and Long, M. C. (2021). The Impact of Climate Change on Ocean Submesoscale Activity. *J. Geophys. Res. Ocean*. 126, 1–15. doi:10.1029/2020JC016750.

Riebesell, U., Czerny, J., von Bröckel, K., Boxhammer, T., Büdenbender, J., Deckelnick, M., et al. (2013). Technical Note : A mobile sea-going mesocosm system – new opportunities for ocean change research. *Biogeosciences* 10, 1835–1847. doi:10.5194/bg-10-1835-2013.

Riebesell, U., and Gattuso, J. P. (2015). Lessons learned from ocean acidification research. *Nat. Clim. Chang*. 5, 12–14. doi:10.1038/nclimate2456.

Riebesell, U., Oschlies, A., and Körtzinger, A. (2009). Sensitivities of marine carbon fluxes to ocean change. *Proc. Natl. Acad. Sci. U. S. A*. 106, 20602–20609.

Riebesell, U., Schulz, K. G., Bellerby, R. G. J., Botros, M., Fritsche, P., Meyerhöfer, M., et al. (2007). Enhanced biological carbon consumption in a high CO_2 ocean. *Nature* 450, 545–548. doi:10.1038/nature06267.

Righetti, D., Vogt, M., Gruber, N., Psomas, A., and Zimmermann, N. E. (2019). Global pattern of phytoplankton diversity driven by temperature and environmental variability. *Sci. Adv*, 5.

Rivière, P., and Pondaven, P. (2006). Phytoplankton size classes competitions at sub-mesoscale in a frontal oceanic region. *J. Mar. Syst*. 60, 345–364. doi:10.1016/j.jmarsys.2006.02.005.

Rodríguez, J., Tintoré, J., Allen, J. T., Blanco, J. M., Gomis, D., Reul, A., et al. (2001). Mesoscale vertical motion and the size structure of phytoplankton in the ocean. *Nature* 410, 360–363. doi:10.1038/35066560.

Ross, O. N., and Sharples, J. (2007). Phytoplankton motility and the competition for nutrients in the thermocline. *Mar. Ecol. Prog. Ser*. 347, 21–38. doi:10.3354/meps06999.

Sabine, C. L., Feely, R. A., Gruber, N., Key, R. M., Lee, K., Bullister, J. L., et al. (2004). The oceanic sink for anthropogenic CO_2. *Science* (80-.). 305, 367–371. doi:10.1126/science.1097403.

Sangrà, P. (1995). Perturbación de un Flujo Geofísico Por un Obstáculo: Aplicación a la isla de Gran Canaria. Doctoral dissesrtation, University Of Las Palmas de Gran Canaria, Spain.

Sangrà, P., Auladell, M., Marrero-Díaz, A., Pelegrí, J. L., Fraile-Nuez, E., Rodríguez-Santana, A., et al. (2007). On the nature of oceanic eddies shed by the Island of Gran Canaria. *Deep. Res. Part I Oceanogr. Res. Pap*. 54, 687–709. doi:10.1016/j.dsr.2007.02.004.

Sangrá, P., Basterretxea, G., Pelegrí, J. L., and Arístegui, J. (2001). Chlorophyll increase due to internal waves on the shelf break of Gran Canaria (Canary Islands). *Sci. Mar*. 65, 89–97. doi:10.3989/scimar.2001.65s189.

Sangrà, P., García-Muñoz, C., García, C. M., Marrero-Díaz, Á., Sobrino, C., Mouriño-Carballido, B., et al. (2014). Coupling between upper ocean layer variability and size-fractionated phytoplankton in a non-nutrient-limited environment. *Mar. Ecol. Prog. Ser.* 499, 35–46. doi:10.3354/meps10668.

Sangrà, P., Pascual, A., Rodríguez-Santana, Á., Machín, F., Mason, E., McWilliams, J. C., et al. (2009). The Canary Eddy Corridor: A major pathway for long-lived eddies in the subtropical North Atlantic. *Deep. Res. Part I Oceanogr*. Res. Pap. 56, 2100–2114. doi:10.1016/j.dsr.2009.08.008.

Sangrà, P., Pelegrí, J. L., Hernández-Guerra, A., Arregui, I., Martín, J. M., Marrero-Díaz, A., et al. (2005). Life history of an anticyclonic

eddy. *J. Geophys. Res. C Ocean*. 110, 1–19. doi:10.1029/2004JC002526.

Sangrà, P., Troupin, C., Barreiro-González, B., Desmond Barton, E., Orbi, A., and Arístegui, J. (2015). The Cape Ghir filament system in August 2009 (NW Africa). *J. Geophys. Res. C Ocean*. 120, 4516–4533. doi:10.1002/2014JC010514.

Santana-Falcón, Y., Álvarez-Salgado, X. A., Pérez-Hernández, M. D., Hernández-Guerra, A., Mason, E., and Arístegui, J. (2017). Organic carbon budget for the eastern boundary of the North Atlantic subtropical gyre: Major role of DOC in mesopelagic respiration. *Sci. Rep*. 7, 1–12. doi:10.1038/s41598-017-10974-y.

Santana-Falcón, Y., Benavides, M., Sangrà, P., Mason, E., Barton, E. D., Orbi, A., et al. (2016). Coastal-offshore exchange of organic matter across the Cape Ghir filament (NW Africa) during moderate upwelling. *J. Mar. Syst*. 154, 233–242. doi:10.1016/j.jmarsys.2015.10.008.

Santana-Falcón, Y., Mason, E., and Arístegui, J. (2020). Offshore transport of organic carbon by upwelling filaments in the Canary Current System. *Prog. Oceanogr*. 186, 102322. doi:10.1016/j.pocean.2020.102322.

Sarmiento, J. L., Slater, R., Barber, R., Bopp, L., Doney, S. C., Hirst, A. C., et al. (2004). Response of ocean ecosystems to climate warming. *Global Biogeochem. Cycles* 18. doi:10.1029/2003GB002134.

Scanlan, D. J., Ostrowski, M., Mazard, S., Dufresne, A., Garczarek, L., Hess, W. R., et al. (2009). Ecological Genomics of Marine Picocyanobacteria. *Microbiol. Mol. Biol. Rev*. 73, 249–299. doi:10.1128/mmbr.00035-08.

Schartau, M., Engel, A., and Schr, J. (2007). Modelling carbon overconsumption and the formation of extracellular particulate organic carbon. *Biogeosciences* 4, 433–454.

Schulz, K. G., Bach, L. T., Bellerby, R. G., Bermúdez, R., Büdenbender, J., Boxhammer, T., et al. (2017). Phytoplankton Blooms at Increasing Levels of Atmospheric Carbon Dioxide : Experimental Evidence for

Negative Effects on Prymnesiophytes and Positive on Small Picoeukaryotes. *Front. Mar. Sci*. 4. doi:10.3389/fmars.2017.00064.

Shulman, I., Penta, B., Richman, J., Jacobs, G., Anderson, S., and Sakalaukus, P. (2015). Impact of submesoscale processes on dynamics of phytoplankton filaments. *J. Geophys. Res. Ocean*. 120, 2050–2062. doi:10.1002/2014JC010326.

Sieburth, J. M., and Smetacek, V. (1978). Pelagic ecosystem structure : Heterotrophic compartments of the plankton and their relationship to plankton size fractions. *Limnol. Oceanogr*. 23, 1256–1263.

Siegel, D. A., Court, D. B., Menzies, D. W., Peterson, P., Maritorena, S., and Nelson, N. B. (2008). Satellite and in situ observations of the bio-optical signatures of two mesoscale eddies in the Sargasso Sea. *Deep. Res. Part II Top. Stud. Oceanogr*. 55, 1218–1230. doi:10.1016/j.dsr2.2008.01.012.

Siegel, D. A., Peterson, P., McGillicuddy, D. J., Maritorena, S., and Nelson, N. B. (2011). Bio-optical footprints created by mesoscale eddies in the Sargasso Sea. *Geophys. Res. Lett*. 38, 1–6. doi:10.1029/2011GL047660.

Siegelman, L., Klein, P., Rivière, P., Thompson, A. F., Torres, H. S., Flexas, M., et al. (2020). Enhanced upward heat transport at deep submesoscale ocean fronts. *Nat. Geosci*. 13, 50–55. doi:10.1038/s41561-019-0489-1.

Sieracki, M. E., Johnson, P. W., and Sieburth, J. M. (1985). Detection, enumeration, and sizing of planktonic bacteria by image-analyzed epifluorescence microscopy. *Appl. Environ. Microbiol*. 49, 799–810. doi:10.1128/aem.49.4.799-810.1985.

Simon, N., Cras, A. L., Foulon, E., and Lemée, R. (2009). Diversity and evolution of marine phytoplankton. Comptes Rendus - *Biol.* 332, 159–170. doi:10.1016/j.crvi.2008.09.009.

Smetacek, V. (2001). A watery arms race. *Nature* 411, 745. doi:10.1038/35081210.

Snyder, S., Franks, P. J. S., Talley, L. D., Xu, Y., and Kohin, S. (2017). Crossing the line: Tunas actively exploit submesoscale fronts to

enhance foraging success. *Limnol. Oceanogr*. Lett. 2, 187–194. doi:10.1002/lol2.10049.

Sobrino, C., Ward, M. L., and Neale, P. J. (2008). Acclimation to elevated carbon dioxide and ultraviolet radiation in the diatom Thalassiosira pseudonana : Effects on growth , photosynthesis , and spectral sensitivity of photoinhibition. *Limnol. Oceanogr.* 53, 494–505.

Sokal, R. R., and Rohlf, F. J. (eds.). (2013). Biometry : The Principles and Practice of Statistics in Biological Research. New York, NY: W. H. Freeman and Co.

Sommer, U., Charalampous, E., Genitsaris, S., and Moustaka-Gouni, M. (2017). Benefits, costs and taxonomic distribution of marine phytoplankton body size. *J. Plankton Res*. 39, 494–508. doi:10.1093/plankt/fbw071.

Spall, S. A., and Richards, K. J. (2000). A numerical model of mesoscale frontal instabilities and plankton dynamics - I. Model formulation and initial experiments. *Deep. Res. Part I Oceanogr. Res. Pap*. 47, 1261–1301. doi:10.1016/S0967-0637(99)00081-3.

Spilling, K., Kremp, A., Klais, R., Olli, K., and Tamminen, T. (2014). Spring bloom community change modifies carbon pathways and C:N:P: Chl a stoichiometry of coastal material fluxes. *Biogeosciences* 11, 7275–7289. doi:10.5194/bg-11-7275-2014.

Spilling, K., and Markager, S. (2008). Ecophysiological growth characteristics and modeling of the onset of the spring bloom in the Baltic Sea. *J. Mar. Syst*. 73, 323–337. doi:10.1016/j.jmarsys.2006.10.012.

Steinacher, M., Joos, F., and Fr, T. L. (2010). Projected 21st century decrease in marine productivity : a multi-model analysis. *Biogeosciences* 7, 979–1005.

Stoecker, D. K., Hansen, P. J., Caron, D. A., and Mitra, A. (2017). Mixotrophy in the Marine Plankton. *Ann. Rev. Mar. Sci*. 9, 311–335. doi:10.1146/annurev-marine-010816-060617.

Stukel, M. R., Aluwihare, L. I., Barbeau, K. A., Chekalyuk, A. M., Goericke, R., Miller, A. J., et al. (2017). Mesoscale ocean fronts enhance carbon export due to gravitational sinking and subduction. *Proc. Natl. Acad. Sci. U. S. A*. 114, 1252–1257. doi:10.1073/pnas.1609435114.

Sulpis, O., Boudreau, B. P., Mucci, A., Jenkins, C., Trossman, D. S., Arbic, B. K., et al. (2018). Current $CaCO_3$ dissolution at the seafloor caused by anthropogenic CO_2. *Proc. Natl. Acad. Sci. U. S. A.* 115, 11700–11705. doi:10.1073/pnas.1804250115.

Swallow, M.(1961) Deep Current in the Open Ocean. *Oceanus*, 7,2-8

Sweeney, E. N., McGillicuddy, D. J., and Buesseler, K. O. (2003). Biogeochemical impacts due to mesoscale eddy activity in the Sargasso Sea as measured at the Bermuda Atlantic Time-series Study (BATS). *Deep. Res. Part II Top. Stud. Oceanogr*. 50, 3017–3039. doi:10.1016/j.dsr2.2003.07.008.

Sydeman, W. J., García-Reyes, M., Schoeman, D. S., Rykaczewski, R. R., Thompson, S. A., Black, B. A., et al. (2014). Climate change and wind intensification in coastal upwelling ecosystems. *Science* (80-.). 345, 77–80. doi:10.1126/science.1251635.

Tanaka, T., Alliouane, S., Bellerby, R. G. B., Czerny, J., De Kluijver, A., Riebesell, U., et al. (2013). Effect of increased pCO_2 on the planktonic metabolic balance during a mesocosm experiment in an Arctic fjord. *Biogeosciences* 10, 315–325. doi:10.5194/bg-10-315-2013.

Taylor, A. G., Goericke, R., Landry, M. R., Selph, K. E., Wick, D. A., and Roadman, M. J. (2012). Sharp gradients in phytoplankton community structure across a frontal zone in the California Current Ecosystem. *J. Plankton Res*. 34, 778–789. doi:10.1093/plankt/fbs036.

Taylor, J. R. (2016). Turbulent mixing, restratification, and phytoplankton growth at a submesoscale eddy. *Geophys. Res. Lett*. 43, 5784–5792. doi:10.1002/2016GL069106.

Taylor, J. R., and Ferrari, R. (2011). Ocean fronts trigger high latitude phytoplankton blooms. *Geophys. Res. Lett*. 38, 1–5. doi:10.1029/2011GL049312.

Thomas, L., and Ferrari, R. (2008). Friction, frontogenesis, and the stratification of the surface mixed layer. *J. Phys. Oceanogr*. 38, 2501–2518. doi:10.1175/2008JPO3797.1.

Thomas, L. N. (2005). Destruction of potential vorticity by winds. *J. Phys. Oceanogr*. 35, 2457–2466. doi:10.1175/JPO2830.1.

Thomas, L. N., and Lee, C. M. (2005). Intensification of ocean fronts by down-front winds. *J. Phys. Oceanogr.* 35, 1086–1102. doi:10.1175/JPO2737.1.

Thomas, L. N., Tandon, A., and Mahadevan, A. (2008). Submesoscale processes and dynamics. *Geophys. Monogr. Ser*. 177, 17–38. doi:10.1029/177GM04.

Thomas, M. K., Kremer, C. T., Klausmeier, C. A., and Litchman, E. (2012). A global pattern of thermal adaptation in marine phytoplankton. *Science* (80-.). 338, 1085–1088. doi:10.1126/science.1224836.

Tortell, P. D., Ditullio, G. R., Sigman, D. M., and Morel, F. M. M. (2002). CO_2 effects on taxonomic composition and nutrient utilization in an Equatorial Pacific phytoplankton assemblage. *Mar. Ecol. Prog. Ser.* 236, 37–43.

Tortell, P. D., Payne, C. D., Li, Y., Trimborn, S., Rost, B., Smith, W. O., et al. (2008). CO_2 sensitivity of Southern Ocean phytoplankton. *Geophys. Res. Lett*. 35, 1–5. doi:10.1029/2007GL032583.

Tréguer, P., Bowler, C., Moriceau, B., Dutkiewicz, S., Gehlen, M., Aumont, O., et al. (2018). Influence of diatom diversity on the ocean biological carbon pump. *Nat. Geosci*. 11, 27–37. doi:10.1038/s41561-017-0028-x.

Tsai, A. Y., Gong, G. C., Chung, C. C., and Huang, Y. T. (2018). Different impact of nanoflagellate grazing and viral lysis on Synechococcus spp. and picoeukaryotic mortality in coastal waters. *Estuar. Coast. Shelf Sci*. 209, 1–6. doi:10.1016/j.ecss.2018.05.012.

Tsutsumi, E., Matsuno, T., Itoh, S., Zhang, J., Senjyu, T., Sakai, A., et al. (2020). Vertical fluxes of nutrients enhanced by strong turbulence

and phytoplankton bloom around the ocean ridge in the Luzon Strait. *Sci. Rep*. 10, 1–12. doi:10.1038/s41598-020-74938-5.

Uitz, J., Claustre, H., Gentili, B., and Stramski, D. (2010). Phytoplankton class-specific primary production in the world's oceans: Seasonal and interannual variability from satellite observations. *Global Biogeochem. Cycles* 24, 1–19. doi:10.1029/2009GB003680.

Utermöhl, H. (1931). Neue Wege in der quantitativen Erfassung des Plankton.(Mit besonderer Berücksichtigung des Ultraplanktons.). *SIL Proceedings*, 1922-2010 5, 567–596. doi:10.1080/03680770.1931.11898492.

Vallina, S. M., Ward, B. A., Dutkiewicz, S., and Follows, M. J. (2014). Maximal feeding with active prey-switching: A kill-the-winner functional response and its effect on global diversity and biogeography. *Prog. Oceanogr*. 120, 93–109. doi:10.1016/j.pocean.2013.08.001.

Vaulot, D., Eikrem, W., Viprey, M., and Moreau, H. (2008). The diversity of small eukaryotic phytoplankton (≤3 μm) in marine ecosystems. *FEMS Microbiol*. Rev. 32, 795–820. doi:10.1111/j.1574-6976.2008.00121.x.

Volkov, D. L., Lee, T., and Fu, L. L. (2008). Eddy-induced meridional heat transport in the ocean. *Geophys. Res. Lett*. 35, 1–5. doi:10.1029/2008GL035490.

Wang, D., Gouhier, T. C., Menge, B. A., and Ganguly, A. R. (2015). Intensification and spatial homogenization of coastal upwelling under climate change. *Nature* 518, 390–394. doi:10.1038/nature14235.

Ward, B. A., Cael, B. B., Collins, S., and Robert Young, C. (2021). Selective constraints on global plankton dispersal. *Proc. Natl. Acad. Sci. U. S. A*. 118, 2021–2024. doi:10.1073/pnas.2007388118.

Ward, B. A., Dutkiewicz, S., and Follows, M. J. (2014). Modelling spatial and temporal patterns in size-structured marine plankton communities: Top-down and bottom-up controls. *J. Plankton Res*. 36, 31–47. doi:10.1093/plankt/fbt097.

Wei, Y., Zhao, Y., Gui, J., and Sun, J. (2021). Phosphorus enrichment masked the negative effects of ocean acidification on picophytoplankton and photosynthetic performance in the oligotrophic Indian Ocean. *Ecol. Indic*. 125, 107459. doi:10.1016/j.ecolind.2021.107459.

Worden, A. Z., Follows, M. J., Giovannoni, S. J., Wilken, S., Zimmerman, A. E., and Keeling, P. J. (2015). Rethinking the marine carbon cycle: Factoring in the multifarious lifestyles of microbes. *Science* (80-.). 347. doi:10.1126/science.1257594.

Wyatt, T. (2014). Margalef's mandala and phytoplankton bloom strategies. *Deep. Res. Part II Top. Stud. Oceanogr*. 101, 32–49. doi:10.1016/j.dsr2.2012.12.006.

Xiu, P., Chai, F., Curchitser, E. N., and Castruccio, F. S. (2018). Future changes in coastal upwelling ecosystems with global warming: the case of the California current system. *Sci. Rep.* 8, 1–9. doi: 10.1038/s41598-018-2 1247-7

Yang, J. W., Wu, W., Chung, C. C., Chiang, K. P., Gong, G. C., and Hsieh, C. H. (2018). Predator and prey biodiversity relationship and its consequences on marine ecosystem functioning - Interplay between nanoflagellates and bacterioplankton. *ISME J.* 12, 1532–1542. doi:10.1038/s41396-018-0111-3.

Yoon, H. S., Hackett, J. D., Ciniglia, C., Pinto, G., and Bhattacharya, D. (2004). A Molecular Timeline for the Origin of Photosynthetic Eukaryotes. *Mol. Biol. Evol*. 21, 809–818. doi:10.1093/molbev/msh075.

Yu, Z., and Metzger, E. J. (2019). The impact of ocean surface currents on global eddy kinetic energy via the wind stress formulation. *Ocean Model*. 139, 101399. doi:10.1016/j.ocemod.2019.05.003.

Zark, M., Broda, N. K., Hornick, T., Grossart, H., and Riebesell, U. (2017). Ocean Acidification Experiments in Large-Scale Mesocosms Reveal Similar Dynamics of Dissolved Organic Matter Production and Biotransformation. *Front. Mar. Sci*. 4, 271. doi:10.3389/fmars.2017.00271.

Zeebe RE,Wolf-Gladrow D. 2001. CO_2 in Seawater: Equilibrium, Kinetics, Isotopes. Amsterdam: Elsevier Sci.

Zeidner, G., Preston, C. M., Delong, E. F., Massana, R., Post, A. F., Scanlan, D. J., et al. (2003). Molecular diversity among marine picophytoplankton as revealed by psbA analyses. *Environ. Microbiol*. 5, 212–216. doi:10.1046/j.1462-2920.2003.00403.x.

Zhang, J., Schmitt, R. W., and Huang, R. X. (1998). Sensitivity of the GFDL modular ocean model to parameterization of double-diffusive processes. *J. Phys. Oceanogr*. 28, 589–605. doi:10.1175/1520-0485(1998)028<0589:SOTGMO>2.0.CO;2.

Zhang, Z., Wang, W., and Qiu, B. (2014). Oceanic mass transport by mesoscale eddies. *Science* (80-.). 345, 322–324. doi:10.1126/science.1252418.

Znachor, P., and Nedoma, J. (2010). Importance of dissolved organic carbon for phytoplankton nutrition in a eutrophic reservoir. *J. Plankton Res*. 32, 367–376. doi:10.1093/plankt/fbp129.

Zubkov, M. V., Sleigh, M. A., and Burkill, P. H. (2000a). Assaying picoplankton distribution by flow cytometry of underway samples collected along a meridional transect across the Atlantic Ocean. *Aquat. Microb. Ecol*. 21, 13–20. doi:10.3354/ame021013.

Zubkov, M. V., Sleigh, M. A., Burkill, P. H., and Leakey, R. J. G. (2000b). Picoplankton community structure on the Atlantic Meridional Transect: A comparison between seasons. *Prog. Oceanogr*. 45, 369–386. doi:10.1016/S0079-6611(00)00008-2.

Zubkov, M. V., and Tarran, G. A. (2008). High bacterivory by the smallest phytoplankton in the North Atlantic Ocean. *Nature* 455, 224–226. doi:10.1038/nature07236.

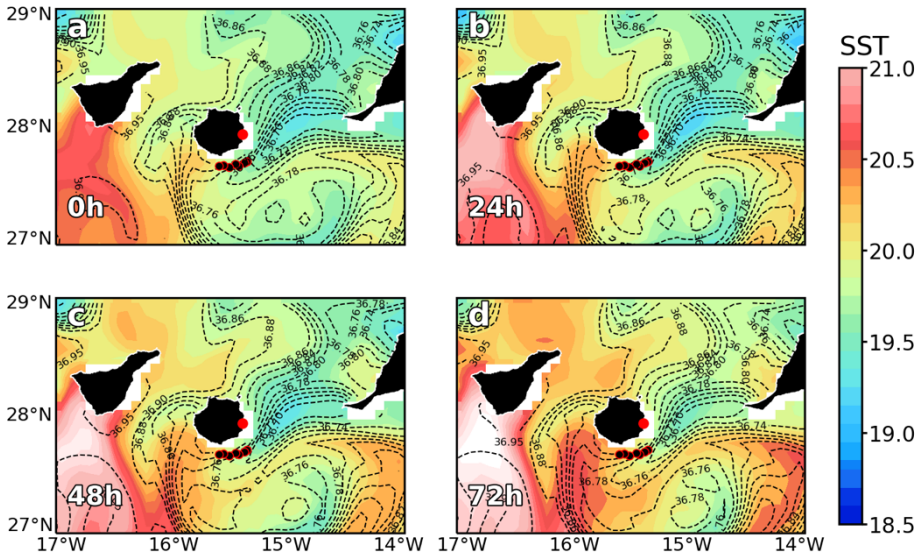

Figure 6.1. Vertical sections of Turner angles (TU; °) for 0 h (a), 24 h (b) and 72 h (c). Stations are indicated in the upper part of the plot. Dashed black line indicates the mixed layer depth. Sampling depths are represented by grey dots. Angles between -90 and -45 are characteristic of diffusive mode; between -45 ° and 45 ° is called doubly stable mode; weak salt fingers mode from 45 ° and 70 ° and salt finger mode for angles larger than 70.

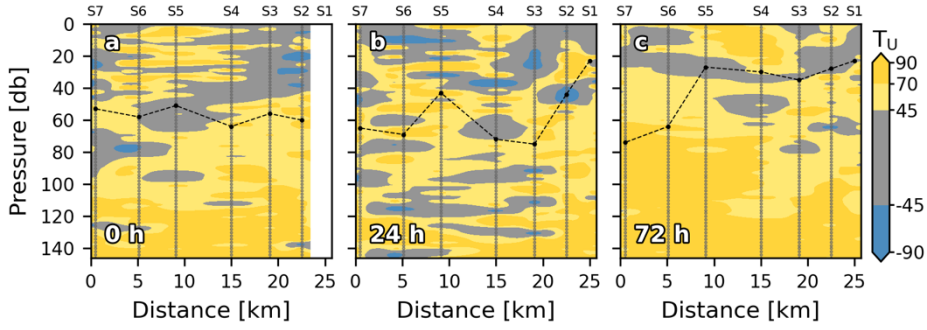

Figure 6.2. Sea surface temperature (°C) time series for (a) May 09th 2011 (0 h), (b) May 10th 2011 (24 h), (c) May 11th 2011 (48 h) and (d) May 12th 2011 (72 h). Salinity contours are superimposed to SST maps. Black dots with red borders indicate stations positions. Red dot indicates Gando airport location.

Table 6.1. Values of nutrient gradients (g_{NOx}; mmol·m^{-4}), vertical eddy diffusivity (K_z (·10^{-5}); m^2·s^{-1}), nutrient fluxes (F_{NOx}; mmol·m^{-2}·d^{-1}) below the MLD for all sampled depths.

St	0 h				24 h			72 h			
	z	g_{NOx}	K_z	F_{NOx}	g_{NOx}	K_z	F_{NOx}	z	g_{NOx}	K_z	F_{NOx}
S1	50	-	-	-	-0.301	3.5	0.033	55	-0.422	4.3	0.066
	75	-	-	-	-0.880	0.1	0.352	75	-0.315	7.8	0.106
	110	-	-	-	-1.323	2.0	0.061	100	-0.818	6.6	0.119
	150	-	-	-	-0.961	7.0	0.116	150	-1.566	6.5	0.175
S2	50	-	-	-	-0.120	-	0.013	75	-0.455	4.1	0.046
	75	-	84.0	-	-0.477	6.3	0.148	95	-0.519	0.1	0.207
	110	-	3.9	-	-1.549	2.6	0.129	110	-0.637	7.3	0.146
	150	-	6.4	-	-2.327	4.0	0.203	150	-0.928	8.7	0.174
S3	50	-	-	-	-	-	-	50	-0.029	3.3	0.003
	75	-0.117	3.9	0.013	-0.128	3.2	0.010	90	-0.222	4.0	0.031
	110	-0.634	3.4	0.050	-0.785	17.0	0.004	120	-0.882	6.8	0.133
	150	-0.862	6.6	0.124	-1.416	6.0	0.244	150	-1.340	7.3	0.169
S4	20	-	-	-	-	-	-	50	0.014	9.1	-0.004
	50	-	-	-	-0.097	1.6	0.006	80	-0.148	1.1	0.006
	75	-0.116	1.7	0.007	-0.816	1.5	0.040	100	-0.620	3.7	0.091
	100	-0.979	2.0	0.044	-1.565	7.8	0.420	132	-0.708	5.1	0.083
	150	-2.037	7.0	0.245	-1.642	7.9	0.622	150	-0.485	7.8	0.065
S5	47	-	-	-	-0.270	3.3	0.031	50	-0.094	3.8	0.012
	79	-0.324	3.8	0.039	0.027	4.7	-0.004	75	-0.423	3.5	0.057
	101	-0.991	7.0	0.168	-1.396	6.4	0.205	110	-0.969	3.4	0.076
	150	-1.537	7.9	0.213	-2.904	6.3	0.397	150	-1.251	6.2	0.135
S6	72	-0.429	3.9	0.057	-0.885	3.7	0.114	72	-0.040	3.3	0.005
	98	-1.076	4.1	0.098	-1.651	4.6	0.167	100	-1.559	4.4	0.144
	150	-1.213	6.4	0.128	-1.475	6.9	0.176	150	-3.017	6.4	0.335
S7	74	-0.691	4.7	0.108	-0.009	3.8	0.001	70	-0.707	2.3	0.056
	100	-1.347	3.7	0.114	-2.270	4.0	0.198	100	-0.600	3.7	0.052
	150	-1.928	7.1	0.238	-4.501	6.5	0.509	150	0.251	7.8	-0.034